


La borsa di dottorato è stata cofinanziata con risorse del
Programma Operativo Nazionale Ricerca e Innovazione 2014-2020,
risorse FSE REACT-EU
Azione IV.4 “Dottorati e contratti di ricerca su tematiche dell’innovazione”
e Azione IV.5 “Dottorati su tematiche Green”

DOTTORATO DI RICERCA IN BIOLOGIA

UNIVERSITY OF NAPLES FEDERICO II

Polytechnic and Basic Sciences School

PhD course in Biological Sciences Cycle 37°

CLASS CHEM-05/A

IDENTIFICATION OF NATURAL PRODUCTS FOR THE DEVELOPMENT OF IMMUNOCEUTICALS AND CANDIDATE DRUGS

Supervisor
Prof. Angelo Fontana

Candidate
Federica Albiani
matr. DR996023

Co-supervisor
Dr. Genoveffa Nuzzo
Dr. Giuliana d'Ippolito

ACADEMIC YEAR 2022-2025

UNIVERSITÀ DEGLI STUDI DI NAPOLI FEDERICO II

Scuola Politecnica e delle Scienze di Base

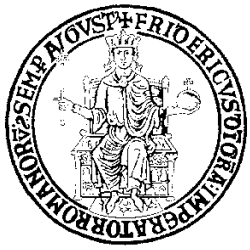

CORSO DI DOTTORATO IN BIOLOGIA 37° CICLO

CLASSE CHEM-05/A

IDENTIFICAZIONE DI PRODOTTI NATURALI PER LO SVILUPPO DI IMMUNOCEUTICI E CANDIDATI FARMACI

Supervisore
Prof. Angelo Fontana

Candidata
Federica Albiani
matr. DR996023

Co-supervisori
Dr. Genoveffa Nuzzo
Dr. Giuliana d'Ippolito

ANNO ACCADEMICO 2022-2024

INDEX

ABSTRACT

Natural Products (NPs) have always represented a huge source of molecules with relevant potential in pharmacological field. In particular, Marine Natural Products (MNPs) are characterized by an enormous structural diversity and potential bioactivity. Many natural products displayed chemo-protective functions, drug-like benefits to skin health, and immunomodulant potential both alone or in association with other treatments.

In this doctoral thesis, I evaluated the activity of MNPs as modulator of the innate immune system with the aim of identifying novel candidates with either defensive properties to use as cosmeceuticals (anti-oxidant and skin protection) or anticancer activity to use in immunotherapy. Conventional chemotherapeutic drugs are cytotoxic substances affecting vitality of normal cells together with tumor cell. In contrast, immunotherapeutic drugs offer a new strategy to fight cancer by stimulating the immune system to recognize and eliminate the malignant cells. Selection of the molecules was based on the ability to bind and activate Dectin-1 and Triggering Receptor Expressed on Myeloid cells 2 (TREM2), two membrane receptors occurring on cells of the innate immune system. Dectin-1 is a pattern recognition receptor (PRR) belonging to the C-type lectin receptors (CLRs) and is predominantly expressed on macrophages and Dendritic cells (DCs), while TREM2 is a transmembrane protein of the immunoglobulin family that is involved in modulation of several physiological and pathological processes, which are involved in several types of diseases, especially neurodegenerative ones. The research activities of this PhD thesis regard eight case studies: *Cacospongia mollior* and *Haliclona vansoesti* (sponges), *Ophiura ophiura (echinoderm),Cyclope neritea* and *Haminoea orbygnana* (molluscs), *Clavelina lepadiformis* (tunicate), *Schizotrix* (cyanobacterium), *Alexandrium andersonii* (dinoflagellate) and *Colpomoenia sp.* (red alga). The marine extracts were submitted to an advanced biological screening platform which includes innovative

approaches of fractionation, with the application of orthogonal chromatographic phases allowing us to both validate the biological response and identify the bioactive products. Moreover, marine extracts were submitted to MS-based deconvolution to find molecules with a specific functional group on the skeleton, that could be correlated to the interaction with a specific immune system receptor. These strategies allowed to isolate new and known active small metabolites of different chemotypes. Between the isolated compounds, the alkaloid Lepadin A resulted to be a good Immunogenic Cell Death (ICD) inducer, whereas the terpene Molliorin F, glycolipids cerebrosides and halisphingosines were found to be cytotoxic, at low concentrations, on human melanoma epithelial cells. Concerning the identification of cosmeceuticals, the research activities were focused on the investigation of three microalgae species- *Tetraselmis chuii*, *Cyclotella cryptica* and *Isocrysis galbana*-already known to be reach of immunomodulant lipids, on which were evaluated the anti-oxidant activity (AOA) and anti-oxidant capacity (AOC). AOA and AOC were assessed through four different assays (DPPH, ABTS, ORAC and FRAP). Also in this case, the extract was submitted to bioassay-guided screening platform, allowing to observe even more promising results for the fractions compared to the extracts. All microalgal extracts exhibited a good scavenging ability in the ABTS assay, but the most promising outcome was obtained with the green microalga *T. chuii*. After fractionation, fraction B of *C. cryptica* showed the best results in DPPH and ORAC assays. Fractions B of *C. cryptica* and *I. galbana*, fractions A and C of *T. chuii* showed a removal of the ABTS radical higher than 90%. Looking for conventional anti-oxidant molecules in each species: the highest phenolic content was found in fractions B and E of *I. galbana* and fraction E of *T. chuii; whereas f*raction B of *I. galbana* was the richest in carotenoids and the highest vitamin content was found in the fraction E of *T. chuii*. Therefore, the highest antioxidant property of the microalgae did not correlate with conventional antioxidant molecules. So, fraction B of *C. cryptica* yielded the best results as candidate for developments of new natural antioxidants,

thus suggesting the presence of different molecules with promising potential as scavenger ingredients. Part of my PhD thesis project was also developed at the company Pharmamar S.p.a (Madrid, Spain), a pharmaceutical company, leader in drug discovery, focused on the exploring of new anti-tumour agents from marine biodiversity. During this period, six different marine extracts, with potential cytotoxic activity, were analyzed and fractionated, through different chromatographic techniques, such as flash chromatography and HPLC, and spectroscopic techniques such as NMR, HRESI-LC-MSMS, to identify sixteen different pure compounds. In compliance with the privacy company policy, only six chemical structures, of the sixteen isolated, are reported in the thesis.

ABSTRACT

I prodotti naturali (NPs) hanno sempre rappresentato un'enorme fonte di molecole con un potenziale rilevante in campo farmacologico. In particolare, i prodotti naturali marini (MNPs) sono caratterizzati da un'enorme diversità strutturale e da una potenziale attività biologica. Molti prodotti naturali hanno mostrato funzioni chemio protettive, benefici simili a farmaci per la salute della pelle e un potenziale immunomodulante sia da soli che in associazione ad altri trattamenti. In questa tesi di dottorato, ho valutato l'attività dei prodotti naturali marini come modulatori del sistema immunitario innato, con l'obiettivo di identificare nuovi candidati con proprietà di difesa, da utilizzare come cosmeceutici (antiossidanti e protettivi della pelle) o attività antitumorali da utilizzare in immunoterapia. I farmaci chemioterapici convenzionali sono sostanze citotossiche che colpiscono la vitalità delle cellule normali insieme a quelle tumorali. I farmaci immunoterapici, invece, offrono una nuova strategia per combattere il cancro, stimolando il sistema immunitario a riconoscere ed eliminare le cellule maligne. La selezione delle molecole si è basata sulla capacità di legare e attivare Dectina-1 e Triggering Receptor Expressed on Myeloid cells 2 (TREM2), due recettori di membrana presenti sulle cellule del sistema immunitario innato. Dectina-1 è un recettore di riconoscimento (PRRs), appartenente alle lectine con dominio di tipo C (CLRs), ed è espressa prevalentemente su macrofagi e cellule dendritiche (DCs), mentre TREM2 è una proteina transmembrana della famiglia delle immunoglobuline che è coinvolta nella modulazione di diversi processi fisiologici e patologici, implicati in vari tipi di malattie, soprattutto neurodegenerative. L'attività di ricerca di questo lavoro di tesi di PhD ha riguardato otto diversi casi studio: *Cacospongia mollior* e *Haliclona vansoesti* (spugne), *Ophiura ophiura (echinoderma), Cyclope neritea and Haminoea orbygnana* (mollusco), *Clavelina lepadiformis* (tunicato) *Schizotrix* (cianobatterio), *Alexandrium andersonii* (dinoflagellato) e *Colpomoenia sp.* (alga rossa). Gli estratti marini sono stati sottoposti a una piattaforma di screening biologico avanzato che comprende approcci innovativi

di frazionamento, con l'applicazione di fasi cromatografiche ortogonali che ci permettono sia di convalidare la risposta biologica sia di identificare i prodotti bioattivi. In genere, gli estratti marini sono stati sottoposti a un processo di deconvoluzione basato sulla spettrometria di massa, per trovare molecole, con uno specifico gruppo funzionale sullo scheletro, che potesse essere correlato all'interazione con uno specifico recettore del sistema immunitario. Queste strategie hanno permesso di isolare piccoli metaboliti attivi nuovi o noti di diversi chemiotipi. Tra i composti isolati, l'alcaloide Lepadin A è risultato un buon induttore di morte cellulare immunogenica (ICD), mentre il terpene Molliorin F, i glicolipidi cerebrosidi e le halisfingosine sono risultati citotossici, a basse concentrazioni, su cellule epiteliali del melanoma umano. Per quanto riguarda l'identificazione di cosmeceutici, le attività di ricerca si sono concentrate sull'indagine di tre specie di microalghe - *Tetraselmis chuii*, *Cyclotella cryptica* e *Isocrysis galbana* - già note per essere portatrici di lipidi immunomodulanti, sulle quali sono state valutate l'attività antiossidante (AOA) e la capacità antiossidante (AOC). AOA e AOC sono state valutate attraverso quattro diversi saggi (DPPH, ABTS, ORAC e FRAP). Anche in questo caso, l'estratto è stato sottoposto a una piattaforma di screening guidata dal saggio, che ha permesso di osservare risultati ancora più promettenti per le frazioni rispetto agli estratti. Tutti gli estratti microalgali hanno mostrato una buona capacità di *scavenging* nel saggio ABTS, ma il risultato più promettente è stato ottenuto con la microalga verde *T. chuii*. Dopo il frazionamento, la frazione B di *C. cryptica* ha mostrato i migliori risultati nei saggi DPPH e ORAC. Le frazioni B di *C. cryptica* e *I. galbana*, le frazioni A e C di *T. chuii* hanno mostrato una rimozione del radicale ABTS superiore al 90%. Per quanto riguarda il contenuto di molecole antiossidanti convenzionali in ciascuna specie: il contenuto fenolico più elevato è stato riscontrato nelle frazioni B ed E di *I. galbana* e nella frazione E di *T. chuii*; mentre la frazione B di *I. galbana* è risultata la più ricca di carotenoidi; il contenuto vitaminico più elevato è stato riscontrato nella frazione E di *T. chuii*. Pertanto, le proprietà antiossidanti

più elevate delle microalghe non erano correlate alle molecole antiossidanti convenzionali. Pertanto, la più alta proprietà antiossidante delle microalghe non era correlata a molecole antiossidanti convenzionali, infatti la frazione B di *C. cryptica* ha dato i migliori risultati come candidato per lo sviluppo di nuovi antiossidanti naturali, suggerendo così la presenza di altri prodotti naturali con un potenziale promettente come *scavenger*. Una parte del mio progetto di tesi di dottorato è stata sviluppata anche presso Pharmamar S.p.a (Madrid, Spagna), azienda farmaceutica leader nella scoperta di farmaci, focalizzata sull'esplorazione di nuovi agenti antitumorali provenienti dalla biodiversità marina. Durante questo periodo, sei diversi estratti marini, con una potenziale attività citotossica, sono stati analizzati e frazionati, attraverso diverse tecniche cromatografiche, come cromatografia flash e HPLC, e tecniche spettroscopiche come NMR, HRESI-LC-MSMS, per ottenere sedici diversi composti puri. Nel rispetto della normativa sulla privacy, nella tesi sono riportate solo sei strutture chimiche, delle sedici isolate.

1) INTRODUCTION

1.1 Natural products (NPs)

Natural products (NPs) are naturally occurring small molecules diversly distributed in microorganisms, fungi, protists, animals and plants. They are traditionally the main source of novel candidates for the pharmaceutical pipeline and, over the past decades, have played a crucial role in the development of medical treatments of human disease. [1] In the last years, a renewed interest in NPs has been driven by the newly recognized value of their structural diversity and chemo-physical properties that make these molecules particularly suitable for the pharmacological applications.[2] According to Newman and Cragg, from 1981 to 9/2019, almost 33% of the new approved drugs were NP or natural derivate (ND), and other 22% were nature-inspired synthetic compounds. Most of the FDA approved drugs during the period from 1981 to 2014 derive from different medicinal terrestrial plants and bacteria.[3] (FIGURE 1) The pharmaceutical development of NPs was not reduced by COVID-19 pandemic, as 37 over the 55 new drugs approved by FDA are related to naturally occurring products.[4,5]

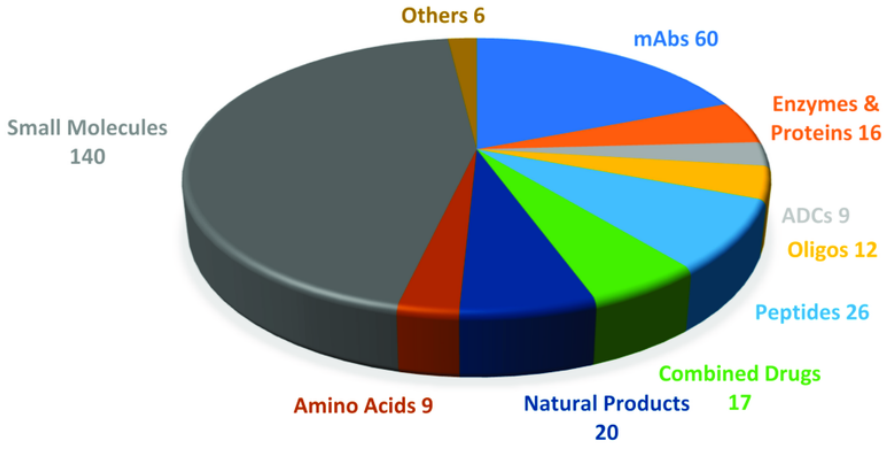

Figure 1: New approved drugs: from all source categories.[5]

Moreover, nowadays, NPs provide an interesting and largely unexplored source also for the discovery of efficient and safe new potential cosmetic ingredients. Indeed, the cosmetic industry is now paying more attention to bioactive natural products from various biological sources for their application in skin care cosmetics, including topical care products, UV protective, and anti-wrinkle products. Starting from natural products isolated from plants and animals, marine bio-discovery and bioavailability became a new trend for searching of marine natural products (MNPs) with potential bioactivity including nutraceutical, cosmetic, and pharmaceuticals field. As per the estimates of a recent report approximately 39,500 marine natural products have been identified with a huge structural variability. Most of these molecules possess potent biological properties; in detail, many marine invertebrates, plants, and bacteria are also source of molecules for prevention and treatment of immune system diseases i.e. impairments in the functionality of the immune system, such as immunodeficiency resulting in infections and tumours, overactivity resulting in autoimmune disease. [3,6–8] In the pharmacological field, small molecules', having a low molecular weight (generally, < 1000 Da), success as drugs has been due to their inherent properties, including their ability to cross biological barriers and to modulate an array of different biological targets through specific chemical interactions, and low toxicity. This offers the opportunity to specifically target various cellular processes and, in particular, signaling pathways that regulate immune responses. [9] The ecological function of small molecules has often driven the research of bioactive molecules. Starting from the need to discover the ecological role of secondary metabolites, many potent different chemical molecules have been found. Structure variability of marine secondary metabolites make them the new frontier for the exploration of novel compounds with potential applications in drug discovery and other fields. [10]

1.2 Drugs from Marine Natural Products (MNPs)

More than 70% of the surface of our planet is covered by oceans. The marine environment is estimated to contain 500,000 species of animals and plants distributed across 28 taxonomic phyla, of which approximately ten have been extensively studied as source of natural products. [11] Marine natural products (MNPs) show a higher incidence of significant bioactivity and structural novelty when compared to their terrestrial counterparts. Oceans are characterized by significant changing in pressure, salinity, temperature, pH, nutrient and light availability. These harsh play a crucial role in the development of the diversity of secondary metabolites of marine organisms,[12] thus, making marine environments a compelling frontier for the exploration of novel compounds with potential applications in drug discovery and other fields. By the late-1950s, the concept of drugs from the sea had attracted some interested. Bergmann published three reports of unusual arabino- and ribo-pentosyl nucleosides obtained from marine sponges collected in Florida, USA. The compounds eventually led to the development of the chemical derivatives ara-A (vidarabine) and ara-C (cytarabine), two nucleosides with significant anticancer properties that have been approved in clinical use.[13] Drug discovery pipeline[14] is the ensemble of stepwise activities intended to identify chemical compounds with a bioactivity of interest, in order to identify candidates for drug development (FIGURE 2). The entire process until drug approval is long, complex and expensive. Since the mid-1960s, several marine-derived compounds have shown promising results in preclinical studies and have been advanced to clinical preliminaries or even confirmed by regulatory bodies. (FIGURE 3)

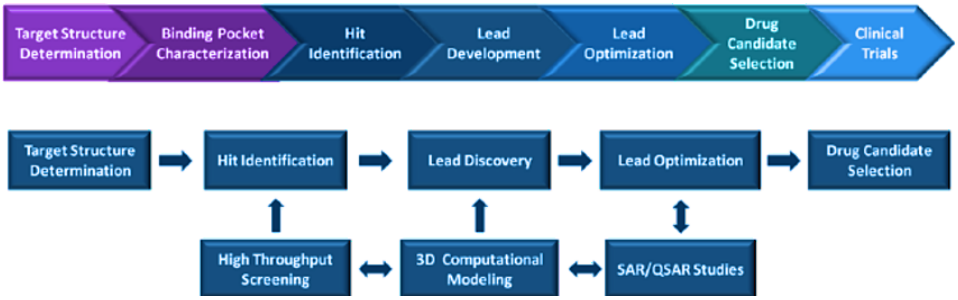

Figure 2: Drug discovery pipeline [14]

The majority of the reported biological activities of these compounds involve cytotoxic which is often related to the ecological function as chemical defenses.[12,15,16]

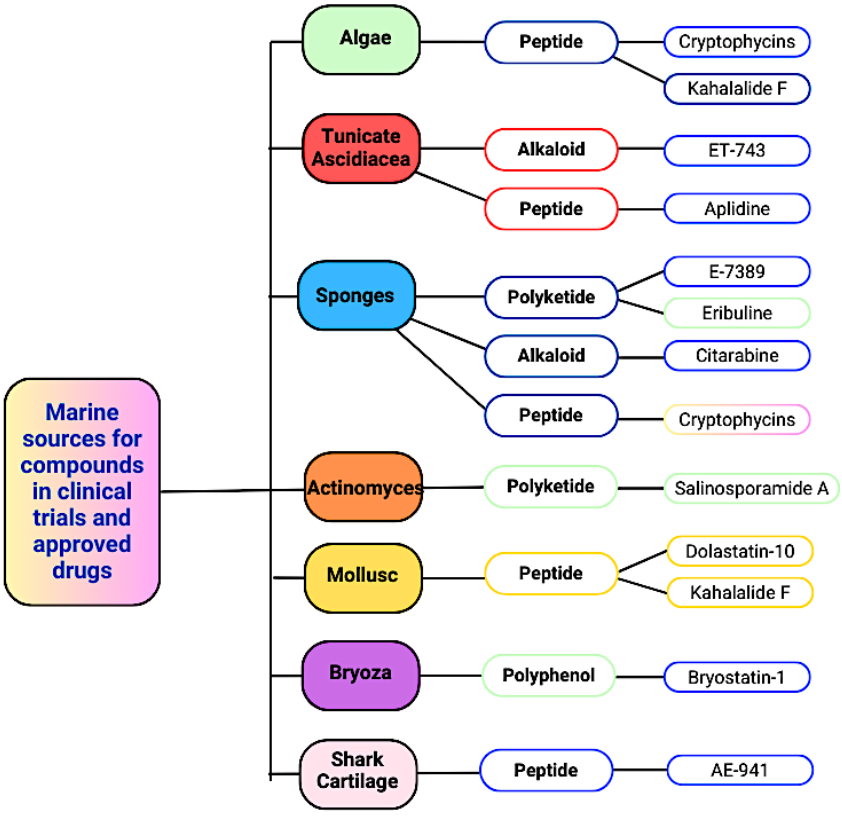

Figure 3: Variety of marine sources of compounds for clinical trials and approved drugs [12]

The number of approved drugs from marine source, by Food and Drug Administration (FDA) is expected to steadily increase. Now days, the number of pharmaceutical compounds in clinical trials has widely increased.[3,13,17] (TABLE 1)

Table 1: Marine-derived compounds that are in clinical trials (Phase I-III) for tumour, anti-inflammatory and neurodegenerative disease. (Mayer, https://www.marinepharmacology.org/)

Drug name	**Origin**	**Organization**	**Class of molecules**
Plitidepsin (Aplidin®)	*Aplidium albicans*	PharmaMar (Colmenar Viejo, Madrid, Spain)	Cyclic depsipeptide
PM00104 (Zalypsis®)	*Joruna funebris*	PharmaMar (Colmenar Viejo, Madrid, Spain)	Alkaloid
Kahalalide F	*Elysia rufescens*	PharmaMar (Colmenar Viejo, Madrid, Spain)	Peptide
Hemiasterlin (E7974)	*Hemiastrella minor*	Eisai (Tokyo, Japan)	Tripeptide
Spisulosine (ES-285)	*Spisula polynyma*	PharmaMar (Colmenar Viejo, Madrid, Spain)	Macrolide
Pseudopterosin A	*Pseudoptergorgia elisabethae*	VimRx Pharmaceuticals (Irvine, CA, USA)	Dyterpene glycoside
Marizomib (Salinosporamide A; NPI-0052)	*Salinispora tropica*	Nereus Pharmaceutical (San Diego, CA, USA)	Macrolide
Tetrodotoxin (TTX)	*Hapalochlaena maculosa*	Canadian WEX Pharmaceuticals Inc., Canada)	Guanidine alkaloid
Neovastat® (AE-941)	Shark cartilage	Æterna (Québec, Québec, Canada)	Water soluble molecules
Conotoxin G (CGX-1160)	*Conus geographus*	Cognetix (Salt Lake City, UT, USA)	Peptide

IPL-576092	*Petrosia contignata*	Aventis (Strasbourg, France)	Polyhydroxylated steroid
DMXBA (GTS-21)	*Paranemertes peregrina*	Comentis (San Francisco, CA, USA)	Alkaloid
Bryostatin 1	*Bugula neritina*	National Cancer Institute (NCI)	Macrolide
Plinabulin (NPI-2358)	*Aspergillus sp.*	Nereus Pharmaceutical (San Diego, CA, USA)	Diketopiperazine

1.3 Cosmeceuticals from MNPs

MNPs have also gained a lot of attention in the cosmeceutical fields. The term "cosmeceutical" was first introduced by Raymond E. Reed in the 1960s. It refers to a hybrid product that combines the esthetical properties of a cosmetic with the efficacy of a dermatological drug. From this perspective, a prerequisite for a product to be claimed as a cosmeceutical is the incorporation of active ingredients into its formulas.[18] Some products meet the definitions of both cosmetics and drugs, but, it's important to clarify that pharmaceuticals and cosmetics follow two distinguished legislations[19], as showed in FIGURE 4.

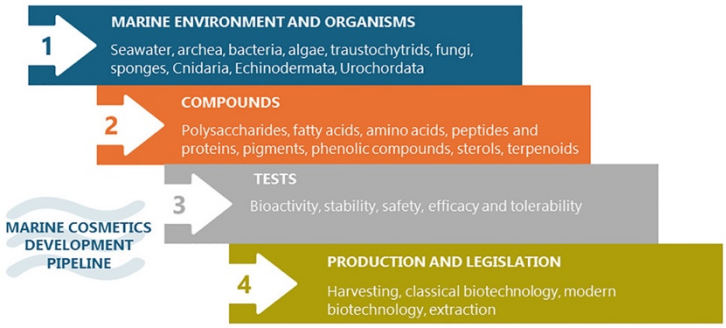

Figure 4: Marine cosmetics development pipeline. [19]

Recently, the cosmeceutical industry is progressively shifting to natural bioactive compounds. Specifically, the demand for algae bioactive compounds in cosmeceuticals is rapidly increasing as they contain natural extracts which are considered safe; thus, rendering fewer side effects on humans.[20] There has been increased evidence proving the beneficial effects of antioxidants when applied topically to the skin,[21] besides acting as a shield against free radicals, antioxidants provide dermo- cosmetic formulations with the necessary protection against oxidative deterioration. This last aspect is not irrelevant with a view to ensuring products with an increasingly long shelf-life.[22]In fact, the fragrance and color of a dermo-cosmetic preparation are decisive factors in the product acceptance by consumers. Therefore, formulating with antioxidants has become imperative in order to launch more effective products onto the market. Despite synthetic anti-oxidant still dominate the market, their use has several limitations, so there is an ongoing search for their replacement with naturally occurring antioxidants.[23] The terms *antioxidant capacity* (AOC) and *antioxidant activity* (AOA) are often used interchangeably, their real meanings are quite distinct. The AOA is referred to a pure compound and corresponds to its rate constant against a given free radical. The AOC is referred, instead, to a complex mixture and measures the moles of a given free radical scavenged, independently from the antioxidant activity of any antioxidant present in the mixture. Many *in vitro* chemical antioxidant assays have been developed and improved in the past few decades. The antioxidant potential shown by microalgae is mainly related to the high content and diversity of antioxidant molecules, some of which are aquatic-specific, while others are shared with terrestrial plants (FIGURE 5). Indeed, microalgae combine several advantages for the development of biotechnological applications: high biodiversity, photosynthetic yield, growth, productivity and a metabolic plasticity that can be orientated using culture conditions. Some of these metabolites are molecules of interest such as pigments (e.g., carotenoids), polysaccharides, vitamins and sterols. Marine algae can survive in harsh conditions (i.e., withstand

heat, cold, ultra-violet radiation, salinity, and desiccation) due to their ability to adapt to physiological changes by producing stress tolerant substances. Algae produce a huge number of primary metabolites; additionally, many research findings reported that secondary metabolites derived from algae such as fucoidan, fucoxanthin, sulphated polysaccharide, polyphenol and fucosterol were shown to possess anti-inflammation, antioxidant, anticancer, antibacterial and anti-aging effects. [24,25]

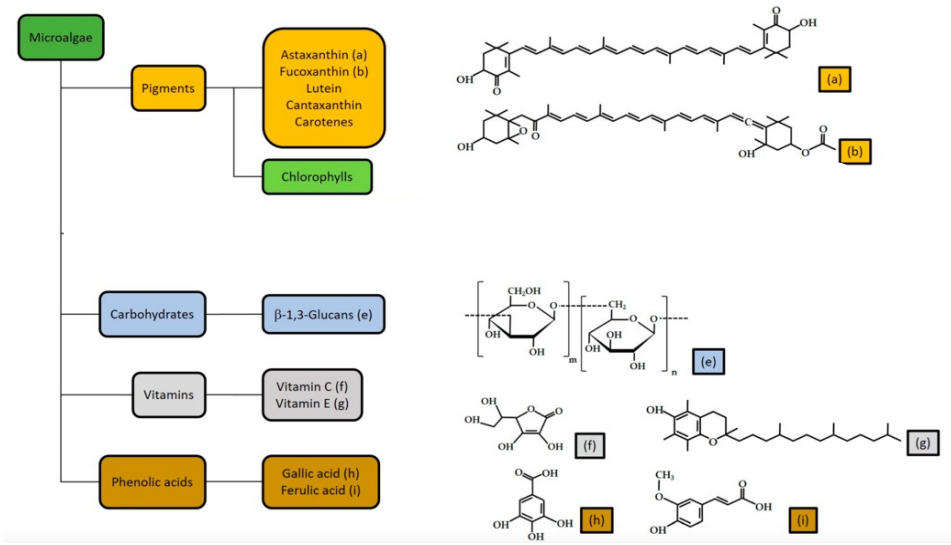

Figure 5: Natural anti-oxidant molecules from microalgae

1.4 Cancer chemotherapy and immunotherapy

The immune system protects the body against illness and infection that bacteria, viruses, fungi or parasites can cause. It is a collection of reactions and responses that the body makes to damaged cells or infection. There are pathological conditions, such as cancers, in which a normal immune response is suboptimal or inappropriate. Tumor development can be controlled by cytotoxic innate and adaptive immune cells; however, as tumor develops from neoplastic tissue to clinically detectable tumors, cancer cells evolve different mechanisms that mimic

peripheral immune tolerance in order to avoid tumoricidal attack. In addition, cancer can weaken the immune system, such as in leukemia or lymphoma, as well as certain cancer treatments can temporarily weaken the immune system. In these cases, pharmaceutical tuning of the immune response is a desired effect to prevent, treat, or augment the effect of traditional treatment. The primary purpose of conventional anti-cancer therapy is to neutralize the cancerous cells, but they can effect on both cancer and healthy cells, showing a toxic effect.[26] (FIGURE 6) The main difference between chemotherapy and immunotherapy lies in their mode of action on the body. While chemotherapy acts directly on cancer cells, immunotherapy exploit the potential of the patient's immune system to fight the tumor. Acting on the patient's immune system, immunotherapy is based on so-called “checkpoint inhibitors”, which modulate or interrupt the immune response. When cancer cells are annihilated, the immune system sends a signal to block the action of immune cells; an exaggerated immune reaction can cause damage to the body, involving even healthy cells. Many natural products displayed chemo-protective and immunomodulant potential both alone or in association with conventional treatment.[2]

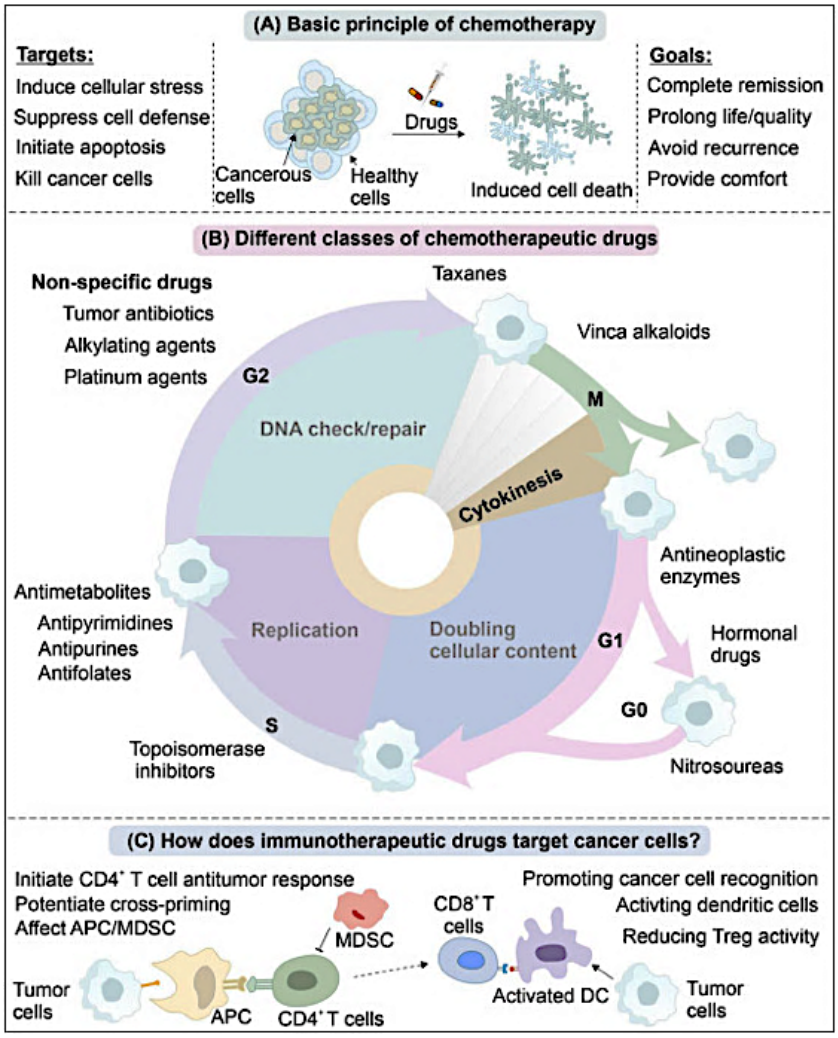

Figure 6: Schematic diagram showing the basic principles of chemotherapy (A), different classes of chemotherapeutic agents/drugs (B), and immunotherapeutic mechanism(s) of targeting cancer cells (C). [26]

The first example of immunotherapy dates back to the late 1800s, when the New York surgeon Coley treated sarcoma patients by vaccination with a mixture composed of attenuated streptococcal and staphylococcal bacteria, also known under the name Coley's toxin.[27]

Among the best-known mechanisms of immunotherapy against tumors there are the ones who involve the antibodies anti-CTLA4 (Cytotoxic T-Lymphocyte Antigen 4) and anti-PD1 (Programmed Death-1). CTLA4 and PD1 are two receptors expressed on the surface of T cells; usually, these receptors modulate negatively, or repress, the immune response. In detail, CTLA4 interacts with its ligands CD80 and CD86 by preventing the proliferation of T cells, such that it promotes the proliferation of tumor cells. PD1 interacts with ligands on the surface of tumor cells, allowing their proliferation. These mechanisms are prevented by the presence of "checkpoint-pathway inhibitors", mentioned above, which block the interaction of the two receptors with their ligands, allowing T cells to remain active long enough to recognize tumor cells and prevent their proliferation. [28,29]
The immune response against the tumor can be further enhanced by unspecific stimulation of the immune system using stimulators such as adjuvants or so-called biological response modifiers (e.g., cytokines). Another peculiar alternative to activate the immune response is the stimulation of dendritic cells (DCs). Dendritic Cells (DCs) represent the most efficient professional antigen-presenting cells (APC) and, in a tumoral field, they recognize, process, and present tumor-associated antigens (TAA) complexed to major histocompatibility complex (MHC) molecules, representing a valuable alternative to chemotherapy. Thanks to this mechanism of action the immune system specifically to target and eliminate tumor cells on the basis of expression of specific markers on their surface.

1.4.1 Chemoimmunotherapy from marine natural products

Chemoimmunotherapy is an emerging treatment option to find and destroy cancerous cells that combines traditional chemotherapy with immunotherapy. The defense against cancerous cells compromises a dynamic and orchestrated interplay of innate and acquired immune response. This process involves three phases and starts with immunosurveillance followed by tumor progression and

escape. Although the field of immunotherapy is still growing, the discovery of immunomodulatory NPs able to stimulate the innate immunity cells represent the new frontier for tumor therapy. In this context, small molecules from marine sources, they are able not only to induce unconventional DC maturation and in vivo antigen-specific immunization, but they can also recognize and bind TAA to reduce immune suppression in the tumor environment or enhance the activation of cytotoxic lymphocyte responses to the cancer.[30,31] (FIGURE 7)

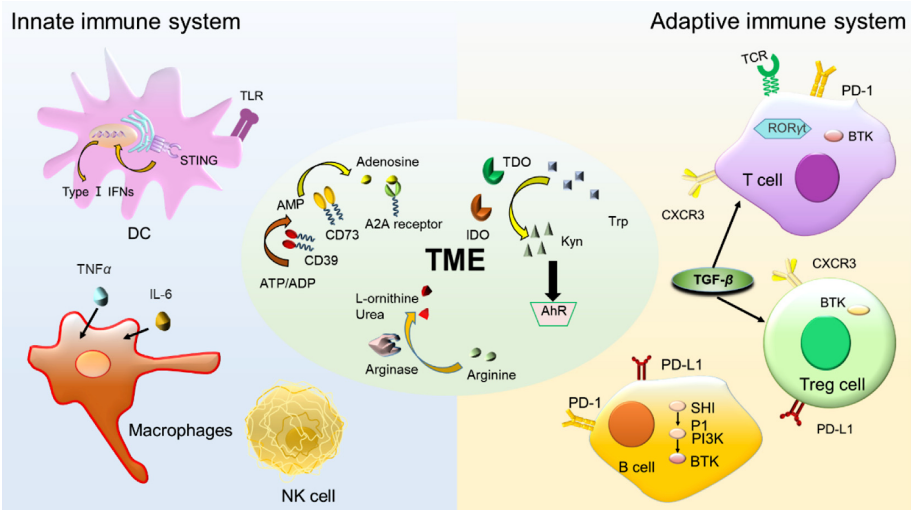

Figure 7: Overview of immune targets related to innate immune system, adaptive immune system, and tumor microenvironment (TME) [31]

Therefore, small molecule-based immune therapies represent an excellent source for the development of new candidate drugs. For example: Bryostatin-1, lactone found in marine Bryozoan, *Bugula neritina,* also showed antitumor and immunomodulatory activity and it is currently in phase 2 of clinical trial. *In vitro* assays displayed cytotoxic effects toward several leukaemia and solid tumor lines;[32] Lissoclibadin 2, a trimeric compound isolated from the tunicate *Lissoclinum cf. badium*, presented several inhibition activities, efficient against human colon tumour cells DLD-1 and HCT116, breast tumour cells MDA-MB-

231, renal tumour cells ACHN and non-small-cell lung tumour cells NCI-H460. [33](FIGURE 8)

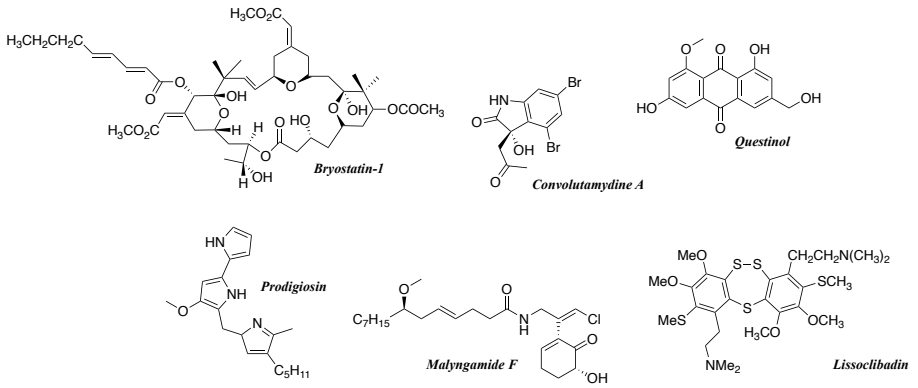

Figure 8: Examples of immunomodulatory Marine Natural Products (MNPs)[2,32–35]

1.4.2 Immunogenic Cell Death (ICD)

Chemotherapeutic agents stimulate both the innate and adaptive arms of the immune system through several modalities. Among the indirect ways of immune cell stimulation, some cytotoxic drugs have been shown to induce an immunogenic type of cell death in tumor cells. Immunogenic Cell Death (ICD) is any type of cell death eliciting an immune response. Both accidental cell death and regulated cell death can result in immune response. ICD represents a mechanism of enhancing T cell-driven response against tumor cells, it depends on the presence and the susceptibility to the activation of Dendritic Cells (DCs) in the TME. In detail, dying cells' exposure or release of several molecules, such as damage-associated molecular patterns (DAMPs), are able to activate the diverse components of the immune system, among which DCs.[36] A canonical example: calreticulin (CRT), a calcium-binding chaperone, expression on the surface of dying cells is considered a clear signal associated to ICD. CRT translocation to the cell surface has been linked with sensitization to the induction of apoptosis of cancer cells after treatment with specific chemotherapeutics. CRT increase on cell surface, translocating from the endoplasmic reticulum (ER), this, grant a sort of

"eat me", stimulating the adaptive immune response known as "immunogenic cell death". Once, CRT gets translocated to the pre-apoptotic tumor cell surface allows the recognition by antigen presenting cells such as DC and the phagocytosis of dying cells. The emission of DAMPs in the course of ICD and their binding to specific pattern recognition receptors (PRRs) expressed by DCs initiates a molecular cascade pathway that activate both innate and adaptive immune response. Now days, just few conventional drugs have been successfully employed as ICD inducers in the pharmacological field, such as Tigilanol tiglate (EBC-46), a novel small molecule belonging to the veterinary pharmaceutical for intratumorally treatment of canine mast cell tumours (MCTs); actually, in Phase II of clinical trials against advanced soft tissue sarcoma.[37,38] (FIGURE 9) (ClinicalTrials.gov ID NCT05755113) Therefore, the identification of new ICD agents is a promising research field.[39,40]

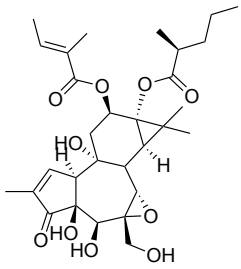

Figure 9: Tigilanol tiglate

1.4.3 Innate immunity and innate immune cells

Immunity has been defined as the ability to resist infections against bacteria or viruses, but also against everything that is recognized by the organism as "not-self", generally called antigen. The immune system is a complex network made up of special cells and proteins that actively fight infections. The immunity system can be sorted in two categories, based on two different forms of defense, which are closely correlated:[41]

- Innate immunity
- Adaptive immunity

The innate immune system response is activated by chemical properties of the antigen, it depends only on the nature of the foreign antigen and the host resistance to a particular antigen is not enhanced by repeated exposure (lack of memory).[42] On the other side the adaptive immune system is able to distinguish structures belonging to the organism (self) and extraneous potentially dangerous structures (not-self). Its response is split in turn in humoral response and cellular response. The humoral response is mediated by lymphocytes B cells and, depending on the nature of the antigen, can need the costimulatory signals of lymphocytes T helper cells (Th cells) or can go forward in a way independent of T helper cells.[43] The cellular response is mediated by the activation of naïve T cells as a result of the recognition of pathogen bound to major histocompatibility complex (MHC) molecules and costimulatory signals from antigen presenting cells (APC), like dendritic cells (DCs) and macrophages. Differently from innate immunity, the peculiarity of the adaptive immune reaction is the specificity of antigen recognition and memory.

1.4.3.1 Dendritic cells (DCs)

Dendritic cells (DCs), specialized antigen presenting cells (APCs), are known as sentinels of the immune system and play a central role in initiating and/or regulating immune responses. DCs were discovered by Ralph Steinman in 1973 and constitute about 1% of mononuclear cell compartments. DCs are found in almost all tissues, mostly in skin, lung, stomach and intestine.[44,45] They reside in peripheral tissue in an immature stage and are specialized in recognizing invading pathogens or antigens. One of the biggest experimental troubles resulted in the low concentration of DCs in tissues and their complex incubation. A general practice to solve this difficulty is to use monocytes as source of DCs because they

can differentiate into dendritic cells (MoDCs) in presence of an inflammatory stimulus preserving the mains APCs' features.[46]

In presence of stimuli or 'danger signals', DCs uptake antigens and go through a maturation process inducing their migration to lymphoid organs. The progression in the maturation state of DCs population involve both changes of the expression of surface receptors and their ability to interact with the environment and surrounding cells. Maturation signals can be exogenous, mediated by activation of pattern recognition receptors (PRRs), or endogenous, mediated by inflammatory molecules (TNF-α, IL- 1, IL-6 and IFN-α), released by damaged tissues or by cells of the immunocompetent system.[47]

The main differences between mature and immature DCs are:

- Inclination to capture antigens
- Production of cytokines
- Ability to antigenic presentation

During their maturation DCs overexpress some chemokines, costimulatory molecules and surface receptors that assist DCs migration to lymphoid tissues and mediate the interaction between DCs and T cells promoting a transient cluster and allowing DCs to match the appropriated T cell receptor (TCR). For this reason, DCs are considered a link between innate and adaptive immune systems. Thanks to the clear differences between immature and mature DCs and the real opportunities to monitor the maturation processes through the evaluation of their phenotypic markers, they can be an excellent tool to estimate the ability of some substances to act as immunomodulatory agents. Immunodulation represents a modulation in the immune system that can turn out in induction, expression, amplification and inhibition of immune response are therefore therapeutic. In this contest, PRRs represents specific targets as they can be 'exploited' by their natural ligands, small organic molecules, in order to trigger immune defense and modulate it to provide adequate protection and to induce immune responses against cancer and infectious diseases. Recently, there has been an increased

interest by the scientific community in searching compounds, such as small molecules from the sea, that are able to modulate the immune response since these molecules have potential applications in the fields of immunopharmacology and oncotherapy.[48]

1.4.3.1.1 Dectin-1

Dectin-1 is one of the most studied and characterized C-type lectin receptors (CLRs). The protein is mainly expressed on myeloid cells, including monocytes, macrophages, DCs and neutrophils. This receptor is best known for its ability to bind β-1,3 glucans, (FIGURE 10) commonly present on fungal cell walls.[49,50]

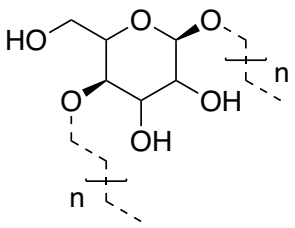

Figure 10: β-1,3-glucans

Several other endogenous ligands, including glycosylated immunoglobulins and galectins, have been recognized for this receptor. The recognition of the ligand by Dectin-1 can trigger and regulate numerous cellular responses, including phagocytosis, autophagy, DC maturation, cytokines and chemokines production. In addition to anti-fungal immunity, there are emerging evidences that Dectin-1 plays a much wider role in immunity, with the ability to recognize other types of pathogens including *Mycobacterium tuberculosis* and *Leishmania infantum*. [51]
Dectin-1 is involved in the regulation of autoimmune diseases, such as arthritis and colitis, thanks to its ability to control excessive inflammation induced by pathogenic fungi and it also performs an important function in the field of anti-cancer immunity. [52,53]. Recently, the receptor Dectin-1 showed a significative role

in the framework of neurodegenerative disease. Knockout of Dectin-1, expressed on microglia, improve neuroinflammation, cognitive function, and neurological damage in $A\beta_{42}$-infused mice; Aβ directly binds to Dectin-1 to initiate Syk/NF-κB signaling and induce inflammatory cytokines. These results suggest the important role of microglia Dectin-1 as a new direct receptor for Aβ in microglial activation and supply a potential therapeutic strategy for neuroinflammation in AD.[54] All this, underlining the crucial importance linked to the research and development of new Dectin-1 ligands, in the pharmacological field.

1.4.3.1.2 Triggering receptor expressed on myeloid cells (TREM-2)

Triggering receptor expressed on myeloid cells-2 (TREM2) is an extracellular innate immune receptor expressed on myeloid lineage cells such as dendritic cells (DCs) and resident tissue macrophages as microglia.[55] Loss-of-function variants of microglial TREM2 are associated with altered microglial responses to β-Amyloids (Aβ) and increased Alzheimer's diseases (AD) risk. Indeed, further evidence for the association of TREM2 in AD is that TREM2 protein levels were found elevated in post-mortem temporal brain tissue taken from AD patients; suggesting this innate immune receptor as a useful therapeutic target. [56] TREM2 makes up part of a receptor complex which binds ligands and initiates signaling; therefore, determining which ligands bind this receptor may help understand the function of TREM2 in microglia.[57]

The identification of endogenous TREM2 ligands is at present at a standstill, in fact TREM2 is commonly referred to as an "orphan receptor". Therefore, several studies have suggested that TREM2 binds anionic ligands, including molecules that are important in AD, such as mycolic acid derivatives and amino phospholipids, such as phosphatidylserine (PS) and phosphatidylethanolamine, (FIGURE 11) that are able to trigger TREM2 signaling in apoptotic cells and macrophages.[55,58]

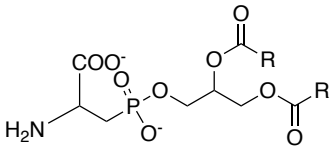

Figure 11: Phosphatidyl serine (R: alkyl chains)

In recent years, ICB-CNR laboratory where I carried out my doctoral research has developed a new synthetic naturally inspired glycolipid, Sulfavant A, (FIGURE 12) which is the first synthetic small molecule ligand of TREM2. The receptor engagement triggers an unconventional maturation of (DCs) with the differentiation of DC towards a novel homeo- stasis-determining phenotype (homeDCs), leading to upregulation of the Major Histocompatibility Complex class II (MHC Class II) and costimulatory molecules (CD83, CD86, DC54) without release of T helper type 1 (Th1) or 2 (Th2) cytokines.[59,60]

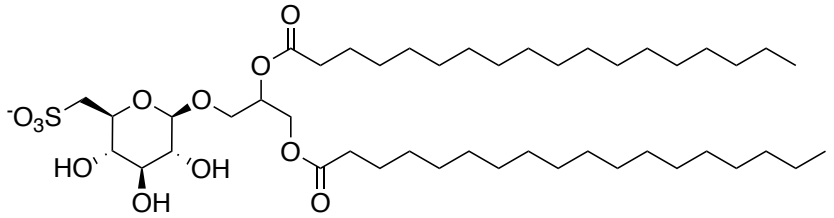

Figure 12: Sulfavant A

1.5 Aim of the work

This PhD work thesis was focused on the identification of bioactive small molecules, potentially able to activate the innate immune system, from marine sources through the use of advanced chromatographic techniques, as well as spectroscopic and spectrometric techniques. This research activities can be framed as basic drug discovery research to find new potential lead compounds for the development of cosmeceuticals and drugs. Bioactive samples were identified from

microalgae and marine invertebrate. In particular, immunotherapeutic candidates were selected by evaluating their chemotherapy potential as ICD induce and the potential interactions between them and two innate immune system receptors: Dectin-1 and TREM2. For what concern the cosmeceuticals applications, the work aimed to investigate the potential application of three microalgal extracts and their enriched fractions. In this regard, the study provided the evaluation of the anti-oxidant activities and the assessment of the investigation of the metabolites involved in this kind of activities.

2) MATERIALS AND METHODS

2.1 General experimental procedures

All the samples described were monitored by thin layer chromatography (TLC) using $Ce(SO_4)_2$ and UV lamp (254nm) as visualizing agents and were analyzed, for structure elucidation, by mono and bi-dimensional NMR on Bruker DRX 600 MHz spectrometer equipped with a TXI CryoProbe (Bruker Bio-Spin, Fällanden, Swiss) and Bruker DRX 400 MHz spectrometer equipped with a TXI CryoProbe (Bruker Bio-Spin, Fällanden, Swiss). The mass spectrometry experiments on a Q-Exactive™ Hy-brid Quadrupole-Orbitrap™ Mass Spectrometer (Thermo Scientific, Waltham, MA, USA) coupled with a 1290 Infinity UPLC System (Agilent Technologies, Santa Clara, CA, USA) with the ESI source. The Q-Exactive™ Hy-brid Quadrupole-Orbitrap™ Mass Spectrometer was operated in data dependent mode with one Full-MS scan at a resolution of 70.000, AGC target $1e^6$, Maximum injection time (IT) 100ms and a scan range of 150-2000 m/z; dd-MS^2 was performed with MS-MS scans at a resolution of 17.500, ACG target $1e^5$, Maximum IT 75ms, isolation window 1.0 m/z, stepped normalize collision energy (NCE) 25,35,40 and a scan range of 70-1500 m/z.

2.2 Bioassay-guided approach

2.2.1 Methanolic extraction

Freeze-dried marine organisms are extracted with methanol (Merk Life Science S.r.l., Milan, Italy) using a tissue homogenizer Precellys Evolution equipped with a cooling system Cryolys Evolution (Bertin Italia, Genoa, Italy). The protocol of extraction consisted of a run at 6200 rpm (3 cycles × 30 s), at the temperature of 16 °C to prevent degradation, followed by centrifugation of the sample at 3600 rpm for 10 min at 4 °C. The organic extract was dried in a rotatory evaporator

using a maximum temperature of 24 °C. This raw sample was weighted and aliquoted using methanol-dichloromethane 2:1 (v/v) and dried under a nitrogen flow and kept at −80 °C until further use. [61]

2.2.2 Solid phase extraction (SPE)-HRX

Once obtained the marine crude extract, appling a Solid Phase Extraction (SPE), based on an hydrophobic polystyrene divinyl-benzene CHROMABOND® HRX cartridges (6 mL/500 mg, Macherey-Nagel, Düren, Germany) on a GX-271 ASPEC Gilson apparatus (Gilson Italy, Cinisello, Italy), by using five different eluents: A) H_2O; B H_2O/CH_3OH 1:1; C) CH_3CN/H_2O 7:3; D) CH_3CN; E) CH_2Cl_2/CH_3OH.[34,61,62]

2.2.3 Solid phase extraction (SPE)-HILIC

According to the screening-platform, the HRX fractions are submitted to a second fractionation step based on an SPE protocol using a hydrophilic interaction liquid chromatography cartridge column (CHROMABOND® HILIC, Macherey-Nagel, Düren, Germany) on the automated GX-271 ASPEC apparatus (Gilson Italy, Cinisello, Italy), again, to obtain five further different fractions eluted with: A) THF/n-hexan; B) THF; C) THF/ CH_3OH; D) THF/ CH_3OH; E) CH_3OH.[34,61,62]

2.2.4 Cytotoxic activity

The cytotoxicity, on human melanoma epithelial cell line (A2058), of the crude extract and the fractions and subfractions was evaluated by 3-(4,5-Dimethylthiazol-2-yl)-2,5-Diphenyltetrazolium Bromide (MTT) assay (Applichem A2231), at concentrations of 1, 10 and 100 μg/mL. 48-hours post-treatment, 10 μL of MTT (5 mg/mL) was added in each well and the plate was incubated in the dark at 37 °C. After 3 hours the media was removed and 100 μL of isopropanol was added to the wells and incubated under agitation for 1 hour to

make purple formazan crystals dissolve. The absorbance was measured with microplate reader at a wavelength of 570 nm (TECAN, Life Sciences). All experiments were performed in triplicate and the anti-proliferative activity was calculated as percentage of cell viability from the ratio of the mean absorbance of each sample and mean absorbance of controls.

For what concern the cytotoxic activity of a panel of nine tumor cell lines: CALU-1 (LC1), HCC827 (LC2), CALU-3 (LC3), A2058 (MEL1) A375 (MEL2) MALME-3M (MEL3), JJN-3 (MM1), KMS-12 (MM2), RPMI 8226 (MM3). Each tumor cell line was cultured at the concentration of 1 × 104 in 0.1 mL of medium, in a 96 well plate. The organic fractions were diluted at maximum concentration of 3 mg/mL in DMSO and tested at 5 and 30 µg/mL or 2.5 and 10 µg/mL for HRX and HILIC samples, respectively. Cells with 1% DMSO in 0.1 mL of medium were used as blank. As positive controls Cisplatin, MEK inhibitor, and doxorubicin were all used at the concentration of 100 µM. All conditions were plated in duplicate and cells were incubated for 24 h. For cell lines growing in adherence, the Sulforodamine B (SRB) Assay Kit (Abcam ab235935, Milan, Italy) was performed. After 24 h of treatment, cells were fixed by a fixation solution for 1 h. After 3 washes in H_2O, cells were stained with SRB solution for 15 min and rinsed with washing solution for 4 times. Protein-bound dye was solubilized, and the optical density was determined at 545 nm according to manufacturer instructions. MTS Proliferation Assay Kit (Abcam, ab197010, Milan, Italy) was used for cells growing in suspension. 10 µL MTS (3-(4,5-dimethylthiazol-2-yl)-5-(3-carboxymethoxyphenyl)-2-(4-sulfophenyl)-2H tetrazolium) was added to each well and incubated at 37 ◦C for 4 h. The absorbance was measured at 490 nm. For all the experiments, percent of cytotoxicity was calculated as: [(O.D. vehicle) × (O.D. sample)/O.D. vehicle] × 100. Background correction was carried out by subtracting the O.D. of culture media. [34]

2.2.5 Dendritic cells (D1) Cell Assay

Dendritic cells (D1) cells were maintained in IMDM supplemented with 30% and then in 15% R1- conditioned medium. These cells were plated on an untreated white flat 96-well plate at a density of 1.5 × 104 cell in 0.2 mL complete culture medium and incubated for 24 h after treatment. Compounds were dissolved in MeOH at the maximum concentration of 0.3 mg/mL. Of this solution, 0.05 mL were used to perform the coating of the plate. After 24 h, plates were centrifuged at 300× g for 3 min and washed with staining buffer (SB) (2% FBS; 0.1% sodium azide in PBS). Staining was performed with monoclonal antibody anti MHC-II APC, CD80 FITC, CD40 PE (REA custom mix from Miltenyi Biotech, Auburn, CA, USA). Before acquisition, each sample was incubated with Propidium iodide solution (Invitrogen, Thermo Fisher Scientific, Waltham, MA, USA) for 5 min at room temperature.

2.2.6 Immunogenic cell death (ICD) assay

Cytotoxicity was tested by the SRB assay kit. Human melanoma A2058 cells were transferred to 96-well plates at a concentration of 1×104 cells per well and treated with Lepadin A, doxorubicin and cisplatin from 2 nM to 100 μM starting from DMSO stock solutions of each compound at concentration of 5 mg/mL. After 24 h, cells were fixed and stained according to manufacturer's instructions. The optical density was determined at 565 nm and cytotoxicity was calculated. Spectrophotometric measurements were performed using EZ Read 2000 microplate readers (Biochrom, Cambridge, United Kingdom).

2.2.7 Anti-oxidant assays

1) DPPH (2,2-Diphenyl-1-Picrylhydrazyl) assay

Methanolic extracts were tested at concentrations of 500, 1000 and 2000 μg mL-1, while enriched fractions at concentrations of 125, 250 and 500 μg mL-1. Dried

extracts and enriched fractions were resuspended in CH_3OH to reach concentrations of 40 and 10 mg mL-1, respectively. The stock DPPH• solution (1 mM) was prepared by diluting 19,72 mg in 50 mL absolute methanol, vortexed and kept in dark at room temperature until its use. In order to reach the concentrations to be tested, 12,5, 25, 50 µL of the sample (extract and enriched fractions) were added to 90 µL of DPPH• stock solution in a plastic cuvette. The final volume of 1 mL was reached with CH_3OH. The mixture was incubated for 30 min in the dark at room temperature and the absorbance was measured at 517 nm by using the UV-VIS spectrophotometer (UV/VIS Spectrophotometer Lambda 35, Perkin Elmer, Waltham, MA, USA). Each measurement was corrected with its background, which was the sample without DPPH• solution. Trolox® was used as a standard. All samples were performed in triplicate. The ability to scavenge DPPH• radical was calculated as the following:

DPPH• inhibition (%) = $[(A0-As)]\ x\ 100\ A0$

where A0 = absorbance of DPPH• and As= absorbance of sample.[63]

2) ABTS (2,2'-Azinobis-3-Ethylbenzothiazoline-6-Sulphonic Acid) assay

To form the ABTS aqueous solution (7 mM), 36 mg of ABTS (CAS No. 30931-67-0, Sigma-Aldrich, St. Louis, MO, USA) were weighted into a 10 mL volumetric flask and mixed with 5 mL of distilled water and dissolved. Distilled water was added to adjust the volume to the mark. Potassium persulfate solution (2,45 mM) was obtained weighting 4,41 mg of potassium persulfate (K2S2O8) (CAS No. 7727-21-1, Sigma-Aldrich, St. Louis, MO, USA) into a 10 mL volumetric flask. 5 mL of distilled water was added, and the final volume of 10 mL was reached with distilled water. To form the ABTS•+ solution, an equal volume of the ABTS aqueous solution (7 mM) and potassium persulfate aqueous solution (2.45 mM) were gently mixed and store in darkness at room temperature for 12 h. The ABTS+• solution was then diluted with methanol (1:49 v/v) to reach

an absorbance of 0.70 ± 0.02 AU, measured in a UV-VIS spectrophotometer (UV/VIS Spectrophotometer Lambda 35, Perkin Elmer, Waltham, MA, USA) at 734 nm. MeOH extracts and enriched fractions were tested at concentrations of 125, 250 and 500 μg mL^{-1}. Dried CH_3OH extracts and enriched fractions were resuspended in CH_3OH to reach concentrations of 10 mg mL^{-1}. To determine AOC, an aliquot of 10 μL of sample, at the desired dilution, was mixed with 990 μL of the ABTS+• solution and kept in the dark for6 min at 30 °C. The absorbance was then read at 734 nm using a UV-VIS spectrophotometer (UV/VIS Spectrophotometer Lambda 35, Perkin Elmer). Methanol and Trolox® were used as negative and positive controls, respectively. A calibration curve of Trolox® was carried out with different concentrations (from 10 nM to 10 mM solutions). The reactions were done in triplicate and the results were calculated according to the equation:

ABTS+• % Inhibition = $[(A0-As)]\ x\ 100\ A0$

where A0= absorbance of ABTS+• and As= absorbance of sample.[64]

3) FRAP (Ferric Reducing Antioxidant Power) assay

In order to make the FRAP reagent, the following solutions were prepared.

- 1 M acetic acid: 5.75 mL of concentrated glacial acetic acid (17.4 M) were added to 94.25 mL of deionized water.
- 1 M sodium hydroxide: 4 g of sodium hydroxide were added to 100 mL of deionized water.
- Acetate buffer (0,1 M, pH 3.6): 3.1 g of sodium acetate anhydrous ($C_2H_3NaO_2$) were weigh ted into a 1 L beaker. 800 mL of distilled water were added, followed by 20 mL of 1 M acetic acid. The pH was adjusted using 1 M acetic acid or 1 M sodium hydroxide. The content was transferred to a 1 L volumetric flask and filled to the mark with distilled water.

- 40 mM HCl: 20 mL of distilled water and 400 µL of 1 M HCl were added and mixed into a volumetric flask. Then, the volume was adjusted to 100 mL with distilled water.
- TPTZ solution (10 mM): 31.3 mg of TPTZ (2,4,6-tris(2- pyridyl)-1,3,5-triazine; C18H12N6) were dissolved into 5 mL of the HCl solution. The final volume of 10 mL was reached with the HCl solution.
- Iron (III) chloride solution (20 mM): 54.1 mg of Iron (III) chloride hexahydrate (FeCl36H2O) were mixed with 5 mL of distilled water. The final volume of 10 mL was reached with distilled water.

The methanolic extracts and the enriched fractions were tested at 500 µg mL^{-1}. The dried extract, and enriched fractions were resuspended in CH_3OH and diluted in CH_3OH to obtain the desired concentrations. Trolox® was used as reference compound. FRAP reagent was prepared immediately prior to the analysis by mixing 0.1 M acetate buffer pH 3.6, TPTZ 10 mM in 40 mM/HCl, and ferric chloride 20 mM/L in ratio 10/1/1. FRAP reagent was heated at 37°C for 5 min. To each well of a 96-well microplate (transparent flat bottom, TPP Techno Plastic Products AG, Trasadingen, Switzerland), 20 µL of sample/Trolox® standard/methanol blank and 180 µL of the preheated FRAP reagent were mixed. The final volume of each well was 200 µL. All the samples were incubated in the dark at 37 °C for 40 min, and then the absorbance was measured at 593 nm using a UV-VIS spectrophotometer (Infinite® M1000 PRO, TECAN, Männedorf, Switzerland). The calibration curve, prepared with Trolox® as standard, was in the range of concentrations from 80 to 480 µM. All the reactions were performed in triplicate. The parameter evaluated to calculate the AOC was the absorbance increase of the sample solution against the absorbance of the blank. The results were expressed as mg Trolox® equivalents (TE) per gram of dried sample (extracts/enriched fractions) (mg TE/g DS).[64]

4) ORAC (Oxygen Radical Antioxidant Capacity) assay

PBS (Phosphate Buffer Saline) (75 mM, pH 7.4), AAPH solution (153 mM) and fluorescein (FL) stock solution (8.16 mM) were prepared as following.

- PBS buffer (75 mM, pH 7.4) was prepared by adding 0.238 g of monosodium phosphate and 1.556 g of disodium phosphate to 100 mL of deionized water and the pH was adjusted to 7.4.
- FL stock solution (8.16 mM) was obtained by weighting 271 mg of fluorescein salt (C20H10Na2O5) into a 100 mL volumetric flask. Then, 50 mL of the phosphate buffer were added and dissolved. The final volume (100 mL) was reached with phosphate buffer.
- AAPH solution (153 mM) was prepared by weighting 415 mg of 2,2′-Azobis (2- methylpropionamidine) dihydrochloride (AAPH; C8H20Cl2N6) into a 10 mL volumetric flask. Subsequently, 5 mL of the PBS were added and dissolved. The final volume of 10 mL was reached with PBS. For a 1:100 v/v dilution, 100 µL of FL stock solution were pipetted into 9.9 mL of PBS and vortex. Then, 10 µL of this solution (81.6 µM) were diluted into 9.99 mL (1:1000 v/v) of PBS to obtain a working concentration (81.6 nM) of FL solution. The MeOH extracts and the enriched fractions were tested at a concentration of 2000 and 500 µg mL- 1, respectively. The dried extracts and enriched fractions were resuspended in MeOH to reach a concentration of 10 mg mL-1 and then diluted in PBS to obtain the desired concentrations. 25 µL of sample/Trolox® standard/PBS blank was mixed with 150 µL of FL solution (81.6 nM) into each well of a black flat-bottom 96-well microplate. The microplate underwent 10-min incubation at 37 °C in the dark on a plate shaker at 20 rpm. Then, 25 µL of AAPH (153mM) were added into each well to reach a final volume of 200 µL. The fluorescence measurements of each well were immediately carried out at 37 °C every minute for 35 min using a microplate fluorometer (Infinite® M1000 PRO, TECAN, Männedorf, Switzerland) at the excitation and emission wavelengths of

495 and 515 nm, respectively. A calibration curve of Trolox® was carried out with different concentrations (from 5 to 50 µM solutions). The ORAC values were reported as micrograms of Trolox® equivalent (TE) per gram of dried sample (extracts/ enriched fractions) (µg TE/g DS).[65]

2.3 Anti-oxidant activity

2.3.1 Biomasses

The freeze-dried biomasses of *Isochrysis galbana,* and *Tetraselmis chuii* were purchased from Phytobloom Necton (Portugal) (https://phytobloom.com/cosmetics/). The freeze-dried biomass of *Cyclotella cryptica* was cultivated at the Institute of Biomolecular Chemistry of National Research Council in Pozzuoli (CNR-ICB). *Cyclotella cryptica* (CCMP 331) was purchased from National Center for Marine Algae and Microbiota (Bigelow Laboratory for Ocean Sciences, East Boothbay, ME, USA) and was maintained in an F/2 medium. *C. cryptica* was grown at 20 ± 2 °C in 2 L of polycarbonate carboy in 2 L of pre-filtered sterile (0.22 µm) f/2 medium at an initial concentration of 1 × 10^4 cells mL^{-1}. Cultures were gently bubbled with sterile air. In heterotrophic conditions, cultures were incubated in the dark and f/2 medium was supplemented with two pulses of 1g/L glucose for each one, at day 0 and day 7. Macronutrient levels were maintained at high regimes, adding nitrates ($NaNO_3$, 882 µmol L^{-1}) and phosphates ($NaH_2PO_4 \cdot H_2O$, 36 µmol L^{-1}) every 48 h, and silicate ($Na_2SiO_3 \cdot 9H_2O$, 107 µmol L^{-1}) every 24 h. Cell growth was monitored using a microscope (Axio VertA1, Carl Zeiss, magnification of 20X, Milan, Italy) and a Bürker counting chamber (depth 0.100 mm, Merck, Leuven, Belgium).

2.3.2 Extraction and fraction of *Tetraselmis chuii*

Freeze-dried *Tetraselmis chuii* was extracted as described in section 2.2.1, to obtain 546.22 mg. About 60 mg of raw extract was subjected to SPE-HRX

(section 2.2.2) to obtain 5 enriched fractions: A (19.47 mg), B (1.51 mg), C (4.43 mg), D (3.65 mg) and E (10.1 mg).

2.3.3 Extraction and fraction of *Cyclotella cryptica*

Freeze-dried *Cyclotela cryptica* was extracted as described in section 2.2.1, to obtain 545.87 mg. About 60 mg of raw extract was subjected to SPE-HRX (section 2.2.2) to obtain 5 enriched fractions: A (16.53 mg), B (1.7 mg), C (3.06 mg), D (1.88 mg) and E (12.71 mg).

2.3.4 Extraction and fraction of *Isocrysis galbana*

Freeze-dried *Isocrysis galbana* was extracted as described in section 2.2.1, to obtain 441.31 mg. About 60 mg of raw extract was subjected to SPE-HRX (section 2.2.2) to obtain 5 enriched fractions: A (13.07 mg), B (3.57 mg), C (3.18 mg), D (2.45 mg) and E (5.81 mg).

2.4 Immunogenic cell death (ICD) and cytotoxic activity

2.4.6 Extraction and fractionation of *Clavelina lepadiformis*

The ascidian *Clavelina lepadiformis sp. B* (150g wet weight) was lyophilized to give 17g of brown powder (dry weight). This material was extracted to obtain 6g of crude extract (section 2.2.1). 150 mg of raw extract were subjected to SPE-HRX (2.2.2) to obtain 5 enriched fractions: A (90 mg), B (15.7 mg), C (6.5 mg), D (8.2 mg) and E (2.3 mg). The HRX fraction C (6.5 mg) was subjected to SPE-HILIC (2.2.3) that led to obtain five new fractions A (0.91 mg), B (0.41 mg), C (0.79 mg), D (0.1 mg) and E (2.6 mg) respectively.

2.4.6.1 Scale up for *Clavelina lepadiformis*

Once identified the HILIC-SPE fraction C (0.79 mg) as the fraction of interest, to collect a greater amount of the pure compound, for spectroscopic and bioactivity analysis, the raw extract (370 mg) was once again fractionated by Sephadex LH-20. The elution step, using CH_3OH as eluent, lead to obtain 49 mg of a crude sample containing the compound of interest. The extract was fractionated on silica column starting with a gradient of petroleum ether/diethyl ether followed with chloroform and chloroform/methanol gradient that led to the elution of the fraction of interest in $CHCl_3$/ CH_3OH 9:1 (*v/v*) (2.8mg), containing the target compound. This silica gel fraction 2.8 mg was further purified on an HPLC column Luna NH_2 (250 × 4.6 mm, 5 µm) in isocratic condition with a mixture of $CH_3CH(OH)CH_3$/ $CH_3(CH_2)_4CH_3$ 5:95 *(v/v)* and 1% of NH_4OH at a flow of 1 mL/min. The pure compound (0.3mg) was analyzed by mono and bidimensional NMR and HRESI-MSMS with the ESI source in positive mode.

2.4.1 Extraction and fractionation of *Cacospongia mollior*

The sponge *Cacospongia mollior* was collected in the Gulf of Naples, Porto Paone (40°47′N, 14°9′E) at depths ranging from 15 to 17 meters (Esposito et al., 2024). *Cacospongia mollior* (35 g wet weight) was lyophilized to give 6.40 g of brown powder (dry weight) and extracted (section 2.2.1). About 112 mg of raw extract was subjected to SPE-HRX (section 2.2.2) to obtain 5 enriched fractions: A (35.25 mg), B (3.43 mg), C (3.18 mg), D (6.49 mg) and E (6.69 mg). Fraction D (6.49 mg) was subjected to further HILIC-SPE (section 2.2.3) fractionation to give other five fractions A (2.89 mg), B (0.55 mg), C (0.57 mg), D (0.46 mg), E (0.53 mg). The HILIC-fraction C (0.57 mg), was analyzed, for structure elucidation, by mono and bi-dimensional NMR and HRESI-MSMS by flow injection analysis (FIA), with the ESI source in negative mode.

2.4.2 Extraction and fractionation of *Haliclona vansoesti*

The sponge *Haliclona Vansoesti* was collected in the Strait of Messina, Faro Lake (80 g wet weight) was lyophilized to give 7 g of brown powder (dry weight) and extracted (section 2.2.1). About 1.2 g of raw extract was obtained and about 100mg were subjected to SPE-HRX (section 2.2.2) to obtain 5 enriched fractions: A (44.2 mg), B (14.8 mg), C (10.6 mg), D (2.1 mg) and E (10.9 mg). After cytotoxic tests and preliminary spectroscopic analysis, fraction D was submitted to further HILIC-SPE (section 2.2.3) fractionation, to obtain five different fractions A (0.8 mg), B (0.2 mg), C (0.1 mg), D (0.2 mg), E (0.1 mg). Both fractions C and D were analyzed, for structure elucidation, by mono and bi-dimensional NMR and HRESI-LC-MS/MSMS with the ESI source in negative mode on a Luna C18 column (150x5 mm, 5µm), using as elution method H_2O and CH_3OH as solvent A and B respectively, starting with an isocratic condition 10:90 A/B (*v/v*) for 15 minutes, followed by gradient condition to 100% of B in 10 minutes, with a flow rate of 0.8 mL/min.

2.5 Chemical approach

2.5.1 Sulphur filtering: sulphated and sukphonated compounds

2.5.1.1 Modified Bligh and Dyer extraction

After methanolic extraction, as described in section 2.2.1, the pellet was further extracted with a modified Bligh and Dyer protocol: it was added on the pellet CH_2Cl_2/CH_3OH 1:2, sonicate. To this solution 0.8 ml H_2O are added to obtain the *ratio* 1:2:0.8. One centrifuges at 3000 g for 5 min 4°C. The organic phase is set aside and unified with the first methanolic extract. The pellet is extracted once

again with $CH_2Cl_2/CH_3OH/H_2O$ 1:2:0.8 sonicated 5', centrifuged at 3000 g for 5 minutes 4°C. The organic phase is unified with the previous ones and we go on with a phase separation with a separating funnel. Observe the following $CH_2Cl_2/CH_3OH/H_2O$ solvent proportions 2:2:0.8 to allow partitioning. The aqueous phase is transferred to another vessel, and the underlying organic phase containing lipids is set aside. The phase separation with a solution $CH_2Cl_2/CH_3OH/H_2O$ 2:2:0.8 is repeated. The upper aqueous phase is removed, and the underlying organic phase is reunited with the previous organic phases, already collected. The organic phase was dried in a rotatory evaporator using a maximum temperature of 24 ◦C. This raw sample was weighted (31.3mg) and aliquoted using methanol-dichloromethane 2:1 (*v/v*). Finally, it was dried under a nitrogen flow and kept at −80 ◦C until further use.[66]

2.5.1.2 Solid Phase Extraction (SPE)-NH_2

The extract was subjected to SPE by using CHROMABOND® NH_2 cartridges (6 mL/500 mg, Macherey-Nagel, Düren, Germany) as follows: the sample is dissolved in 1mL of $CHCl_3/CH_3OH$ 9:1 (*v/v*) and the column in activated through four different steps: 5mL of CH_3OH, 5mL of H_2O, 5mL of HCl 0.1M, 5mL of H_2O and 5mL of CH_3OH, then conditioned with 5mL of $CHCl_3/CH_3OH$ 9:1 (*v/v*). Once loaded the sample on the activated column, the elution gradient allows to obtain four different fractions: A 10mL of $CHCl_3/CH_3OH$ 9:1 (*v/v*); B 10mL of $CHCl_3/CH_3OH$ 8:2 (*v/v*); C 10mL of $CHCl_3/CH_3OH$ 75:25 (*v/v*); D 10mL of $CHCl_3/CH_3OH$ 8:2 (*v/v*) + 100mM CH_3COONH_4+2% NH_3. The last fraction is treated with a solution of KCl 0.9% followed by centrifugation at 3600 rpm for 10 min at 4 ◦C. [67] The distribution of metabolites in the enriched SPE fractions was monitored by thin layer chromatography (TLC) and the plates were burned with a specific reactive, Azure A, to display the presence of sulphur compounds.[68]

2.5.1.3 LC-MS analysis and *MZmine* deconvolution

The extract and the enriched fraction D was analyzed by ^{1}H-NMR and HRESI-MS/LC-MS-MSMS with the ESI source in negative mode using a column Luna C18 (150x2.6 mm, 5µm), with H_2O+NH_4OH/CH_3COOH 0.005% (pH=8) and CH_3OH as solvent A and B respectively, starting with 70:30 A/B (*v/v*) in gradient condition to 100% of B in 30 minutes, with a flow rate of 0.3 mL/min. MZmine 3.9.0 has been used for the deconvolution of raw data. At first, LC-MS raw data were converted by ProteoWizard to generate. mzml data files. [69] After importing the file, mass detection has carried out using following parameters: scan filter, retention time, autorange; ms level filter, all ms levels; polarity, negative; spectrum type, any; scan type (IMS), all scan types; mass detector, exact mass, noise level 1.0E1. Once settled all the parameters for the mass detection, the scatter plot has been obtained setting the following parameters:

- X axis: retention time;
- Y axis, precursor ion m/z;
- Z axis, product ion intensity;
- MS level filter, MSn level ≥ 2;
- Retention time, autorange;
- Product m/z, auto range;
- m/z tolerance, 0.0050 mz or 2 ppm;
- Intensities filtering, number of best fragments 95;
- Diagnostic fragmentation filtering (DFF) for the sulphated group HSO_4^- : m/z 96.958 and for the sulphonated group HSO_3^-: m/z 80.963[70,71]

2.5.1.4 TREM-2 assay

2B4 mouse T cell hybridoma cells stably transfected with enhanced green floruescent protein (eGFP) under consensus sequences of NFAT and human TREM2/DAP12 cDNA then selected by G418 (1 mg/mL) were kindly provided by prof. Marco Colonna from Washington University in St. Louis. Cells were

maintened in RPMI1640 medium (GIBCO) supplemented with 10% of fetal bovine serum (GIBCO) and cultured up to 20 passages (max. confluency $1x10^6$/mL). For the activity assay $2x10^5$ cells were plated in flat 96-well plate in 0.2 mL of medium and incubated overnight. Compounds were dissolved in MeOH and coated in the plate using 0.05 mL of the solution of the molecules at indicated concentration. After overnight incubation reporter cells were assessed by MACSQuant® Analyzer 16 Flow Cytometer (Milteny Biotec) as GFP^+ cells percentage subtracted from background (vehicle control).

2.5.1.5 Extraction and fractionation of selected extracts

2.5.1.5.1 Extraction and fractionation of *Schizotrix*

The cianobacterium (10 g wet weight) was lyophilized to obtain 4 g (dry weight), submitted to the methanolic (2.2.1) and Bligh and Dyer extraction (section 2.5.1.1), to obtain 1.26 g of the final extract. 35.72 mg were submitted to an anionic exchange fractionation on SPE-NH2 support (section 2.5.1.2). This fractionation yielded four enriched fractions: A (17.38 mg), B (3.07 mg), C (2.08 mg), and D (6.89 mg). LC-MS data of extract and the four fractions were submitted to a deconvolution screening according to the section 2.5.1.3.

2.5.1.5.2 Extraction and fractionation of *Alexandrium andersonii*

The dinoflagellate *Alexandrium andersonii* (25 g wet weight) was lyophilized to obtain 1.4 g (dry weight), submitted to the methanolic (2.2.1) and Bligh and Dyer extraction (section 2.5.1.1), to obtain 168 mg of the final extract. 33.93 mg were submitted to an anionic exchange fractionation on SPE-NH2 support (section 2.5.1.2). This fractionation yielded four enriched fractions: A (16.52 mg), B (2.14

mg), C (2.17 mg), and D (3.36 mg). LC-MS data of extract and the four fractions were submitted to a deconvolution screening according to the section 2.5.1.3.

2.5.1.5.3 Extraction and fractionation of *Colpomoenia sp.*

The red alga *Colpomoenia sp.* (210 g wet weight) was lyophilized to obtain 14 g (dry weight), submitted to the methanolic (2.2.1) and Bligh and Dyer extraction (section 2.5.1.1), to obtain 120 mg of the final extract. 19.14 mg were submitted to an anionic exchange fractionation on SPE-NH2 support (section 2.5.1.2). This fractionation yielded four enriched fractions: A (9.23 mg), B (1.78 mg), C (4.39 mg), and D (2.9 mg). LC-MS data of extract and the four fractions were submitted to a deconvolution screening according to the section 2.5.1.3.

2.5.1.5.4 Extraction and fractionation of *Cyclope neritea*

The mollusc *Cyclope neritea* (343 g wet weight) was lyophilized to obtain 210 g (dry weight), submitted to the methanolic (2.2.1) and Bligh and Dyer extraction (section 2.5.1.1), to obtain 14.97 mg were submitted to an anionic exchange fractionation on SPE-NH2 support (section 2.5.1.2). This fractionation yielded four enriched fractions: A (5.4 mg), B (0.3 mg), C (0.88 mg), and D (1.69 mg). LC-MS data of extract and the four fractions were submitted to a deconvolution screening according to the section 2.5.1.3.

2.5.1.6 Extraction and fractionation of *Ophiura ophiura*

The echinoderm *Ophiura ophiura* (131 g wet weight) was lyophilized to obtain 1.3 g (dry weight), submitted to the methanolic (2.2.1) and Bligh and Dyer extraction (section 2.5.1.1) to obtain 150 mg of the extract. 30 mg of the extract was submitted to an anionic exchange fractionation on SPE-NH2 support (section

2.5.1.2). This fractionation yielded four enriched fractions: A (9.15 mg), B (3.19 mg), C (2.64 mg), and D (3.36 mg). LC-MS data of extract and the four fractions were submitted to a deconvolution screening according to the section 2.5.1.3.

2.5.1.6.1 Scale up of *Ophiura ophiura*

Since the extraction and fractionation yields weren't satisfying, to accumulate a greater amount of material for more accurate spectroscopic analysis, the echinoderm *Ophiura ophiura* (495 g, wet weight) was once again lyophilized (237 g) and submitted to a methanolic extraction (section 2.2.1) to obtain 17g of crude extract. The raw extract was subjected to SPE-HRX (section 2.2.2) to obtain 5 fractions, enriched of metabolites of interest: A (10.4 g), B (1.55 g), C (697.8 mg), D (2.1 g) and E (1.72 g). Fraction D was further fractionated on SPE-NH_2 (section 2.5.1.2), as described above, to obtain four fractions: A (98.6 mg), B (6.5 mg), C (12.6 mg) and D (62 mg). After preliminary analyses with ^{1}H-NMR and through MZmine software, with diagnostic product ions (m/z) 96.958 (HSO_4^-), the SPE-NH_2 fraction D (62 g) was subjected to a successive SPE-HILIC, with a little modification in the protocol, described as follows: sample is dissolved in 1 mL of THF/*n*-hexane 50:50 (*v/v*) and the column is activated with 2 mL H_2O and 10 mL THF *n*-hexane 50:50 (v/v). Elution steps led us to obtain four new fractions A (8 mg), B (2 mg), C (36.4 mg) and D (18.9 mg), eluted with: A 10 mL of THF; B 10 mL of THF/ CH_3OH 90:10 *v/v*; C 10 mL THF/ CH_3OH 80:20 *v/v*; D 10 mL o. f CH_3OH 10:90 *v/v* (10 mL). The HILIC fraction B (2 mg) was analyze through mono and bi-dimensional NMR and HRESI-MSMS.[61]

2.5.2 Pyridine-moiety filtering

2.5.2.1 Acetonic extraction

Freeze-dried marine organisms were immersed in Acetone (Merk Life Science S.r.l., Milan, Italy) and submitted to ultrasound vibration for 1 min. Only the

metabolites present in the mantle (external part) were extracted by this procedure. The solvent was removed and the animals were pestle and treated with acetone, to obtain the extract of the internal part. Both were dried in a rotatory evaporator using a maximum temperature of 24 °C. Internal and external extracts were aliquoted using methanol-dichloromethane 2:1 (v/v) and were dried under a nitrogen flow.

2.5.2.2 LC-MS analysis and *MZmine* deconvolution

MZmine 3.9.0 has been used for the deconvolution of raw data. The distribution of metabolites in the acetonic extracts were monitored by ^{1}H-NMR and HRESI-MS/LC-MS-MSMS with the ESI source in positive mode using a column Omega PS C18 (50x2.1 mm, 3µm), with H_2O and CH_3CN as solvent A and B respectively, starting with 80:20 A/B (v/v) in gradient condition to 60:40 A/B (v/v) in 3 minutes, to 30:70 A/B (v/v) in 15 minutes and to 100% of B in 2 minutes, with a flow rate of 0.5 mL/min. LC-MS raw data were converted by ProteoWizard to generate. mzml data files.[69] After importing the file, mass detection has carried out using following parameters: scan filter, retention time, autorange; ms level filter, all ms levels; polarity, negative; spectrum type, any; scan type (IMS), all scan types; mass detector, exact mass, noise level 1.0E3. Once settled all the parameters for the mass detection, the scatter plot has been obtained setting the following parameters:

- X axis: retention time;
- Y axis, precursor ion m/z;
- Z axis, product ion intensity;
- MS level filter, MSn level ≥ 2;
- Retention time, autorange;
- Product m/z, auto range;
- m/z tolerance, 0.0050 mz or 2 ppm;
- Intensities filtering, base peak percentage 15;

- Diagnostic fragmentation filtering (DFF) for the ethylpyridine moiety: m/z 106.05[70,72]

2.5.2.3 Dectin-1 assay

HEK-Blue™ hDectin-1b Cells (SEAP reporter cells) (Invivogen, San Diego, CA, USA) were plated in 96-well plates at 4×10^5 cells/well in 0.2 mL/well of HEK-Blue™ medium (Invivogen, San Diego, CA, USA) and incubated overnight. MeOH was used as solvent to dissolve compounds and by performing the coating of the plate with 0.05 mL of solution of lipids at indicated concentration. Reporter cells activity was assessed after overnight incubation as quantification of secreted alkaline phosphatase (SEAP) released in the medium by reading the optical density (OD) at 655 nm. Zymosan was used as positive control under the same conditions at concentration of 100 μg/mL according to manufacturer's instructions. Quantitative data (ng/mL) were obtained by a standard curve for the SEAP protein.

2.5.2.4 Extraction and fractionation of *Haminoea orbygnana*

The mollusc *Haminoea orbygnana* was collected in the Gulf of Naples, Miseno Lake (three specimens, average length of 2 cm) and the individuals were threated through an acetonic extraction, as described in section 2.6.1, to obtain 30 mg of first external extract, 6.5 mg of second external part and 32 mg of internal extract, that were kept at −80 °C. The result LC-MS data were submitted to a mass deconvolution screening according to the section 2.6.2. All the extracts were purified on silica gel column with a gradient of petroleum spirit and $CH_3CH_2OCH_2CH_3$ to a gradient of $CHCl_3$ and CH_3OH, this led to the elution of the interesting fractions in petroleum spirit/$CH_3CH_2OCH_2CH_3$ 40:60 (*v/v*) (0.6 mg) and $CHCl_3$/CH_3OH 98:2 (*v/v*) (0.4 mg).

2.5.2.4.1 Ion mobility analysis of *Haminoea orbygnana* sonicate

The same LC-MSMS conditions were used for the experiment with Ion mobility spectrometry (IMS). The LC/MS/MS data were acquired on a conventional U(H)PLC system formed from an ACQUITY I-Class LC system (Waters Corporation, Milford, MA), coupled to a Synapt XS Q-ToF mass spectrometer (Waters Corporation, Wilmslow, UK) using positive electrospray ionization (ESI+) at a capillary voltage of 3.0 kV and source temperature of 100 °C with a desolvation gas flow of 600L/h at a temperature of 300 °C and the nebulizer gas flows was set at 6 bar. Data were acquired in data independent mass spectrometry mode (MS^E) generating two discrete and independent interleaved acquisition functions using low collision energy of 4eV and high collision energy 30eV over the m/z range 50−750 Da operating at a mass resolution of 30000, FWHM. The time-of-flight (TOF) mass analyzer of the mass spectrometer was externally calibrated with a Major Mix mixture from m/z 50 to 2000. Leucine Enkephaline (m/z 556.2771 in positive mode) provided the external lock mass and a scan was collected every 200 s using a fixed cone voltage of 40 V.

3) RESULTS AND DISCUSSION

3.1 Anti-oxidant activity

To evaluate the anti-oxidant capability (AOC) and anti-oxidant activity (AOA) were employed four anti-oxidant assays (section 2.2.7):

1) 2,2-Diphenyl-1-picrylhydrazyl (DPPH) assay: in the presence of antioxidant compounds, DPPH• can accept an electron or a hydrogen atom from the antioxidant scavenger molecule, to be converted to a more stable DPPH molecule. As the reduced form of DPPH is pale yellow (due to the picryl group still present), this reaction is accompanied with the color change of the reaction mix.[73] (FIGURE 13)

2) 2,2'-azino-bis(3-ethylbenzothiazoline-6-sulfonic acid (ABTS) assay: the assay measures the ability of antioxidants in the sample to scavenge the radical cation ABTS•+, a blue-green chromophore with maximum absorption at 734 nm to the non-radical ABTS., ABTS•+ may absorb at different wavelengths, namely 645, 734, 815, and 415 nm. However, the wavelength of 734 nm was chosen owing to the reduced interferences and sample turbidity. [73] (FIGURE 13)

3) Ferric ion reducing antioxidant power (FRAP) assay: it is based on a simple redox reaction in which a key oxidant, in the form of an aqueous ferric tripyridyltriazine (Fe3+-TPTZ) salt solution, is reduced by the electron donating (reductive) antioxidants in the reaction mixture. This redox reaction can be followed macroscopically due to the color change. Indeed, the ferric salt solution has a pale-yellow color but when reduced to the ferrous form, this changes to blue, and absorbance at 593 nm increases. Reaction conditions (temperature, pH, reagent and sample volumes,

reaction duration) are fixed. The Fe^{3+} in the reaction mixture is in large excess.[74] (FIGURE 13)

4) Oxygen Radical Absorbance Capacity (ORAC) assay: at controlled temperature the azo compound AAPH is the most used peroxyl radical generator in hydrophilic systems. AAPH undergoes thermal decomposition giving an alkyl radical (RO•) that reacts with molecular oxygen to generate ROO•. The ROO• further reacts with fluorescein resulting in the loss of fluorescence, which can be recorded with a fluorometer. As oxidative degeneration continues, the fluorescent intensity decreases, and this intensity is recorded on average for half an hour after the addition of the azo initiator.[75] (FIGURE 13)

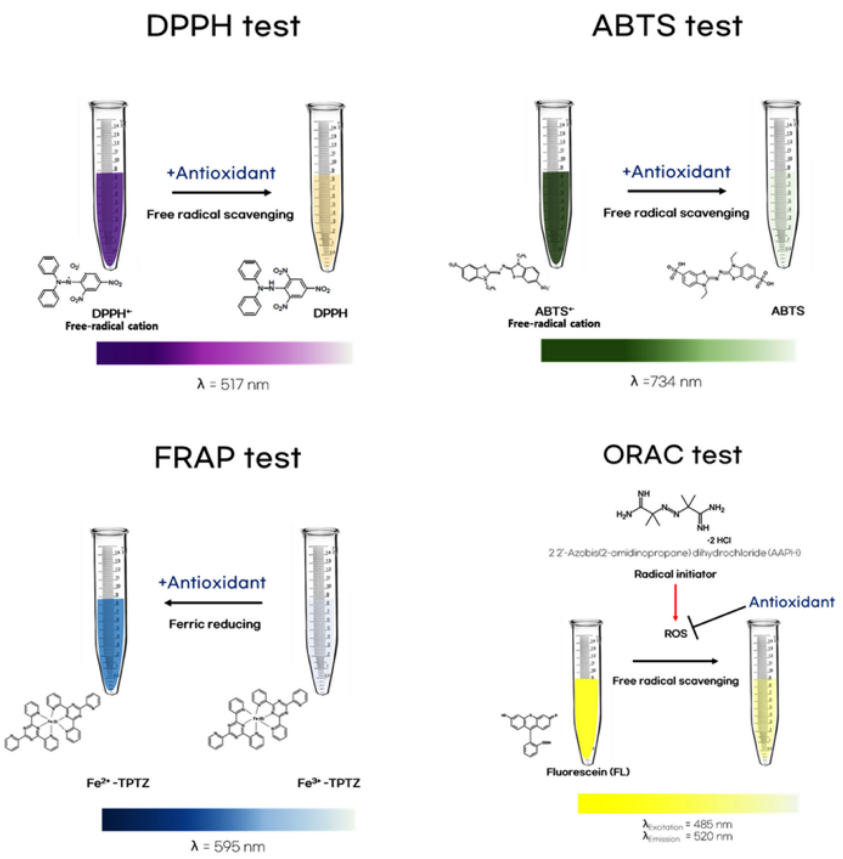

Figure 13: Chemical in vitro anti-oxidant activity [76]

Microalgal extracts have been described as promising source of natural anti-oxidant metabolites and, as described in section 1.3, microalgae are also known to possess immunomodulatory properties. An example, among many described in literature, are immunomodulatory lipids isolated from the diatom *Thalassiosira weissflogii* [34,61,62] this allowed to isolate families of lipids such as α-sulfoquinovosyl diacylglycerols (α-SQDGs) and atypical phosphoglycolipids (PGDGs), which are able to maturation of DCs in the micromolar range, clear evidence of immunomodulation, as described in section (1.4.3.1). [77,78]

So, starting from these assumptions, in this PhD thesis we decided to employ a "bioassay guided platform" (FIGURE 14) to investigate the potential anti-oxidant

capability (AOC) and anti-oxidant activity (AOA) of both methanolic extracts and enriched fractions of three microalgae by the conventional anti-oxidant assays, described above, for the development of cosmeceutical formulations. The investigation of enriched fractions represents an added value in the research of dermo cosmetic ingredients, as most of the studies reported in the literature use crude extracts, this additional step, led to higher relative concentrations of active ingredients in the fractions, thus increasing the chances of a positive response in the biological tests.

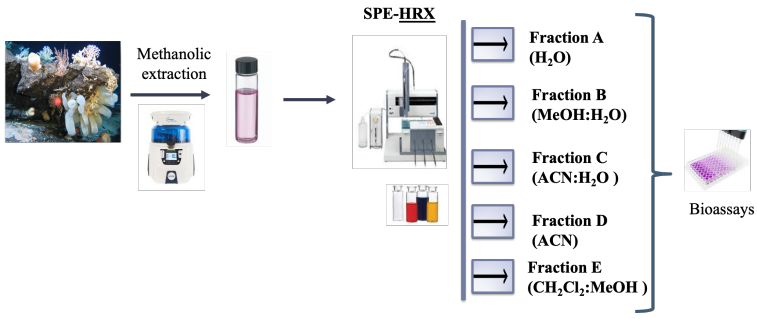

Figure 14: Bioassay-guided screening platform.[34,61,62]

3.1.1 *Tetraselmis chuii*

1) DPPH assay: the methanolic extract was tested at concentrations of 500, 1000, and 2000 µg mL^{-1}, while the enriched fractions at concentrations of 125, 250, and 500 µg mL^{-1}. Surprisingly, the highest DPPH$^{\bullet}$ radical scavenging activity (23,98%) was recorded at the minimum concentration assayed, i.e., 500 µg mL^{-1}. The absence of DPPH$^{\bullet}$ radical inhibition at 2000 µg mL^{-1} is an altered finding due to the presence of interfering compounds in the sample. Taking enrichment into account, lower concentrations of 125, 250 and 500 µg mL^{-1} were tested for the fractions. Figure 48 clearly shows a dose-dependent inhibition of the DPPH$^{\bullet}$ radical for all fractions, excluding the fraction B. Fractions A and C exhibited a

similar DPPH• radical scavenging capacity as the extract at the same concentration of 500µg mL^{-1} (23,59% and 21,79%, respectively, vs. 23,98%). Interestingly, due to the enrichment, the same percentage of inhibited DPPH• in the extract at 500 µg mL^{-1} concentration was detected in fraction B, but at a lower concentration of 125 µg mL^{-1}. Therefore, among the fractions, fraction B was the most promising in DPPH• radical scavenging.[63] (FIGURE 15) (TABLE S1)

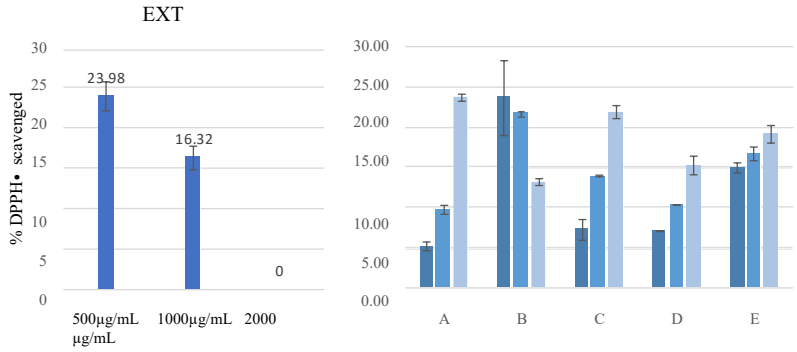

Figure 15: Radical scavenging capacity of T. chuii extract (EXT) (left) and enriched fractions (A-E) (right) on DPPH•. Each value represents the mean ± SD of three replicates.

2) $ABTS^{+\bullet}$ assay: it was performed in concentrations of 125, 250, and 500 µg mL^{-1} were chosen for both methanolic extract and enriched fractions. Lower concentrations were chosen for the methanolic extract than those adopted in the DPPH assay, as the ABTS assay showed higher sensitivity than the DPPH assay in the microalgal strains involved in this screening. The *T.chuii* extract showed a strong $ABTS^{+\bullet}$ radical inhibition ability: at 125 µg mL^{-1} concentration, it scavenged 88,53% $ABTS^{+\bullet}$ radical. Intriguingly, no differences were recorded in the scavenging activity of $ABTS^{+\bullet}$ radicals at higher concentrations, which means that the antioxidant system of the sample, at a concentration of 125 µg mL^{-1}, was already able to inhibit almost all radicals present in the reaction mixture.

In the case of fractions, a dose- dependency in the inhibition of $ABTS^{+\bullet}$ was found only in fractions A, D and E. For all fractions, the scavenging properties at concentrations of 250 and 500 µg mL^{-1} were almost identical, suggesting that cation radicals in the reaction environment were almost all scavenged as early as 250 µg mL^{-1}. However, fraction B and E exerted the highest $ABTS^{+\bullet}$ radical scavenging ability. At 125 µg mL^{-1}, they inhibited 88,32% and 87,4% of $ABTS^{+\bullet}$, respectively.[64] (FIGURE 16) (TABLE S2)

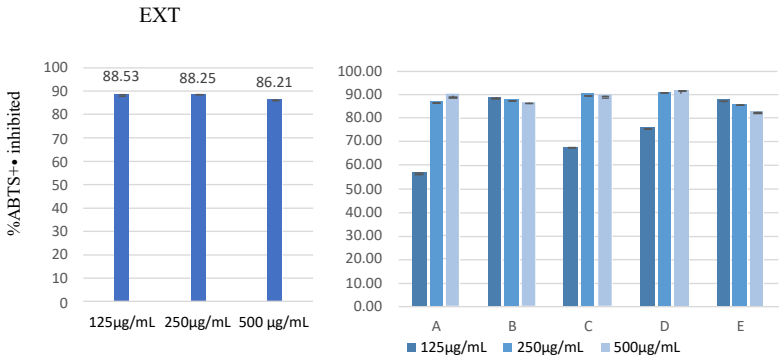

Figure 16: ABTS+• radical scavenging activity of extract (EXT) (left) and enriched fractions (A-E) (right) of T.chuii. Values are given as mean ± SD of three replicates.

3) FRAP assay: the methanolic extract was analyzed at concentrations of 500 and 2000 µg mL-1, and enriched fractions at a concentration of 500 µg mL-1. According to the present results, *T.chuii* extract did not reduced Fe3+ in a dose-dependent manner. At the lowest concentration tested (500 µg mL-1), the extract exhibited a higher FRAP value of 290,58± 0,64 mg TE g-1 DS. As regards enriched fractions, fractions E and B showed ferric reducing capabilities stronger than the extract. Their FRAP values were 353,90 ± 22,32 and 322,98 58 ± 3,93 mg TE g^{-1} DS, respectively. On the other hand, fraction A proved to be the weakest in reducing the ferric cation.[64] (FIGURE 17) (TABLE S3)

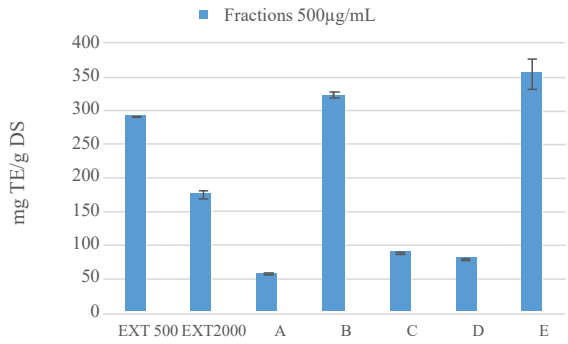

Figure 17: FRAP values (mg TE/ g DS) of extract (EXT) and enriched fractions (A-E) of T.chuii. TE= Trolox Equivalent. DS=Dried Sample. Values are given as mean ± SD of the three replicates

4) ORAC assay: the methanolic extract were tested at a concentration of 2000 µg mL^{-1}, while enriched fractions at a concentration of 500 µg mL^{-1}. The strongest chain breaking capacity against peroxyl radicals was found in fraction C with an ORAC value of 13,16 ± 0,33 mg TE g^{-1} DS. On the other hand, the lowest value was recorded in fraction B (1,05 ± 0,05 mg TE g^{-1} DS). It should be noted that neither the extract nor the fraction E resulted positive to this test.[65] (FIGURE 18) (TABLE S4)

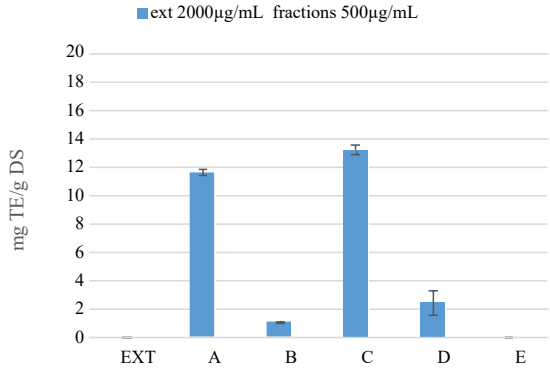

Figure 18: ORAC values (mg TE/g DS) of extract (EXT) and enriched fractions (A-E) of T.chuii TE=Trolox Equivalent. DS=Dried Sample. Each value is expressed as mean ± SD of the three replicates.

3.1.2 *Cyclotella cryptica*

DPPH assay: methanolic extract was tested at concentrations of 500, 1000, and 2000 μg mL^{-1}, while the enriched fractions at concentrations of 125, 250, and 500 μg mL^{-1}. The methanolic extract, inhibiting 23,45 % of DPPH• at a concentration of 500 μg mL^{-1}, showed a modest capacity to scavenge DPPH•. Additionally, there was no increase with increasing concentration. Rather, at a concentration of 2000 μg mL^{-1}, a higher absorbance was recorded, suggesting the presence of interfering compounds which masked any reduction of DPPH•. The interfering molecules were eluted in fraction D. Significative inhibition of the DPPH• radical (58,91%) was recorded in fraction B at the highest concentration tested (500 μg mL^{-1}). In particular, this fraction showed the greatest potency in DPPH• radical scavenging of all samples under investigation.[63] (FIGURE 19) (TABLE S5)

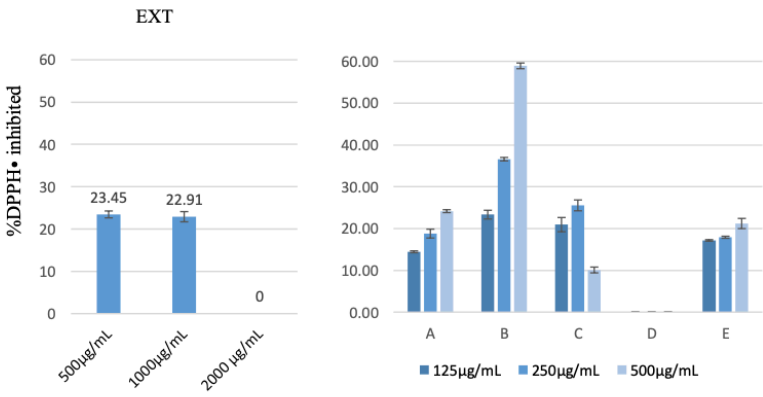

Figure 19: Radical scavenging capacity of C. cryptica extract (EXT) (left) and enriched fractions (A-E) (right) on DPPH•. Each value represents the mean ± SD of three replicates.

1) ABTS+• assay: was performed at concentrations of 125, 250, and 500 µg mL^{-1} were chosen for both methanolic extracts and enriched fractions. According to the obtained results, the MeOH extract showed good and dose-dependent ABTS+• scavenging activity. At the highest concentration tested (500 µg mL-1), it had the ability of scavenging 89,62% of ABTS+• in the reaction mixture. A similar percentage of inhibited ABTS+• was recorded in all fractions, with the exception of fraction A, at the same concentration (500 µg mL^{-1}). However, the strongest antioxidant potential against ABTS+• was performed by fractions D and E, which always inhibited ~90% of ABTS+•, but at a lower concentration of 250 µg mL^{-1}.[64] (FIGURE 20) (TABLE S6)

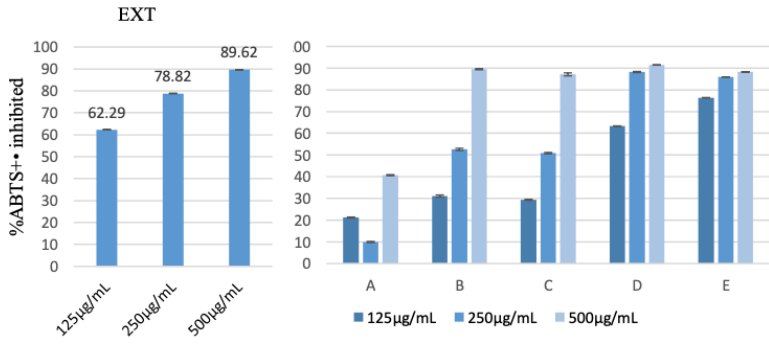

Figure 20: ABTS+• radical scavenging ability of C. cryptica extract (EXT) (left) and enriched fractions (A-E) (right). Values are given as mean ± SD of three replicates.

2) FRAP assay: methanolic extract was analyzed at concentrations of 500 and 2000 µg mL^{-1}, and enriched fractions at a concentration of 500 µg mL^{-1}. In the extract, the results of the present study showed the greatest reducing power (238,83 ± 2,04 mg TE g-1 DS) at the lowest concentration tested (500 µg mL^{-1}). Concerning fractions, the ferric reducing ability was found to increase progressively as the polarity of the extraction solvents decreased. Fraction E, thus, presented the highest FRAP value of 104,14 ± 3,87 mg TE g^{-1} DS.[64] (FIGURE 21) (TABLE S7)

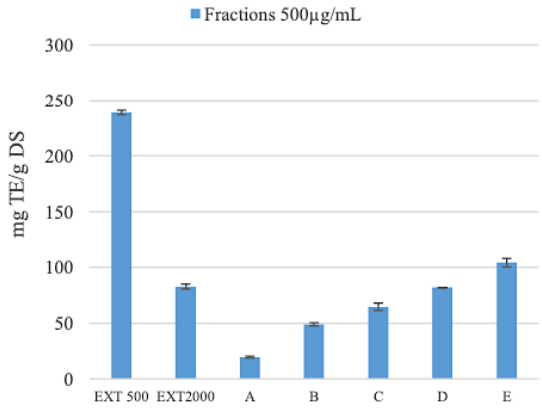

Figure 21: FRAP values (mg TE/g DS) of the extract (EXT) and enriched fractions (A-E) of C. cryptica. TE= Trolox Equivalent. DS=Dried Sample. The extract was assayed at 500 and 2000 µg mL-1 concentrations (EXT500 and EXT2000, respectively). Each value is expressed as mean ± SD of the three replicates.

3) ORAC assay: the methanolic extract was tested at a concentration of 2000 µg mL^{-1}, while enriched fractions at a concentration of 500 µg mL^{-1} The highest chain breaking capacities against peroxyl radicals were detected in fractions C and B, with ORAC values of 19,09 ± 0,82 and 18,61 ± 0,35 mg TE g^{-1} DS, respectively. Fractions A and E, the most and least polar, respectively, showed very similar values (~12 mg TE g^{-1} DS). Finally, the lowest ORAC value was found in the extract, whilst fraction D showed no effectiveness in breaking the radical chain reactions triggered by peroxyl radicals.[65] (FIGURE 22) (TABLE S8)

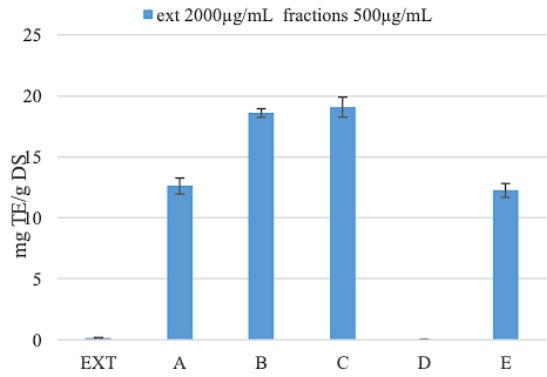

Figure 22:ORAC values (mg TE/g DS) of the extract (EXT) and enriched fractions (A-E) of C. cryptica. TE= Trolox Equivalent. DS=Dried Sample. Results are represented as mean± SD of the three replicates.

3.1.3 *Isocrysis galbana*

1) DPPH assay: methanolic extract was tested at concentrations of 500, 1000, and 2000 µg mL^{-1}, while the enriched fractions atconcentrations of 125, 250, and 500 µg mL^{-1}. The extract displayed a low capacity of DPPH inhibition with only 21,12 % of DPPH scavenged at the concentration of 1000 µg mL^{-1}. The enriched fractions, except fraction D, showed a low and dose dependent DPPH radical scavenging activity. However, fractions B and C, at 500 µg mL^{-1} concentration, showed a good scavenging activity, with fraction C as the major DPPH scavenger (41,37% DPPH• removed). Unexpectedly, in the extract, at 2000 µg mL^{-1} concentration, an increase in absorbance was recorded, thus suggesting the potential presence of interfering compounds, possibly carotenoids. As can easily be noticed in figure 83, the interference was then found in the enriched fraction D, indicating that the potential interfering molecules might have been eluted in this fraction.[63] (FIGURE 23) (TABLE S9)

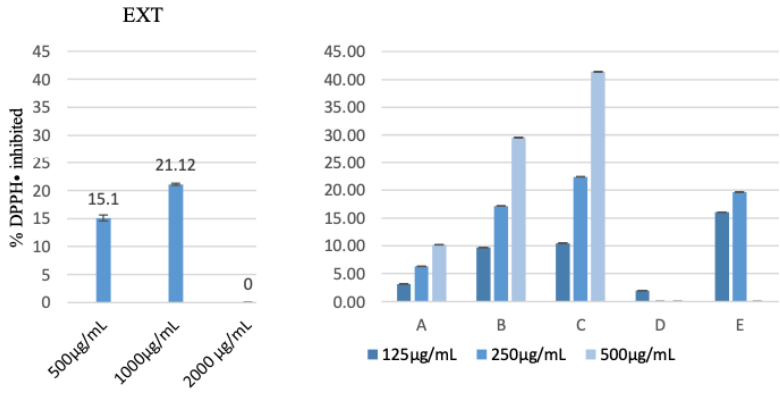

Figure 23:DPPH• radical scavenging activity of the extract (EXT) (left) and enriched fractions (A-E) (right) of I. galbana. Each value represents the mean ± SD of three replicates.

2) ABTS+• assay: it was performed at concentrations of 125, 250, and 500 µg mL^{-1} were chosen for both extract and enriched fractions. Addition of extract concentrations of 125, 250 and 500 µg mL^{-1} resulted in a dose-dependent reduction (54,41%, 84,63% and 91,52%, respectively) of the blue-green radical ABTS+• into the pale blue reduced form. The fractions showed similar antioxidant potential as the extract, except for fractions D and E, which, at a concentration of 125 and 250 µg mL^{-1}, inhibited lower and higher percentages of ABTS+• than the extract, respectively. Overall, our data revealed that fraction E exhibited the strongest antioxidant potency against ABTS+•.[64] (FIGURE 24) (TABLE S10)

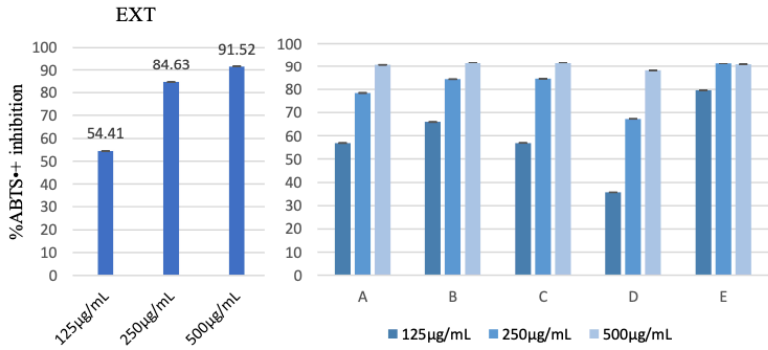

Figure 24: DPPH• radical scavenging activity of the extract (EXT) (left) and enriched fractions (A-E) (right) of I. galbana. Each value represents the mean ± SD of three replicates.

3) FRAP assay: the extract was analyzed at concentrations of 500 and 2000 µg mL^{-1}, and enriched fractions at a concentration of 500 µg mL^{-1}. The extract exhibited a higher reducing power at the lowest concentration tested (500 µg mL^{-1}). Fractions E and D had similar FRAP values and proved to be the most potent in reducing the ferric cation of all fractions and the extract. On the other hand, the lowest reducing potential was found in fraction A.[64] (FIGURE 25) (TABLE S11)

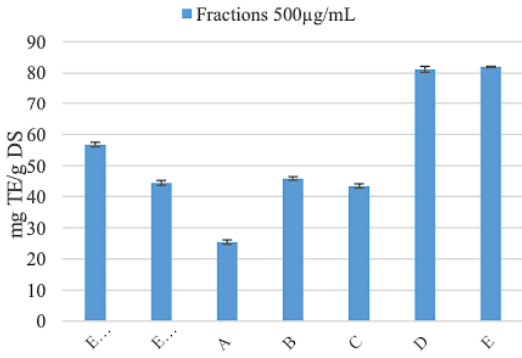

Figure 25: FRAP values (mg TE/g DS) of the extract (EXT) and enriched fractions (A-E) of I. galbana. TE= Trolox Equivalent. DS=Dried Sample. Each value represents the mean± SD of three replicates.

4) ORAC assay: the extract was tested at a concentration of 2000 µg mL^{-1}, while enriched fractions at a concentration of 500 µg mL^{-1}. The ORAC values varied from 25,48 ± 0,52 to 0,62 ± 0,05 mg TE g^{-1} DS. The highest and lowest values were found in fraction B and extract, respectively. For what concern the most polar enriched fractions proved to be more effective in chain breaking against peroxyl radicals formed in the reaction environment.[65] (FIGURE 26) (TABLE S12)

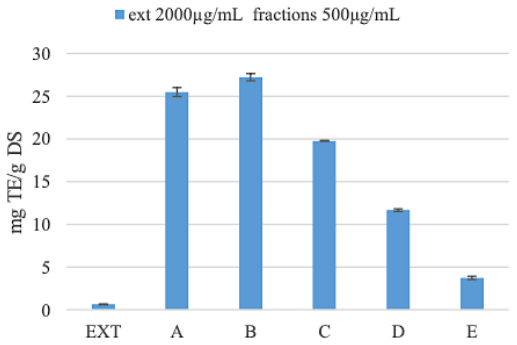

Figure 26: ORAC values (mg TE/g DS) of the extract (EXT) and enriched fractions (A-E) of I. galbana. TE= Trolox Equivalent. DS=Dried Sample. All results represent the mean ± SD of the three replicates.

3.2 Immunogenic cell death (ICD) and cytotoxic activity

With the aim to identify new potential chemotherapy agents, we have applied the bioassay-guided approach. Compared to the case study reported above, in this case the approach was implemented through a second fractionation step. The combination of the sequential hydrophobic and hydrophilic phases determines an orthogonal chromatographic approach that allows quick dereplication of complex mixtures of small organic molecules. (FIGURE 27)

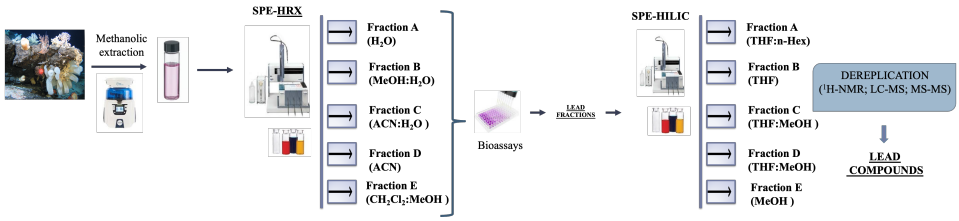

Figure 27: Bioassay-guided screening platform.[34,61,62]

3.2.1 *Clavelina lepadiformis*

The phylum ascidian represents the most abundant class of marine invertebrates, with 3000 species from shallow water to deep sea, already reported. Most secondary metabolites isolated from ascidians stand out for their potential as putative therapeutic agents in the treatment of microbial infections, but ascidians are also recognized because they contain abundant, potently toxic secondary metabolites that are implicated in chemical defense, such as Clavepictine A from *Clavelina picta*.[79,80] In 1991, from the species *Clavelina lepadiformis* collected in the North Sea, a compound with decahydroquinoline alkaloid moiety was isolated: Lepadin A; some years later founded, together with other two analogs, in a flatworm who feed himself with this ascidian.[81,82] More recently, it was reported the isolation of other analogs: the lepadin family, constituted with eleven decahydroquinoline members, was identified from ascidians belonging to the genera *Clavelina*, *Didemnum*, and *Aplidium* as well as their predators.
[83,84] In addition, again from the tunicate *Didemnum,* collected in the Bahamas sea, three new variants Lepadins I–K, differing by the presence of a rare 3-methylthioacrylate ester at C-3, were isolated.[85] Raw extract of the colonial ascidians *Clavelina lepadiformis*, collected from the dock walls of the Fusaro Lake channel and the related five SPE-HRX fractions (sections 2.2.2; 2.4.1) were tested on the panel of cancer cell lines of the bioassay platform (section 2.2.4) (FIGURE 28A) and at the same time, they were used also to treat immature mouse dendritic cells (D1) in the bioassay performed to evaluate the activation (growth factor-dependent assay) (section 2.2.5) (FIGURE 28B). Considering the result of

both cytotoxic and D1 assays, we identified fraction C as the sample of interest, due to the capability to increase the expression of the phenotypic markers at both concentrations 5 and 30 μg, but with a slight level of toxicity. Indeed, during their maturation process Dendritic Cells (DCs) are able to overexpress some surface receptors, such as costimulatory molecules CD80, CD40, and MHC II, that represent phenotypic markers to monitor the maturation process of DCs, highlighting the difference between mature and immature DCs. So, the expression of phenotypic markers can be an excellent tool to estimate the ability of some substances to act as immunomodulatory agents.

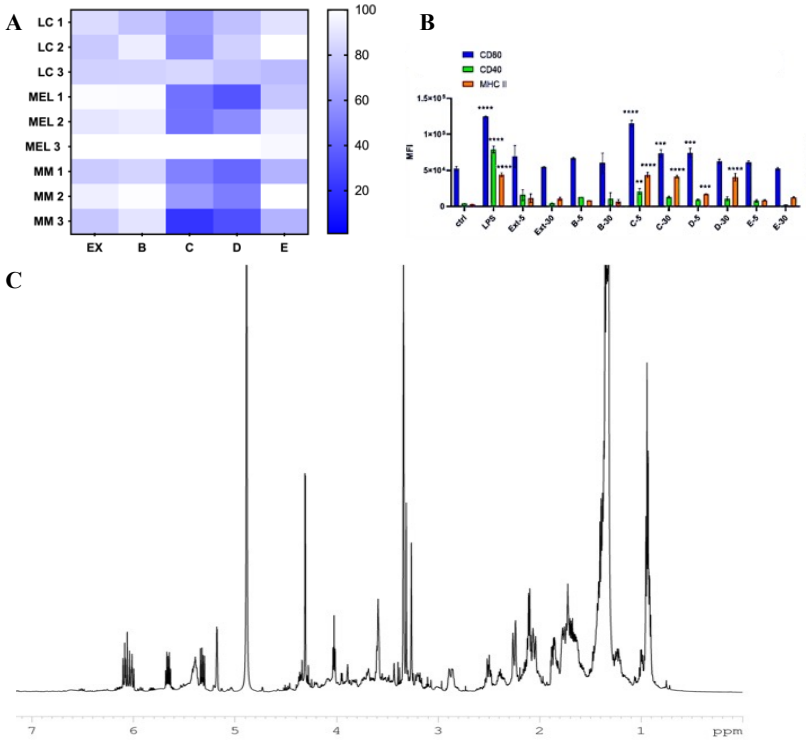

Figure 28: A) Biological screening assay carried out on the panel of nine different cell lines CALU-1 (LC1), HCC827 (LC2), CALU-3 (LC3), A2058 (MEL1) A375 (MEL2) MALME-3M (MEL3), JJN-3 (MM1), KMS-12 (MM2), RPMI 8226 (MM3). (Y axis) treated at 5 and 30 ug/mL (media) with positive controls, total extract (Ext) and HRX-SPE fractions (B–E) of C. lepadiformis. Values reported in the color bar legend on the right indicate the % of viability; B) Surface expression analysis of CD80, CD40, and MHC-II on D1 treated at 5 and 30 ug/mL with the vehicle (Ctrl), LPS

((positive control), extract (Ext) and HRX-SPE of C. lepadiformis. Data are expressed as MFI (mean fluorescence intensity) measured for each marker; C) ^{1}*H NMR of HRX fraction C (600 MHz,* CD_3OD*).*

Therefore, the fraction C was further fractionated on hydrophilic HILIC-SPE (sections 2.2.3; 2.4.1), in five different fractions, that once assayed reported an increase of cytotoxicity against cancer cells and immunomodulatory activity, on D1 cells, at non-toxic concentrations on the new Fraction C. (FIGURE 29) The combination of the two effects is expected to increase the anticancer properties by, both, the role of mature DCs in the generation of anti-tumor activity and the potential release of immunogenic molecules by dying cells.

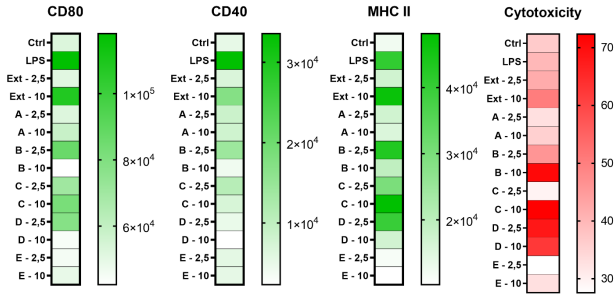

Figure 29: Surface expression analysis of CD80, CD40, and MHC-II, and percentage of vitality on D1 treated at 2.5 and 10 µg/mL with fraction C from the HRX-SPE and fractions A–E from the HILIC- SPE. All data were compared to cells treated with vehicle (Ctrl) or LPS used as positive control. The color bar on the right shows the MFI (mean fluorescence intensity) measured for each marker

Spectroscopic studies of the active HILIC fraction C showed the presence of a predominant metabolite (FIGURE 30), characterized by a structural framework of cis-decahydroquinoline alkaloid, compared to the literature.

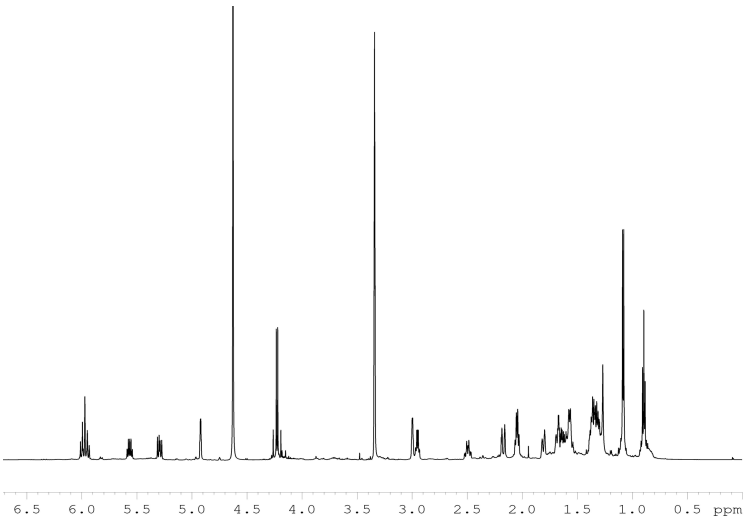

Figure 30: ^{1}H NMR of HILIC fraction C (600 MHz, $CD_3OD/CDCl_3$ 1:1 (v/v)).

^{1}H-NMR data showed the presence of at δ_H 4.23 (2H, AB system, *J*=16.5 Hz) ascribable to the butadienyl system two methyl groups at δ_H 1.10 ppm (3H, d, *J*=6.5 Hz) and at 0.92 ppm (3H, t, *J*=7 Hz), respectively the first on the position C-2 of the chain and the terminal one. A conjugated system of double bonds between δ_H 5.32–5.98 ppm. (4H, dd, *J*=14.5, 10, 8.5, 7.0 Hz) which correlated to each other in the COSY experiment. ^{13}C spectrum confirmed the presence of a C-2 methyl group in the ring; showed the presence of C-3 oxygenated related to the acyloxy group, and the C-5 of the ring substituted with an eight-carbon side chain. (FIGURE S13-S15) HR-ESIMS spectrum showed a major peak at *m/z* 336.2462 for $[M+H]^+$ in agreement with the molecular formula $C_{20}H_{34}NO_3$ (calcd. for *m/z* 336.2533). (FIGURE S16). As showed in TABLE 2, comparing all the data with the literature, structural hypothesis of 2,3,5-trisubstituted cis-decahydroquinoline alkaloid, Lepadin A (FIGURE 31) was confirmed.[86]

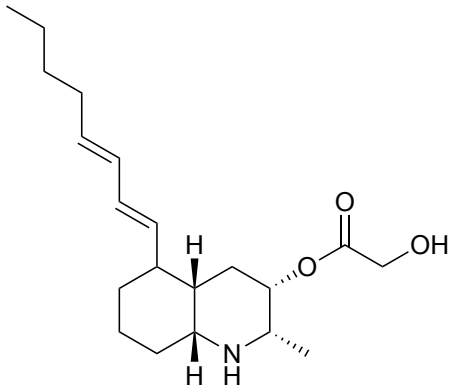

Figure 31: Lepadin A

Table 2: NMR Data[a] of Lepadin A in CD_3OD at 600 MHz.

C	**Type**	**δ_C**	**δ_H, m (*J* in Hz)**
2	CH	56.4	2.98, q (6.0)
3	CH	72.4	4.91, m 1.70, m
4	CH_2	33.3	2.16, dt (15.0;2.0)
4a	CH	39.5	1.38, m
5	CH	41.0	2.57, m
6	CH_2	35.3	1.12, m 1.66, m
7	CH_2	21.4	1.58, m 1.85, m
8	CH_2	32.8	1.65, m
8a	CH	56.0	3.02, s
1’	CH	137.6	5.31, dd (14.5; 8.5)
2’	CH	133.2	6.04, dd (14.5; 10.0)
3’	CH	131.7	5.98, dd (14.5; 10.0)
4’	CH	133.5	5.59, dd (14.5; 7.0)
5’	CH_2	33.1	2.09, q (7.0)
6’	CH_2	23.2	1.40, m
7’	CH_2	32.1	1.37, m
8’	CH_3	14.5	0.92, t (7.0)
1’’	N.D.	N.D.	

2''	CH_2	61.6	4.23, AB system (16.5)
2-Me	CH_3	17.8	1.10, d (6.5)

[a] The structure assignment was obtained by ^1H-^1H COSY, HSQCedited and ^{13}C correlations.

To obtain a major amount and validate the biological activity of Lepadin A, the raw extract was fractionated through size exclusion chromatography (Sephadex LH-20) followed by silica gel column and HPLC fractionation. (section 2.4.1.1) By spectroscopic analysis was confirmed the chemical structure of the metabolite. (FIGURE 32)

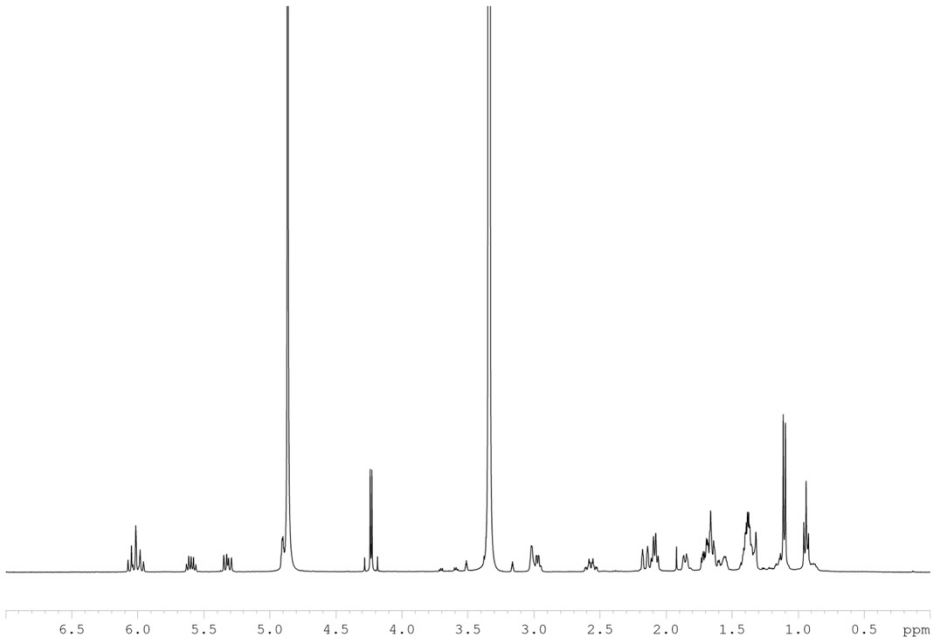

Figure 32: ^1H NMR of Lepadin A (600 MHz, CD_3OD).

So, pure Lepadin A was used to calculate EC_{50} (FIGURE 33A) and IC_{50} (FIGURE 33B) on D1 cells, resulted respectively: 1.64 ± 0.02 µg/mL and 4.20 ± 0.14 µg/mL.

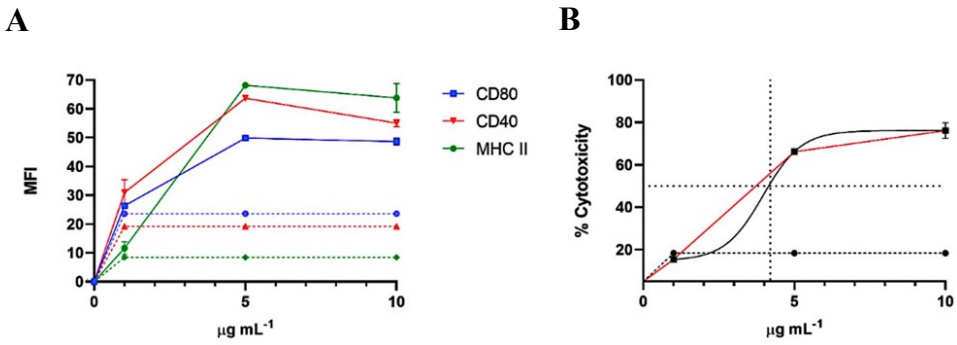

Figure 33: A) Maturation and toxicity on D1 cells induced by the active product purified from the extract of C. lepadiformis. (A) Expression of cell surface markers of D1 cells after treatment with the active molecule from 1 to 10 µg/mL (n = 3). Data are expressed as Mean Fluorescence Intensity (MFI) of CD80, CD40 and MHC-II compared to cells treated only with vehicle (dashed lines) after 24 h; B) Cell viability expressed as percentage of cytotoxicity after stimulation of D1 cells with the active molecule in the same range of concentrations. A nonlinear regression analysis was performed for the estimation of the IC50 value as plotted in the figure.

3.2.1.1 Immunogenic Cell Death activity evaluation for Lepadin A

Biological results made Lepadin A a good candidate as ICD inducer and prompt us to deep in the immune-based anticancer activity. (section 1.4.2) To verify this hypothesis, it was evaluated the exposure of CRT, as ICD marker in human melanoma A2058 cells and the consequent response of monocyte-derived dendritic cells (MoDCs). (section 2.2.6). It was compared the activity of Lepadin A (1) to the chemotherapy drugs doxorubicin (2), a known ICD inducer, and cisplatin (3), which is incapable of triggering translocation of CRT to the surface of dying cells.[87,88]

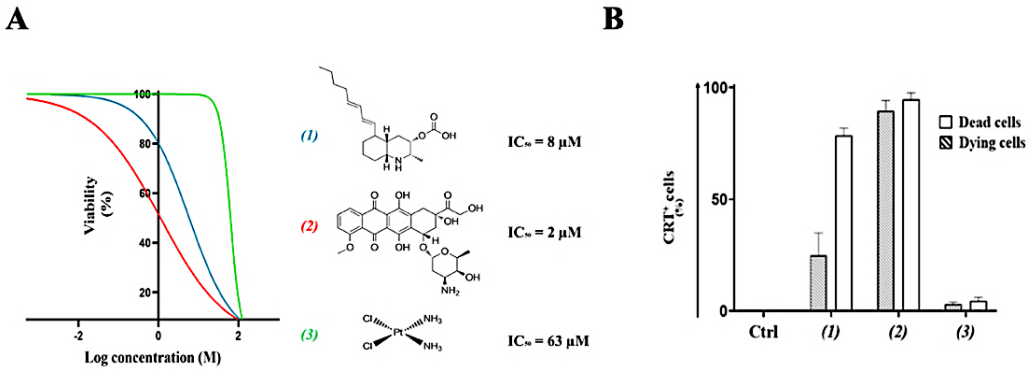

Figure 34: A) Cytotoxic activity of Lepadin A (1), doxorubicin (2) and cisplatin (3) in the concentration range from 2 nM to 100 µM on human A2058 melanoma cells. A nonlinear regression analysis was performed for the estimation of the EC50 (50% of the effective concentration) reported alongside the chemical structures of the tested molecules. B) CRT exposure in A2058 cells treated with Lepadin A (1), doxorubicin (2) and cisplatin (3). Percentage (n = 3) of CRT exposed on the surface of dead and dying cells after 24 h from the addition of compounds 1–3 at the EC50 concentrations. Ctrl = untreated cells.

Significant presence of CRT in the membrane of dying A2058 cells also occurred with doxorubicin (2) (about 90% of the whole population) and Lepadin A (1) (about 40% of the whole population), which is in agreement with the translocation of the protein in an early phase of the anti-cancer mechanism. On the other hand, no signal for CRT was detected after treatment with 63 µM cisplatin (3) despite the intrinsic toxicity of this drug. (FIGURE 34) Starting from these preliminary results, to support the idea of considering Lepadin A a potential ICD inducer and to determinate his role in cancer immunotherapy, it was tested the response of MoDCs from healthy human donors in co-cultures with A2058 cells, treated with Lepadin A, using cells exposed to doxorubricin as positive control. As described in section 1.4.2 chronic exposure of damage-associated molecular patterns (DAMPs) attracts receptors and ligands on dendritic cells (DCs) and activates the maturation process of DCs to transition to a mature phenotype and allowing the antigen presentation, thus stimulating specific T cell responses, evidence of ICD activity.[89] Indeed, biological tests showed that the exposure to Lepadin A allowed

to induced maturation of DCs with several evidences such as release of IL-6, reduction of the immunosuppressive IL-10 and upregulation of the costimulatory molecules, CD86 and CD91. The activity of Lepadin A was comparable to that of doxorubicin, validating the possibility of considering it a good ICD inducer.[90]

3.2.2 *Cacospongia mollior*

Marine sponges of the genus *Cacospongia* (order Dictyoceratida, family Thorectidae) has been reported to produce different bioactive terpenoids; in particular diverse cyclic sesterterpenes, collectively named scalaranes, characterized by a *trans*-fused 6/6/6/6 carbocyclic. Among the wide structural variations, several scalaranes, that have been previously isolated from the genus *Cacospongia* from the Gulf of Naples, contain a heterocyclic five-membered rings, such as lactone, furan, lactam or pyrrole: C_{21}-difuran terpenoid cacospongienone A from *C. scalaris*, manoalide-type sesterterpenoid cacospongionolide from *C. mollior*, and tetracyclic scalarane-type sesterterpenoid scalarin from *C. scalaris*. [91–94] whereas, the group of scalarin-like pyrrolterpenes, molliorin A-E, was reported from *Cacospongia mollior*.[95–97]

The crude extract of the sponge *C. mollior* and its HRX-SPE (sections 2.2.1; 2.4.2) fractions were submitted to biological assays on human melanoma epithelial cell line (A2058). (FIGURE 35A) The Fraction D showed a promising cytotoxic activity with a percentage of cell viability of 65% at 10 µg/mL, a concentration at which it was not toxic to normal cells used as control. (section 2.2.4)

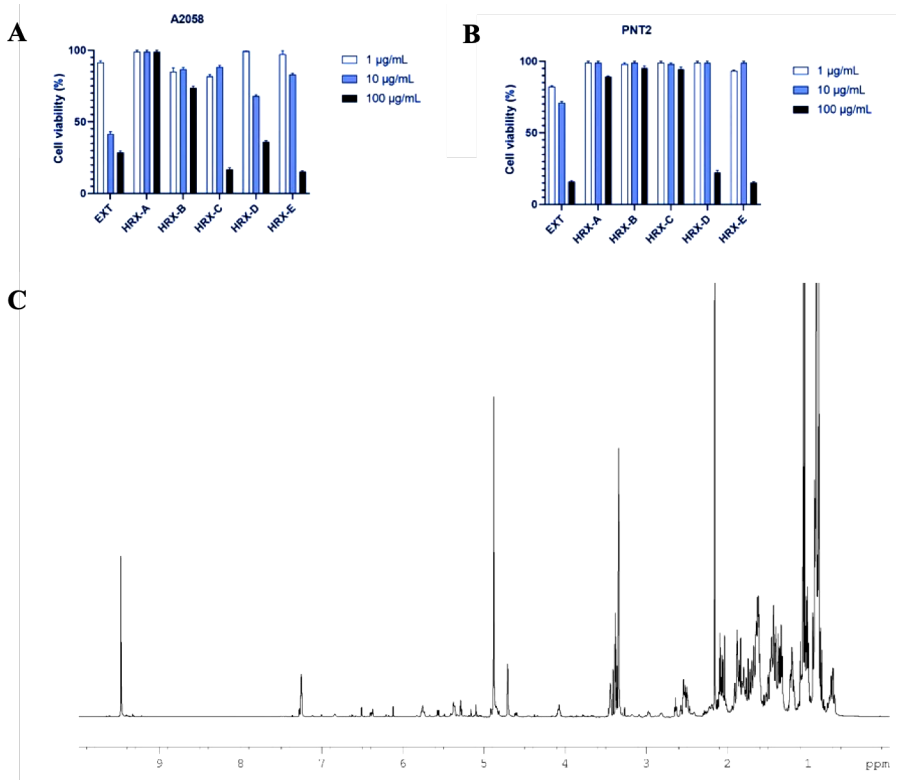

Figure 35: A) Percentage cell viability of human melanoma epithelial cell line (A2058) treated with total extract (EXT) and HRX-B, C, D and E fractions at concentrations of 1, 10, and 100 µg mL^{-1}; B) Percentage cell viability of human cell lines somatic prostate epithelium (PNT2) immortalized with SV40 treated with total extract (EXT) and HRX-B, C, D and E fractions at concentrations of 1, 10, and 100 µg mL^{-1}; C) ^{1}H NMR of HRX fraction D (600 MHz, CD_3OD).

Following the results of the bioassays, guided screening platform, the HRX-fraction D (sections 2.2.3; 2.4.2) was further fractionated on HILIC-SPE. The five new fractions obtained by this second chromatographic step were then tested on A2058 cells again (FIGURE 36A), showing further enrichment of the biological activity in the HILIC-fraction C, highlighting a dose-dependent cytotoxicity on the human melanoma epithelial cells, with a decreasing of viability of 40%. Driven by these results, dereplication analysis with ^{1}H-NMR and HR-ESIMS showed the presence of a single metabolite in the active fraction C, a new pyrrole-terpene derivative, named Molliorin F (FIGURE 36B).

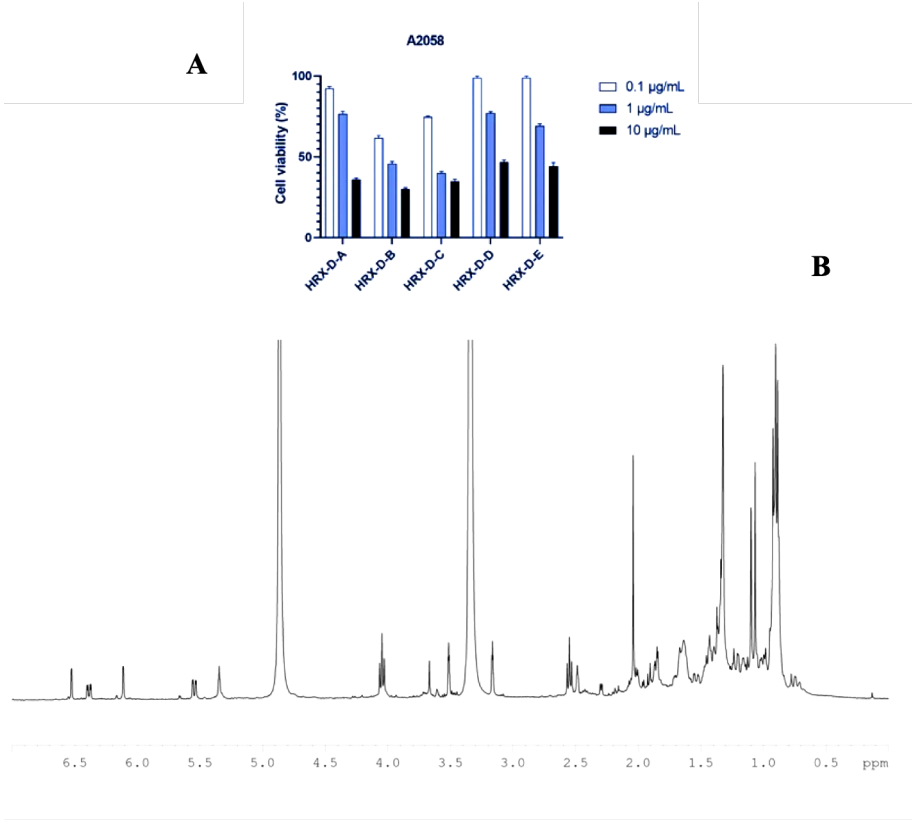

Figure 36: A) Percentage cell viability of human melanoma epithelial cell line (A2058) treated with total extract (EXT) and HILIC-B, C, D and E fractions at concentrations of 1, 10, and 100 µg mL⁻¹; B) ^{1}*H NMR of HILIC fraction C (600 MHz, CD₃OD).*

Spectroscopic studies of HILIC-fraction C showed the presence of several methyl group typical of a scalarane skeleton. HR-ESIMS spectrum showed a major peak at *m/z* = 480.3137 for $[M-H]^-$ in agreement with the molecular formula $C_{30}H_{43}NO_4$ (calcd. for *m/z* 481.3192), together with the adduct $[2M-H]^-$ at *m/z* = 961.6343. Moreover, in our case, NMR data revealed the diagnostic signals of a pyrrolic moiety at δ_H 6.52 (1H, d, *J* = 1.9 Hz, H-19) and 6.11 ppm (1H, d, *J* = 1.9 Hz, H-20), two olefinic signals at 6.38 (1H, dd, *J* = 9.8, 2.9 Hz, H-15) and 5.54 (1H, dd, *J* = 9.8, 2.9 Hz, H-16), five methyl singlet (δ_H 1.05, 1.08, 0.93, 0.88, 0.88), one acetoxy group (δ_H 2.03), a methine at δ_H 5.37 ppm correlating with an acetylic group, and two methylenes at δ_H 4.05 (2H, t, *J* = 14.5, 7.3 Hz, H-26) and 2.54 (2H,

t, *J* = 14.5, 7.3 Hz, H-27) which correlated to each other in the COSY experiment. Heterocorrelations in 2D NMR spectra indicated the presence of a propionic substituent on the ring. Indeed, the protons 2.54 ppm correlated with the carboxylic group (179.5 ppm). In the HMBC experiments C=O correlated also with the protons at 4.05 ppm (H-26), which showed also a cross peak with the carbon signals at 119.5 (C-19) and 108.6 (C-20) ppm of the pyrrole ring. Further spectroscopic studies, by the infrared (IR), supported the structural hypothesis with bands at 1567.64 and 1581.34 cm^{-1} for the acetyl and carboxylic group respectively. The diagnostic MSMS fragment at m/z 408.2963 due to the neutral loss of the propionic acid also confirmed the predicted structure. (FIGURE S17-S21) As reported in TABLE 3 the remaining NMR signals were ascribable to a scalarane skeleton, thus leading to the assignment of the new compound named Molliorin F (FIGURE 37), in agreement with the analogs previously reported. The determination of the stereochemistry was obtained comparing our data with the one present in literature for these skeletons. According to this, the absolute configuration of Molliorin F is proposed to be 4a*S*,4b*R*,6*S*,6a*S*,7*R*,10a*S*,10b*R*,12a*S*.[98]

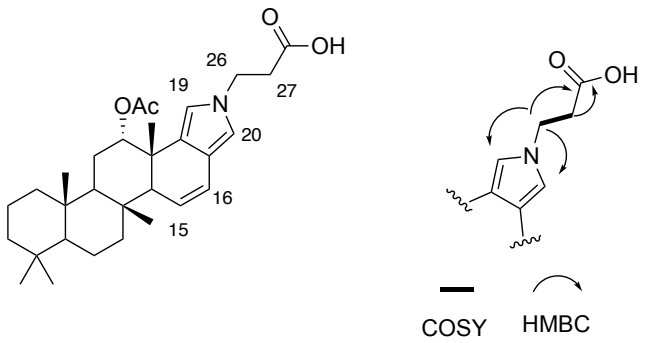

Figure 37: Molliorin F; key COSY and HMBC correlations

Table 3: NMR Data[a] of Molliorin F in CD_3OD at 600 MHz.

C	**Type**	**δ_C**	**δ_H, m (*J* in Hz)**
1	CH_2	31.7	1.30, overlapped
2	CH_2	21	1.64, 1.41, overlapped
3	CH_2	43.8	1.4, 1.19, overlapped
4	C	54.1	-
5	CH	58	0.90, bt (12.4)
6	CH_2	41.8	1.64, m
7	CH_2	20.7	1.50, m 1.30, m
8	C	139.2	
9	CH	54.2	1.42, m
10	C	149.4	
11	CH_2	24.7	1.84, m
12	CH	76.8	5.37, m
13	C	129.8	
14	CH	55.1	2.48, bd (5.6)
15	CH	119.9	6.38, dd (9.8, 2.9)
16	CH	120.6	5.54, dd (9.8, 2.9)
17	C	120.4	
18	C	129.7	
19	CH	119.5	6.52, d (1.9)
20	CH	108.6	6.11, d (1.9)
21	CH_3	25.6	1.05, s
22	CH_3	20.2	1.08, s
23	CH_3	17.6	0.93, s
24	CH_3	34.3	0.88, s
25	CH_3	22.3	0.88, s
26	CH_2	48.8	4.05, t (14.5, 7.3)
27	CH_2	42.1	2.54, t (14.5, 7.3)
28	C	179.5	
OAc	CH_3	22.3	2.03, s
OAc	C	174.4	

[a] The structure assignment was obtained by ^1H-^1H COSY, TOCSY, HSQCedited and HMBC correlations.

Pure compound Molliorin F was used to define the IC_{50} of 0.4 µg/mL, representing the first cytotoxic pyrrole-terpene showing anticancer activity at sub molar concentrations on human melanoma cells. (section 2.2.4) (FIGURE 38)

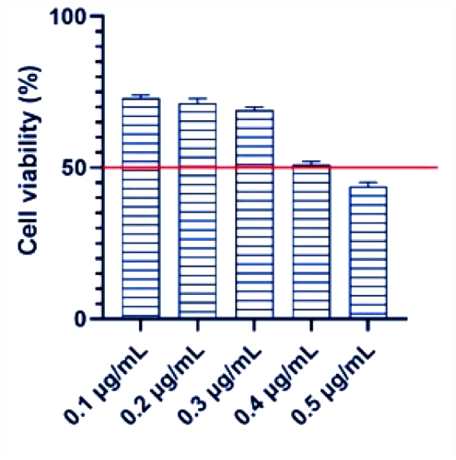

Figure 38: IC_{50} of HRX-D-C fraction of C. mollior at concentrations of 0.1, 0.2, 0.3, 0.4 and 0.5 µg mL^{-1} on human melanoma cells (A2058).

3.2.3 *Haliclona vansoesti*

The sponge genus *Haliclona* (class Demospongiae) belongs to the family Chalinidae and it's likely a low-bacterial-density sponges. Marine sponges of *Haliclona* genus led to more than 200 various bioactive metabolites including steroids, alkaloids, macrolides, polyketides, cyclic peptides, long-chain sphingoid bases, merohexaprenoids, and cyclic bis-1,3-dialkylpyridinium salts. Different activities, including cytotoxic and antitumor effects, have been reported.[99] Recently, from the genus *Haliclona (Reniera) sp.* were reported several anti-cancer potential polar lipids. Through the orthogonal SPE guided fractionations, we identified two active sphingoid-based lipid classes, characterized by nuclear magnetic resonance and mass spectrometry, as the main components.[100,101]

The crude extract of the *Haliclona* and its HRX-SPE (sections 2.2.2; 2.4.3) fractions were submitted to biological assays to evaluate cytotoxicity on human melanoma epithelial cell line (A2058) (FIGURE 39A) and normal human prostate cell line (PNT2) as a control, at three different concentrations (1, 10 and 100 µg/mL) (FIGURE 39B). (section 2.2.4). Biological assays indicated that the HRX fractions C and D were the most active. However, due to the strong cytotoxic effect of sample C against normal human PNT2 cells at 100 µg mL^{-1}, only fraction D was selected for subsequent analysis: ^{1}H-NMR experiments showed the presence of a mix of metabolites in this fraction, as showed in FIGURE 39C, confirmed by HR-ESIMS analysis.

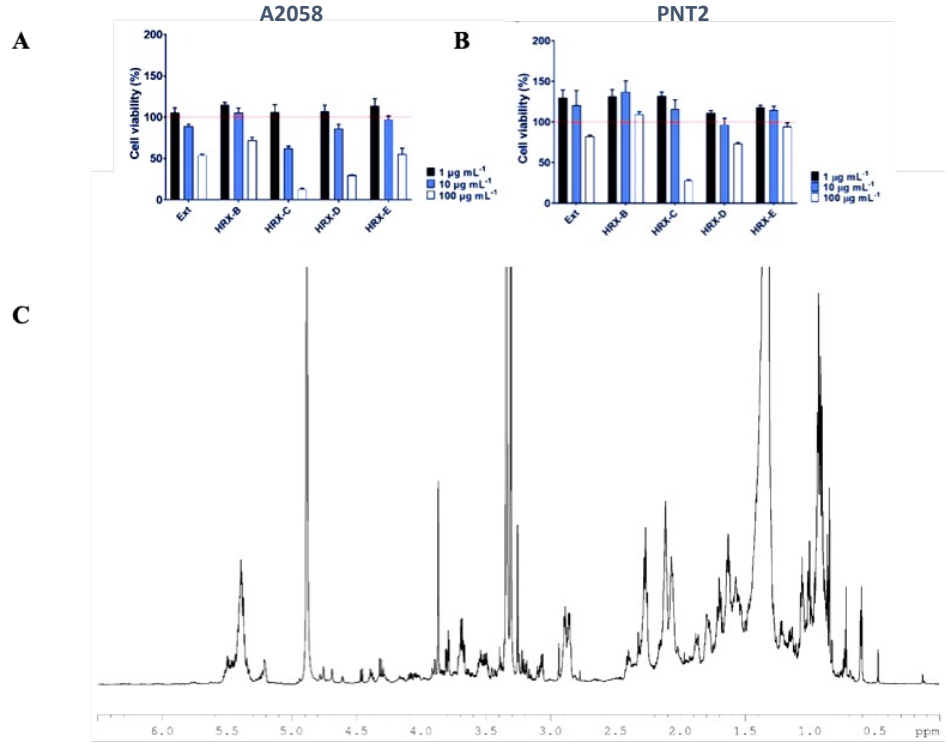

Figure 39: A) Percentage cell viability of human melanoma epithelial cell line (A2058) treated with total extract (EXT) and HRX-B, C, D and E fractions at concentrations of 1, 10, and 100 µg mL^{-1}; B) Percentage cell viability of human cell lines somatic prostate epithelium (PNT2) immortalized with SV40 treated with total extract (EXT) and HRX-B, C, D and E fractions at concentrations of 1, 10, and 100 µg mL^{-1}; C) ^{1}H NMR of HRX fraction D (600 MHz, CD_3OD).

Moving forward, with the second step of fractionation by HILIC-SPE on the most active sample HRX-D (sections 2.2.3; 2.4.2), the biological assays on the new five fractions confirmed the cytotoxic activity of new samples C and D (FIGURE 40A-41A); chemical analysis indicated that both fractions contained a family of lipidic compounds, as showed from ^{1}H-NMR spectra in FIGURE 40B-41B.

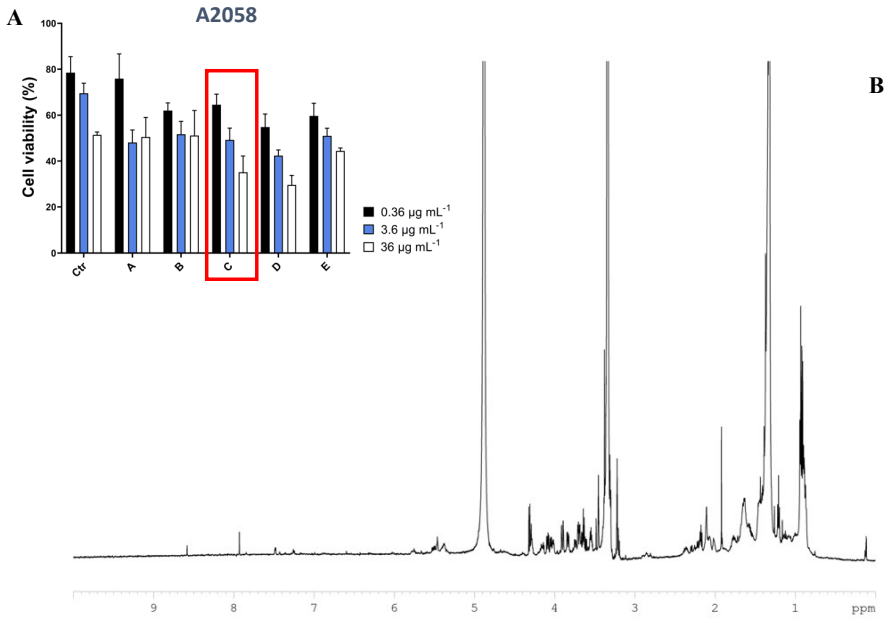

Figure 40: A) MTT assay of the HILIC fractions (A–E) and sample HRX-D (Ctr) on the human melanoma cell line A2058. Cell viability at IC_{50} concentration (36 µg mL^{-1}) and two ten-fold dilutions (3.6 and 0.36 µg mL^{-1}, respectively) was reported as a percentage.; B) ^{1}H NMR of HILIC fraction C (600 MHz, CD_3OD).

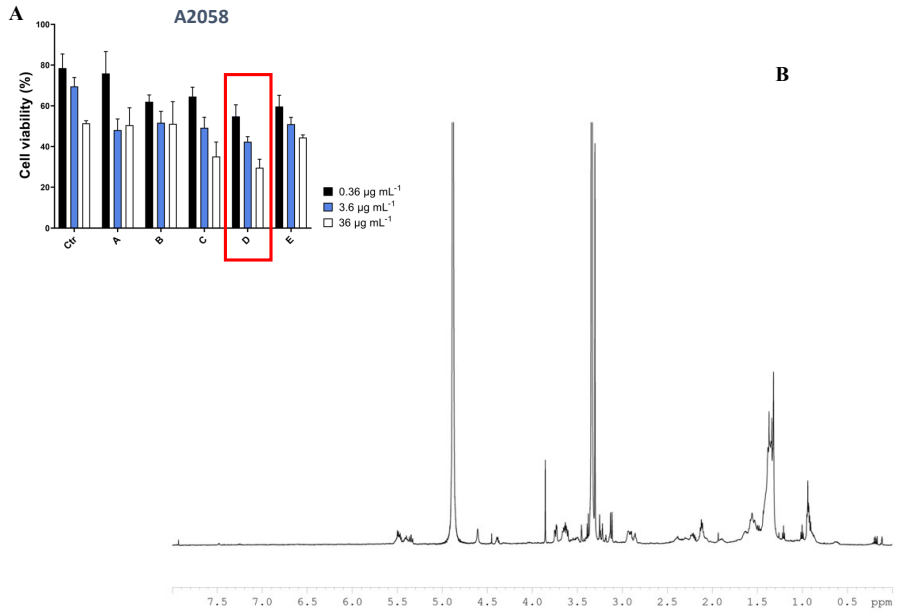

Figure 41: A) MTT assay of the HILIC fractions (A–E) and sample HRX-D (Ctr) on the human melanoma cell line A2058. Cell viability at IC_{50} concentration (36 µg mL^{-1}) and two ten-fold dilutions (3.6 and 0.36 µg mL^{-1}, respectively) was reported as a percentage.; B) ^1H NMR of HILIC fraction D (600 MHz, CD_3OD).

From a first dereplication analysis, it was evident that fraction C contained glycolipids given the presence of the peculiar signal of the anomeric proton at δ_H 4.31 (1H, d, J = 7.7 Hz, β orientation) in ^{1}H-NMR and the diagnostic ion peaks of the sugar moiety in LC-MS-MSMS: *m/z* 179.06 (loss due to the break between the sugar and the chain), *m/z* 161.04 (loss due to the break between the anomeric carbon and anomeric oxygen), *m/z* 89.02 (loss due to the break between the anomeric caron and the endocyclic oxygen). From the study of the different fragmentation pattern, it was possible to differentiate each compound for chain length, degree of oxygenation and instauration (TABLE S13). Spectroscopic data (mainly COSY and TOCSY experiments) also suggested the presence of two different spin system along the chain from carbon C-1 to C-6 with a common 2-amino-1,3-dioxynated moiety as reported for compounds 1a-1e. These evidences were corroborated by the HMBC correlation with the correlation between the

methine H-2 at 4.28 or 4.02 ppm (δ_C 51.5 or 54.5 ppm in agreement with a carbon resonance bonded to a nitrogen atom) with C-1' at 176.5 ppm of the sphingosine chain. Analyzing heterocorrelation spectra and comparing chemical shift data with literature, we could confirm not only the presence of α-glucopyranose with signals of a methylene C-6''at 62.5 ppm, δ_H 6.52 (2H, dd, J = 12, 3 Hz) and the diagnostic signal for the anomeric carbon, with β orientation, C-1" at 104.1 ppm, δ_H 4.31 (1H, d, J = 7 Hz). All the data, compared to the literature, were ascribable to cerebroside moiety (FIGURE 42) with different grades of insaturations and oxygenations on the alkyl chain, whereas the sphingosine chain remains unchanged, as showed in TABLE 4.[102–104] (FIGURE S22-S25)

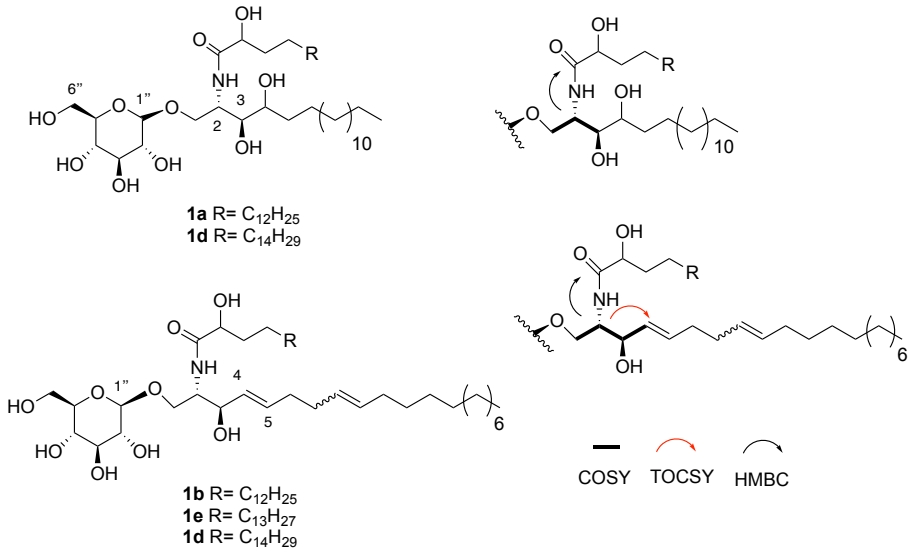

Figure 42: Cerebrosides; key COSY, TOCSY and HMBC correlations

Table 4: Relevant NMR Data [a] of HILIC fraction in CD_3OD at 600 MHz.

		1)	1)	2)	2)
C	**Type**	**δ_C**	**δ_H, m (*J* in Hz)**	**δ_C**	**δ_H, m (*J* in Hz)**
1	CH_2	69.7	4.08, dd (10.5, 6.0)	69.5	4.14, m
2	CH	51.5	4.28, m	54.4	3.75, dd (10.5, 3.8)
3	CH	75.2	3.64, t (6.0)	72.4	4.02, m
4	CH	72.9	3.55, m	130.9	5.51, dd (15.0, 7.0)
5	CH	32.6	1.44, m	134.3	5.77, dd (15.0, 7.0)
6	CH_2			33.3	2.10, m
7	CH_2			33.4	2.11, m
8, 9	CH			131.0	5.45, m
10	CH_2			34.8	2.00, m
11	CH_2			23.9	1.37, m
1’	C	176.5	-	176.5	-
2’	CH	72.7	4.05, dd (8.0, 4.2)	72.7	4.05, dd (8.0, 4.2)
3’	CH_2	35.2	1.64, m	35.2	1.64, m
4’	CH_2	30.0	1.30, m	30.0	1.30, m
1”	CH	104.1	4.31, d (7.7)	104.1	4.31, d (7.7)
2”	C	74.8	3.21, m	74.8	3.21, m
3”	C	77.5	3.38, m	77.5	3.38, m
4”	CH	71.7	3.30, m	71.7	3.30, m
5”	CH	77.3	3.31, m	77.3	3.31, m
6”	CH_2	62.5	3.70, dd (12.0, 3.0)	62.5	3.70, dd (12.0, 3.0)

[a] The structure assignment was obtained by ^{1}H-^{1}H COSY, TOCSY, HSQCedited, and HMBC correlations.

Regarding the HILIC-fraction D, spectroscopic data indicated the presence of another, and more simplified, class of sphingolipids: halisphingosines (FIGURE 43), already reported in this genus of sponge. In detail, it was immediately clear the similarity between our compounds and Halisphingosine A, the main

component of the fraction showed in the MS spectra as main peaks those at *m*/*z* 316.2844, 297.2740 and 280.2633, related to the $[M+H]^+$, $[M-H_2O+H]^+$, $[M-2H_2O+H]^+$, respectively. [105,106] In the NMR spectra, the sphingosine moiety was confirmed by the HSQC heterocorrelation between H-2 at δ_H 2.96 and his carbon C-2 at 58.4, indicating the bond with the amino group and three different sites of oxygenation δ_H 3.94, 3.62 (2H, H-1), C-1 61.8; δ_H 3.66 (1H, H-3), C-3 69.7; δ_H 4.39 (1H, H-6), C-6 67.8. Correlations corroborated also by the COSY correlation between H-2 and H-1, H-2 and H-3; the homocorrelation spectrum confirmed also the presence of the instauration, thanks to the correlation between H-6, of the oxygenated methine and H-7 δ_H 5.35 (1H, dd, *J*= 10, 9 Hz) of the double bond. [102] (FIGURE S26-S27) (TABLE 4)

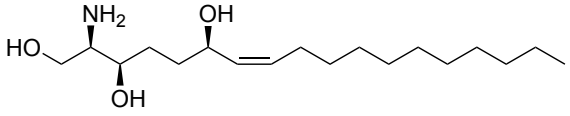

Figure 43: Halisphingosine A

Table 5: Relevant NMR Data [a] of HILIC fraction C in CD_3OD at 600 MHz.

C	**Type**	**δ_C**	**δ_H, m (*J* in Hz)**
1	CH_2	61.8	3.74, dd (11.0, 3.7) 3.62, m
2	CH	58.4	2.96, m
3	CH	69.7	3.66, m
4	CH_2	35.0	1.50-1.44, m
5	CH_2	38.0	1.50-1.44, m
6	CH	67.8	4.39, m
7	CH	134.2	5.35, dd (10.0, 9.0)
8	CH	133.0	5.44, m
9	CH_2	28.6	2.08, m
10-17	CH_2		1.40-1.25, m
18	CH_3	14.0	0.90, t (7.0)

[a] The structure assignment was obtained by ^{1}H-^{1}H COSY, HSQC correlations.

Thus, applying our bioassay-guided fractionation approach, we highlighted the potential anti-cancer and pharmacological properties of *Haliclona vansoesti* metabolites, against human melanoma cells. Interestingly, the second SPE fractionation allowed to differentiate the activity: between two new fractions containing two different classes of sphingolipids: fraction C was composed of the more complex lipid, cerebrosides, whereas fraction D contained sphingolipids of halisphingosine family. These compounds isolated from the sponge, namely cerebrosides and sphingolipids were found to be the most pro-apoptotic on melanoma cells, with a reduction cell viability of 55–65%.

3.3 MS-based approach

3.3.1 Sulphur filtering: sulphated and sulphonated compounds

Human Triggering Receptor Expressed on Myeloid Cells 2 (TREM2) is an immune receptor playing an important role in pathophysiological processes and widely expressed on Dendritic cells (DCs) and macrophages, innate immune cells able to regulate T cell responses to either immunity or tolerance. TREM2 is known to bind different anionic molecules, specifically lipids, mostly associated to tissue damage or cellular stress. (section 1.4.3.1.2) Recently in our laboratory was synthetized a sulfoquinovoside glycerolipid, Sulfavant A, a novel immunomodulatory naturally inspired sulfolipid able to induce maturation of human DC and recognized as the first synthetic TREM2 ligand. The sulfoquinovoside group mimics the polar head of phospholipids with a strong acidic property of the sulfonic acid that increases the negative charge density in comparison to phospholipids, promoting the interaction with TREM2, according to the current model of binding.[58–60] Thus starting from this consideration of chemical structure of TREM2 ligands, with the aim to find new putative immunomodulant molecules, several marine organisms were tested on a mouse reporter cell line expressing human TREM2-WT receptor, to evaluate the percentage of GFP^+ cells. After incubation with the extracts or enriched natural products, cell increase GFP surface expression upon receptor stimulation and reporter activity can be easily measured by flow cytometry as % GFP^+ cells. Beside the biological assays, we developed an MS-based workflow described in FIGURE 44 to identified new metabolites able to target TREM2 receptor: otherwise characterized by an anionic functional group on the structure, specifically sulphur compounds. To set up and test this approach four different species were selected: *Colpomoenia sp.*, *Alexandrium andersonii*, and *Schizotrix*

sp. and *Cyclope neritea*. After a modified Bligh and Dyer procedure (section 2.5.1.1), the extracted was processed through a fractionation on an SPE-NH_2 resin active to allow an anionic exchange, for the enrichment in one fraction, fraction D, all the anionic compounds. (section 2.5.1.2). Both the extracts and the enriched fraction were analyzed by LC-MS using as described in section 2.5.1.3 a buffer solution at pH 8.2, to achieve a successful ionization, in ESI source, taking advantage of the acid properties of the sulphate and sulphonate groups. Raw data were analyzed through a deconvolution method with the MZmine software with the selection of a DFF, a filtering for the loss of a diagnostic fragment: 96.958 m/z for compounds with sulphated moiety on the structure (HSO_4^-); 80.963 for compounds with sulphonated moiety (HSO_3^-). (section 2.5.1.3) (FIGURE 50) This was necessary to highlight only sulphur compounds and remove from the *MZmine* "scatter plot" (X axis Retention time; Y axis *m/z*) (FIGURE 44) other anionic species such as phospholipids, contained in the SPE-NH_2 fraction D.

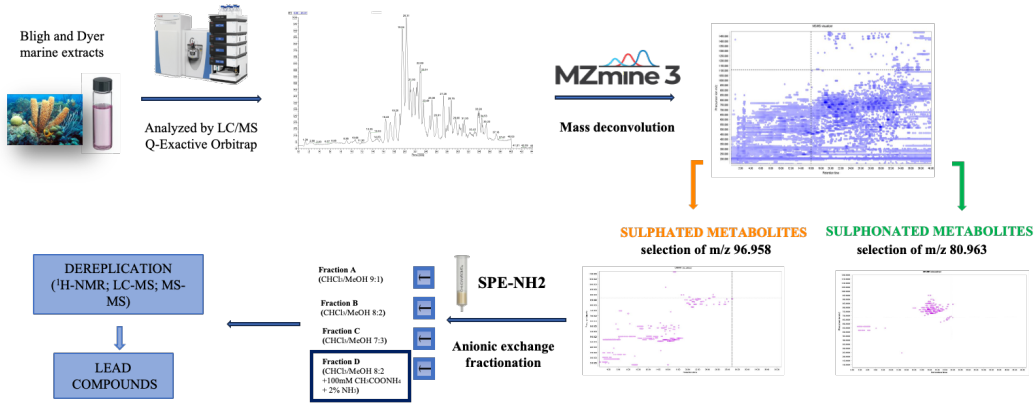

Figure 44: Work flow for sulphur compounds screening.

Regarding sulphated compounds (FIGURE 45), in almost all the samples, the workflow (section 2.5.1.3; section 3.3.1) allowed the identification of known compounds such as sterol sulfates (StS): cholesterol sulfate, brassicasterol sulfate and beta-sitosterol sulfate.

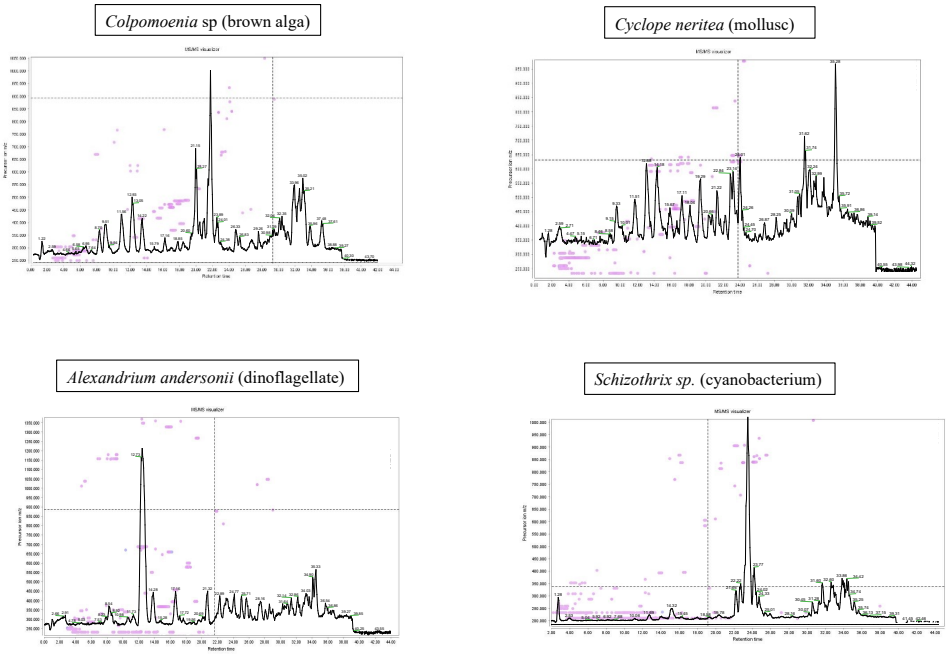

Figure 45: MZmine scatter plot (X-axis Retention time; Y-axis Precursor m/z) for the LC-MS deconvolution screening of sulphated compounds of selected extracts

Likewise, the data were processed to evaluate the presence of sulphated compounds. (FIGURE 46) In this case, the work flow (section 2.5.1.3; section 3.3.1) allowed the enrichment, for all the extracts analyzed, of known glycero-lipids such as sulfoquinovosyl diacylglycerols (α-SQDGs) and their lyso-form sulfoquinovosyl monoacylglycerols (α-SQMGs), differing in the alkyl chains. For both families, it was also found the presence of alkyl chains with odd-numbered carbons, probably imputable to a bacterial metabolism.

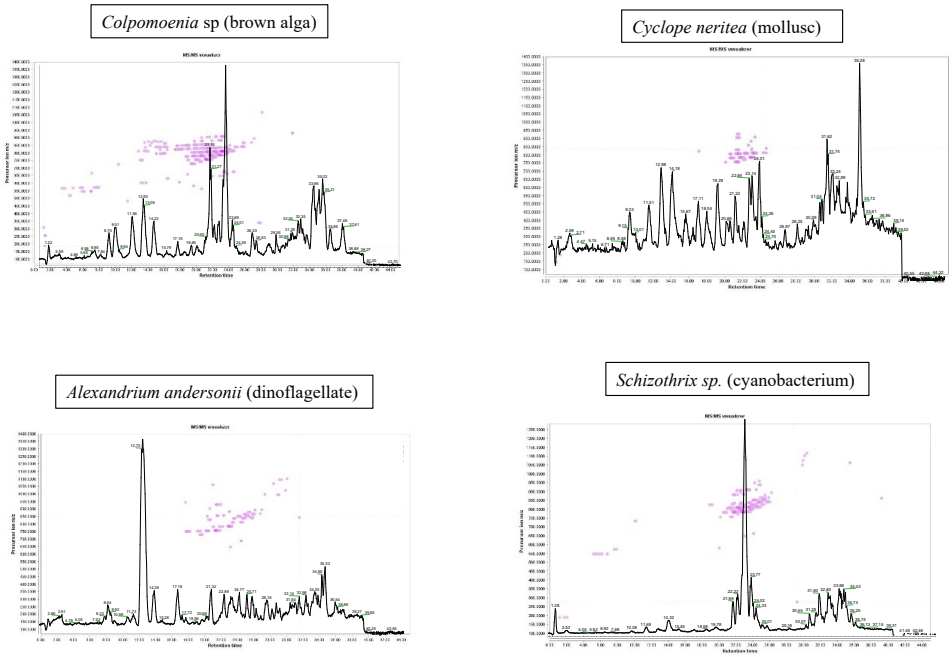

Figure 46: MZmine scatter plot (X-axis Retention time; Y-axis Precursor m/z) LC-MS deconvolution screening of sulphonated compounds of selected extracts.

This hypothesis of bacterization was corroborated by the isolation of a class of bacterial sulfonolipids (FIGURE 47), from the dinoflagellate *A. andersonii* and the brown alga *Colpomoenia sp.*, named cystenolides, already reported in literature from the marine *Roseobacter* clade.[107]

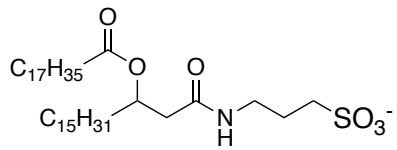

Figure 47: Sulfonolipids

3.3.1.1 *Ophiura ophiura*

Echinoderms dominate the marine environment, holothurians and ophiuroids are usually the most abundant genus observed. Echinoderms have been poorly studied with regard to their medicinal applications, despite their chemical diversity. From Ophiuroid species several saponins, disulfate polyhydroxylated steroids and hamigrene sesquiterpenes were isolated from all species investigated.[108] From echinoderms, like *Ophiura ophiura,* were reported several sulphated steroid scaffold and chlorine porphyrinic compounds.[109–111] Evaluating the biological activity of the extract and related HRX-SPE of the starfish *Ophiura ophiura*, collected in the Gulf of Naples, we found that HRX fractions D and E were strongly active for the TREM2 receptor assays (FIGURE 48); from a chemical point of view these fractions are usually enriched of lipidic compounds, so we apply the workflow above described to search potential active sulphur lipids.

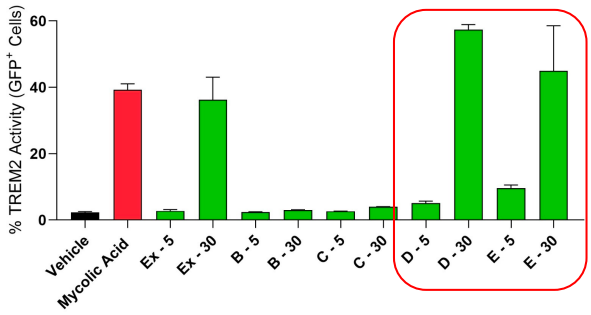

Figure 48: Dose-dependent hTREM2 activity (GFP⁺ cells) of extract and HR-X fractions of Ophiura ophiura on 2B4 transfected cell line. Control positive Mycolic acid (10 μg/mL); vehicle methanol.

So, moving forward with our workflow, after a modified Bligh and Dyer procedure (section 2.5.1.6), the extracted was processed through a fractionation on an anionic exchange support (section 2.5.1.6). The fraction D, in which anionic compounds were eluted, was analyzed with the MZmine software with the selection of a DFF, a filtering for the loss of a diagnostic fragment: 96.958 m/z for compounds with sulphated moiety on the structure (HSO_4^-). (section 2.5.1.3; section 3.3.1) (FIGURE 49) Besides known compounds such as phospholipids and sulfate sterols, the screening highlighted also the presence of other lipidic compounds with a MS/MS not ascribable to reported compounds.

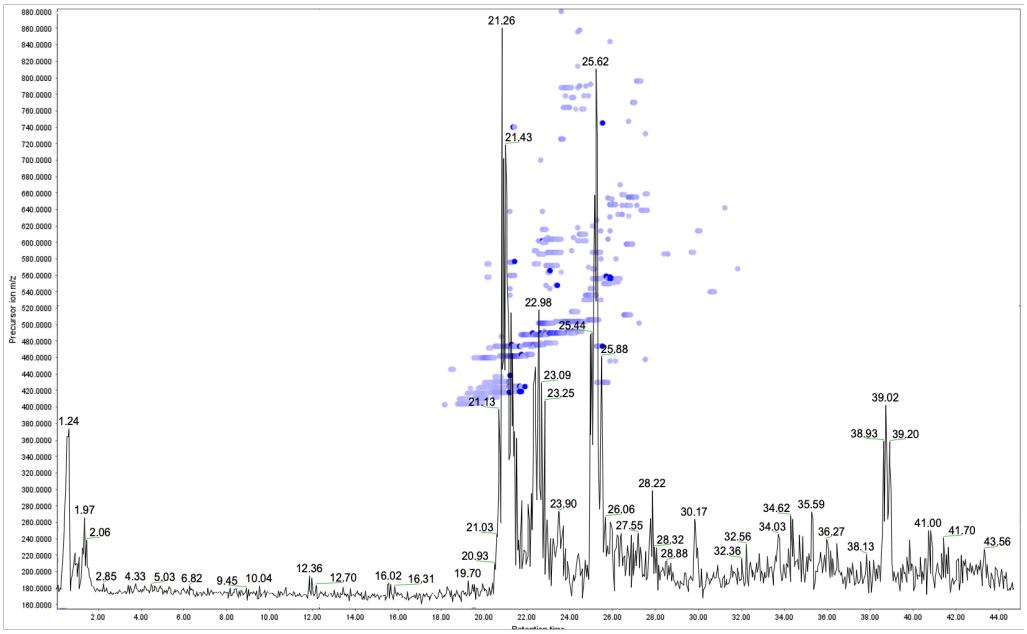

Figure 49: MZmine scatter plot (X-axis Retention time; Y-axis Precursor m/z) of NH2-SPE fraction D; (DFF: 96.058 m/z).

Since this method of extraction yielded a very low amount of product for further purification and structural characterization, the raw material was once again processed by methanolic extraction and consecutive HRX-SPE fractionation. All the new samples were analyzed by the mass spectrometry screening, and it was clear that the metabolites of interest were still preserved in HRX fraction D, as provided by the preliminary analysis. (section 2.5.1.6.1) (FIGURE 50)

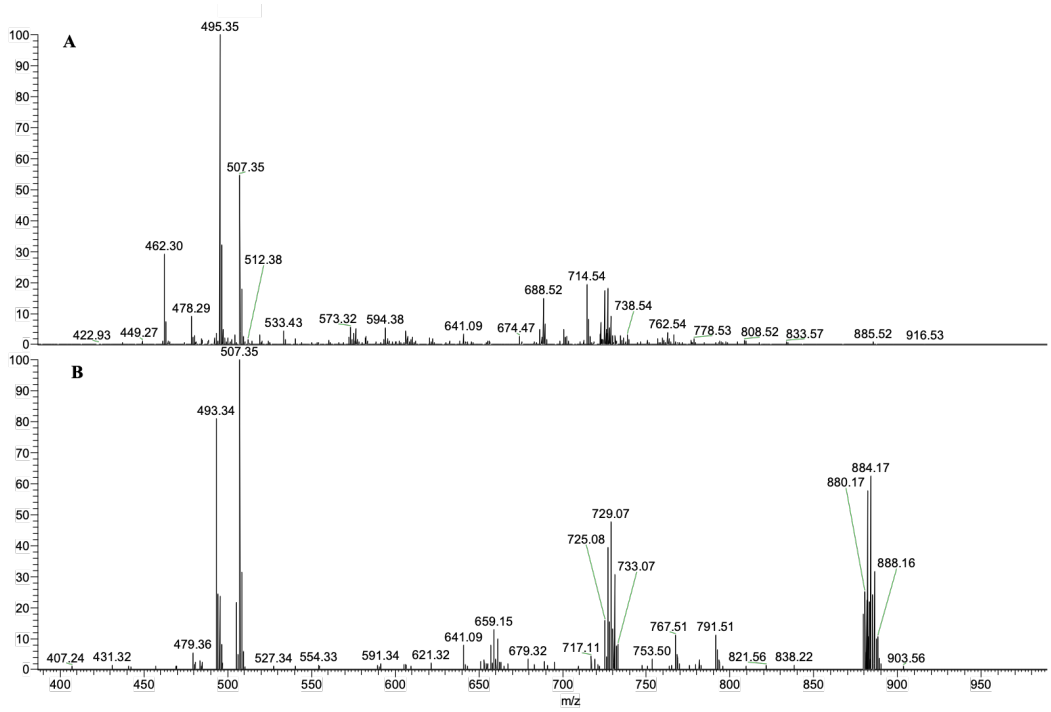

Figure 50: HRESI-MS/MS (ESI mode (-)) of SPE-NH2 fractions of A) Bligh and Dyer extract; B) HRX-Fraction D.

So, this fraction was submitted to the anionic exchange fractionation to enrich in one fraction all the sulphated compounds and discord neutral metabolites. Indeed, the NH_2-SPE fraction D contains the same compounds as that derived from the Bligh and Dyer extract. Trying to further purify the sample, the NH_2 -SPE fraction D was further fractionated through HILIC-SPE; the family of target compounds

was enriched in the fraction B with THF/CH_3OH 80:20. (section 2.5.1.6.1) Dereplication analysis of the HILIC fraction B by HRESI-LC-MS/MS suggested the presence of a family of lipids (FIGURE S28-S30). The MS/MS spectrum highlighted the presence on the structural moiety of a sulphated group with the diagnostic fragments 96.958; brominated atoms due to the presence of the diagnostic losses of 78.917 and 80.916, ascribable to the two Br isotopes; chlorinated atoms due to the several neutral losses of 36Da imputable to the loss of HCl on the linear carbon chain. (FIGURE 51) Searching by molecular weight at high resolution, we can suggest that one of the compounds in the mixture has the same molecular formula as the algal metabolite Halo-sulpholipid. (FIGURE 52) Biological assays to evaluate halo-sulpholipids TREM2 activity are still on going.

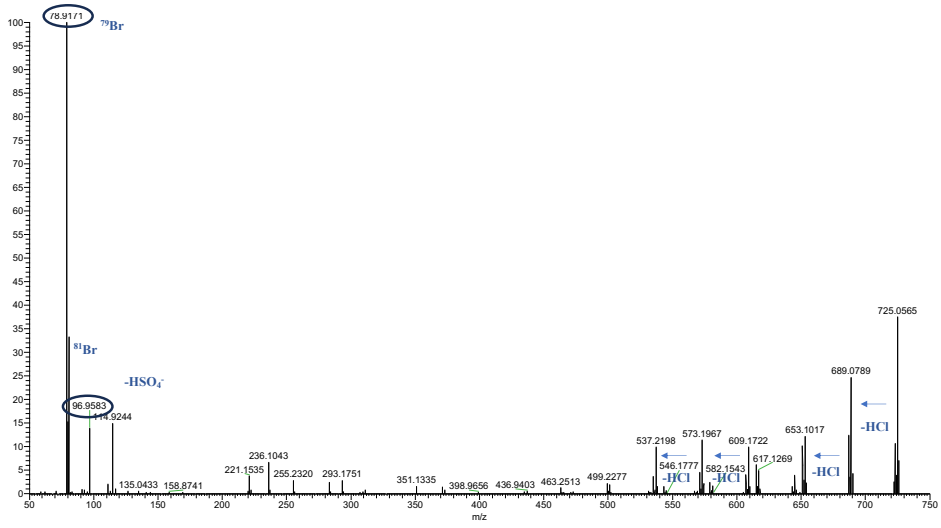

Figure 51: HRESI-MS/MS (ESI mode (-)) of Halo-sulpholipid with m/z 725.056 (HILIC fraction B of Ophiura ophiura).

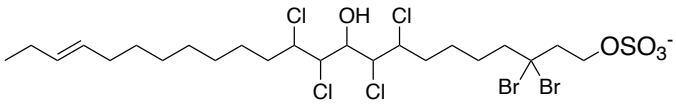

Figure 52: Halo-sulpholipids

Our case study, was the first evidence of the presence of this kind of compounds, sulphur-halo lipids, in this species. In literature, were reported several sulphur-halo lipids; the first chlorosulpholipid, Danicalipin A (FIGURE 53), was isolated in the late 1960s from the freshwater alga *Ochromonas danica*, but have since been observed in other species of algae and have been isolated from toxic shellfish and corals from the marine environment.[112,113] Several years later, White et al. reported that these kind of compounds could contain a bromination functionalization on the structure, when the alga *O. danica* is grown under modified conditions, containing excess bromide ion.[114] Our case syudy represent the first evidence of the presence of this kind of sulphur-halo lipids in the studied specie.

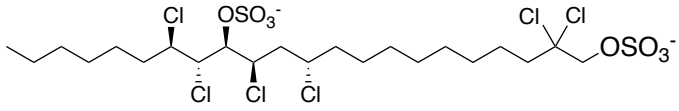

Figure 53: Danicalipin A

3.3.2 Pyridine-moiety filtering

3.3.2.1 *Haminoea orbygnana*

Cephalaspidean opisthobranchs are characterized by a shell that can be conspicuous, thin and fragile, or internal. Finally, some cephalaspideans lose the shell when mature. Most of cephalaspideans are carnivorous, feeding upon molluscs, polychaetes from shallow marine environments, but not in the case of the animals from *Haminoidea* family, who are herbivorous. From this genus were found several 3-alkylpyridine alkaloids, derived by single or multiple units of a basic 3-alkylpyridine motif with variability along the chain concerning insaturations and oxidations. An extensive study of many Mediterranean species belonging to the genus *Haminoea* (*H. navicula*, *H. fusari*, *H. orteai*, *H. orbignyana*) led the

characterization of a series of 3-alkylpyridines, named haminols, structurally related to the already described navenone-A. [115,116]

Alkaloids evolved as a chemical defense mechanism against predators; in the marine environment, they have been described as functional for antihypertensive, antitumor, and against neurological diseases. [117] From this genus were reported, over the years, also several compounds with polypropionates skeleton, such as fusaripyrones A and B. [118] Thus, suggesting that in Cephalaspidea, molecules, with different scaffolds, play different ecological roles, intra-specific communication for the alkylpyridines, and inter-specific defensive role for the polypropionates.[119]

Moved always by the need to research new potential immunomodulant bioactive small molecules from the sea, in the framework of the innate immunity, another target of our research was the receptor Dectin-1, a C-type lectin receptor (CLR) expressed in DC2 mainly involved in antifungal immunity and in other inflammatory human disease. Several studies have shown that Dectin-1 can cooperate with TLRs, but the synergistic signaling via Dectin-1 and TLR does not only result in proinflammatory cytokine production, but also in augmented secretion of anti-inflammatory IL-10, consistent with induction of a regulatory phenotype and reduced activation of T cells.[120–122] (section 1.4.3.1.1)

As for TREM2 receptor, extracts and HRX-SPE fractions of the mollusc *H. orbygnana*, were tested at two different concentrations, on the reporter cells, that express Dectin-1 protein, resulted to be one of the most potential active species. In detail, the HRX-SPE fraction C showed a potent activity at 5µg/mL, resulting more active than the Zymosan, a polysaccharide used as positive control since is widely described as well characterized ligand for Dectin-1 receptor. (FIGURE 54A) Dereplication analysis on the active sample showed in the ^{1}H-NMR spectrum signals ascribable to pyridine moiety, see region between 7 and 8.5 ppm. (FIGRE 54B)

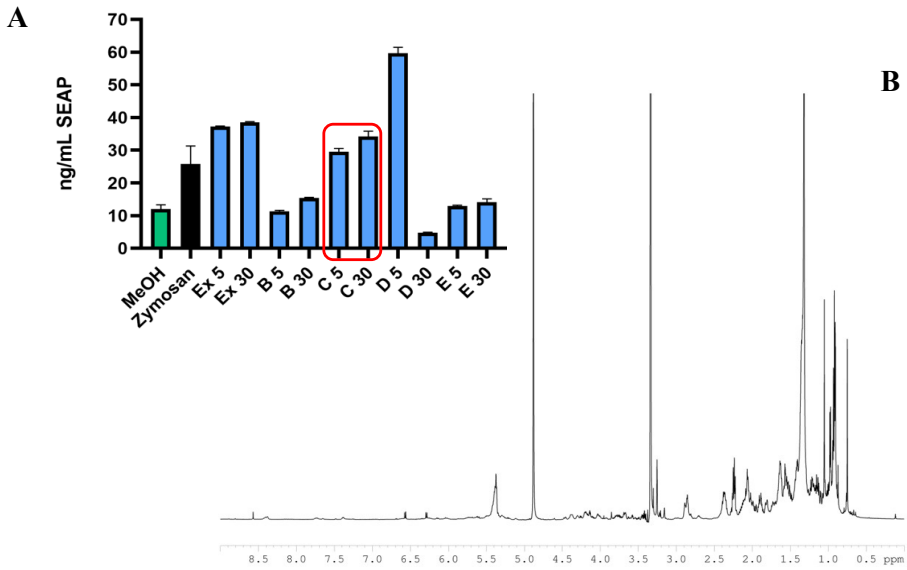

Figure 54: A) Dose-dependent SEAP Dectin-1b activity of extract and HR-X fractions of haminoea orbygnana on HEK293 transfected cell line. Control positive Zymosan (100 μ g/mL); vehicle methanol; B) 1H-NMR of HRX-SPE fraction C (600 MHz, CD_3OD)

So, starting from these results, we applied an MS-based approach to look for putative bioactive molecules containing this chemical moiety. The mollusc was collected once again and extracted with acetone, typically applied for chemical studies of organisms belonging to the phylum mollusc. This extraction protocol provides the separation of external extract (mantle) and internal extract (viscera) by a first gentle sonication followed by a second step of grinding tissue. (section 2.5.2.1) The localization and distribution of the secondary metabolites is strictly correlated to their function, so the acetonic extraction allowed us to recover a greater amount of bioactive compounds with a higher degree of purity.

The extracts were submitted to a first spectroscopic screening through ^{1}H-NMR (FIGURE 55) and HRESI-LCMS/MSMS, applying the chemical approach, based on the mass deconvolution with the selection of a DFF for the ethylpyridine group (m/z 106.05), peculiar for pyridine compounds (section 2.5.2.2).[123] (FIGURE 56)

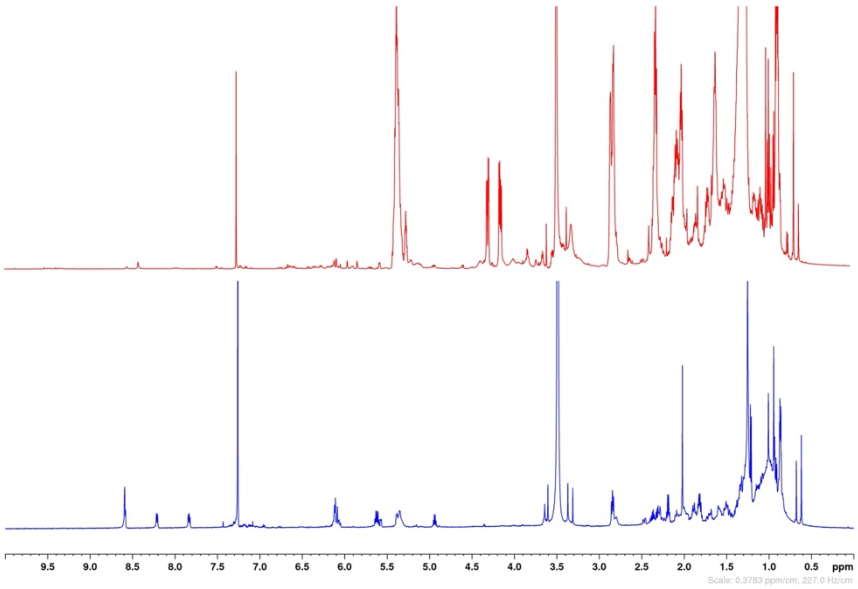

Figure 55: ^{1}H NMR of Haminoea orbygnana external extract (blue) and internal extract (red) (600 MHz, $CDCl_3$)

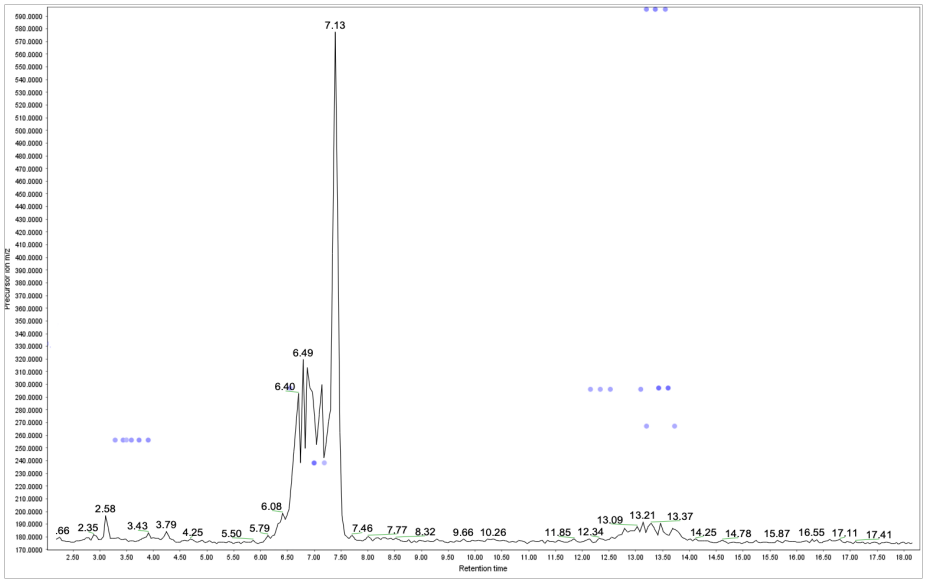

Figure 56: MZmine scatter plot (X-axis Retention time; Y-axis Precursor m/z) of external part; DFF (106.06 m/z)

The chemical approach confirmed the presence of the already reported Haminol-1 and Haminol-2, confirmed by the ^{1}H-NMR spectra of pure fractions obtained by silica purification of the first external extract. Haminols are 3-alkylpyridines characterized by a linear alkyl chain containing twelve carbons and a hydroxy, or acetoxy, function at C-2 and distribution of the two (or three) insaturations, along the chain. (FIGURE 57)

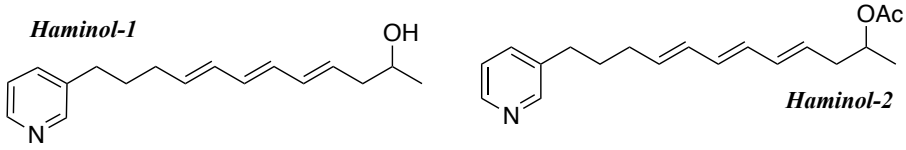

Figure 57: Chemical structure of haminol 1 and 2 [72,115]

Moreover, the mass deconvolution showed also the presence of another minority compound with *m/z* = 597.3694. (FIGURE S31) that suggests the presence of a dimeric structure, in agreement with the molecular formula $C_{38}H_{49}N_2O_4^+$ (calcd. for *m/z* 597.8194). Indeed the MS/MS fragmentation pattern supposedly ascribable to a dimeric alkylpyridine, due to the peaks with *m/z* = 537.3640 and *m/z* = 477.3268 ascribable to the loss of two acetyl groups on the alkyl chain; *m/z* = 300.1963 corresponding to $[M+H]^+$ of Haminol-2, properly. (FIGURE S32-S33)
To fully characterize the new compound, the external extract was fractionated with silica gel to obtain the pure molecule (section 2.5.2.4), on which perform spectroscopic analysis. Although the NMR data are not complete due to the limited material available and the low resolution of the experiments, we hypothesized the dimeric 3-alkylpyridine structure as depicted in FIGURE 58.

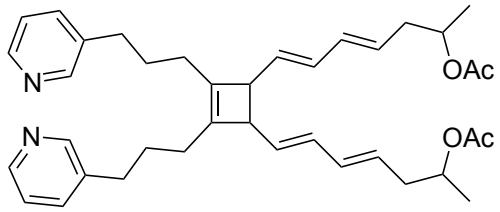

Figure 58: Structural hypothesis of dimeric alkylpyridine

To achieve further evidences of the presence of the new metabolite, Ion Mobility Spectrometry (IMS) experiments combined with HRESI-LC-MS and data (section

2.5.2.4.1) using Waters Synapt Mass Spectrometer, an instrument designed for spectral acquisition and data processing with an increased specificity associated with exact mass measurement, ideal for compound and fragment identification. The configuration of the SYNAPT system, where collision cells are placed one before (Trap) and one after the ion mobility cell (Transfer), allows an acquisition mode known as HD-MS^E. It is possible to select a precursor ion of interest in the first collision cell (TRAP, low collision energy) and achieve its fragmentation in the second collision cell (TRANSFER, high collision energy). The low collision energy provides unfragmented ions and of both unfragmented and fragmented ions by generating two discrete and independent interleaved accurate mass information, while the high collision energy provides fragmented ions. The time an ion takes from the start of the drift tube to the detector is referred to as the drift time. As the ion travels through the drift tube, it undergoes collisions with the buffer gas; this observational property which averages all geometric orientations and ion-gas interaction types during the experiment is referred to as the collision cross section (CCS). The larger an ion, the larger also its CCS. This means that ions with a large CCS require more time to traverse the drift tube and therefore exhibit a longer drift time.[72,124,125]

Table 6: Observed CCS and Drift time values for all the compounds observed in H. orbygnana first sonicate. All data were elaborated with Waters connect software.

Component name	Observed mass (Da)	Observed m/z	Observed RT (min)	Observed drift (ms)	Observed CCS (Å2)
Dimer	597,3689552	597,3684066	10,56783676	6,680603504	234,533905
Dimer	597,3689565	597,3684079	12,4254179	6,965553284	242,2054443
Dimer	597,3752366	299,1870697	12,60033226	3,457336426	288,5695974
Monomer	299,1886891	300,1959655	14,70965385	4,012108803	163,8813934
Monomer	299,1888873	300,1961637	13,49994946	4,052464485	165,0654297
Monomer	299,1891053	300,1963818	5,618355274	4,011295319	163,8560791
Monomer	299,1890508	300,1963273	7,003068447	4,05335474	165,0856781

So, as shown in FIGURE 59 the difference in drifts time and in CCS (TABLE 6) between the ion at m/z 300.19 (monomer) and the ion at m/z 597.39 (dimer) supported the hypothesis of monomer and dimer, each. (FIGURE S34) Biological assays to evaluate alkylpyridines Dectin-1 activity are still on going.

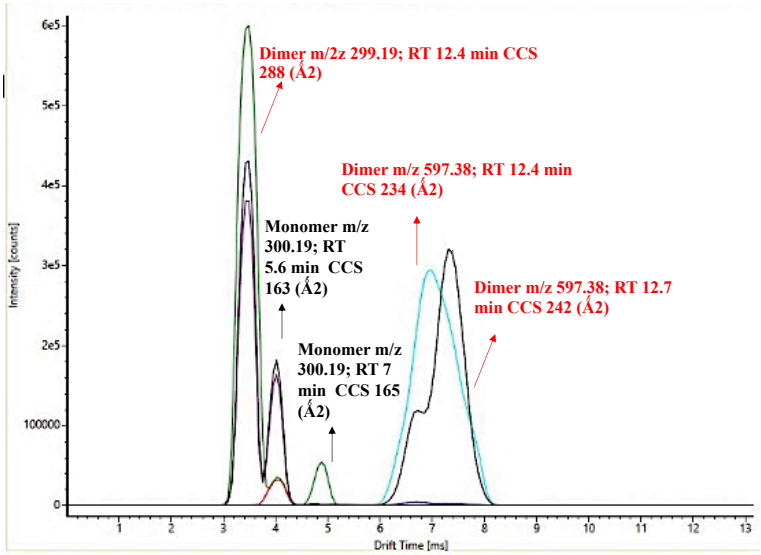

Figure 59: Mobility trace of selected monomeric and dimeric compounds from H. orbygnana first sonicate

3.4 Summary description of scientific activity

This PhD thesis presented the discovery of bioactive marine natural products with potential applications in the cosmeceutical and pharmaceutical industries, combining chemistry, biology, and immunology, through a wide range of techniques for the isolation, purification, and identification of different structural classes of marine natural products from various marine organisms. All the study of state of art for bioactive marine natural products were published in a review.[2] Between all our achievement, the results related to the compounds Lepadin A and Molliorin F were reported in three published papers, in which my contribute deal with the isolation and structure elucidation of the bioactive molecules, as well as the drafting of part of the manuscripts. [86,90,98]

4) EXPERIENCE ABROAD: PHARMAMAR S.P.A (Madrid, Spain)

4.1 First screening of marine extracts

In the framework of my PhD project, I did a collaboration with the company Pharmamar (Madrid, Spain), leader in the drug discovery for the research of anti-cancer compound from marine sources. During my period there I was able to isolate bioactive natural products from marine organisms, in detail, six organisms from their personal library, collected in the Indonesian sea, were selected:

- *Nephtheidae*
- *Verongida*
- *Lissoclinum*
- *Mycale*
- *Sarcophyton*
- *Mycarpa*

The organisms were lyophilized and all treated, as provided by the company procedures, by methanolic and acetonic extraction. The extracts were fractionated by flash chromatography and purified by HPLC. Overall, sixteen pure compounds of different chemical nature were isolated. Structural elucidation of theses active metabolites was carried out by using the most advanced Nuclear Magnetic Resonance (NMR) and Mass Spectrometry (MS) techniques. For reasons of company privacy, not all the chemical structure can be reported in this thesis, at present.

4.1.1 *Nephtheidae*

Nephtheidae is a family of soft corals in the phylum Cnidaria. From the first ^{1}H-NMR (FIGURE 60) screening of the methanolic extract it was evident the presence of several methyl signals ascribable to a cembranoid moiety.

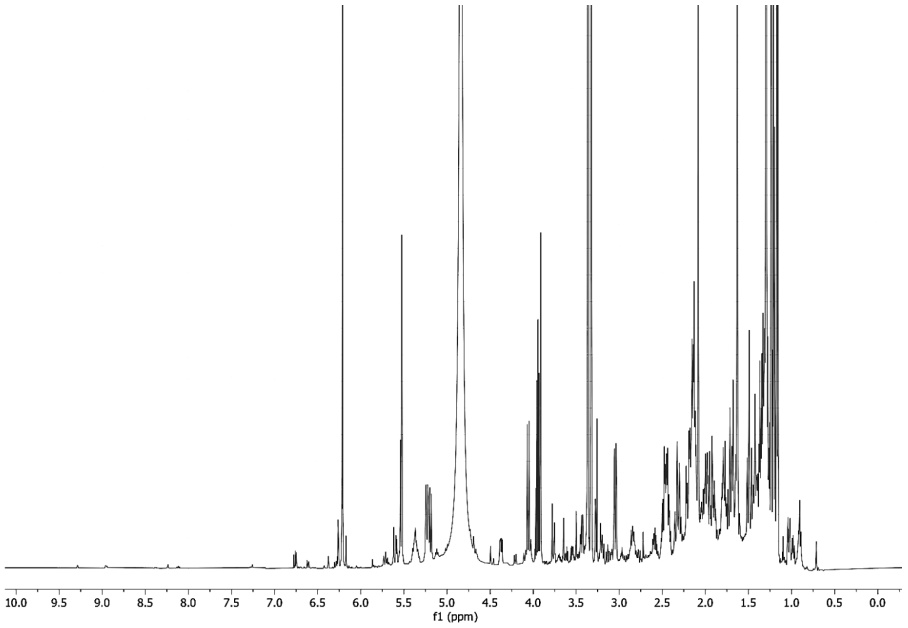

Figure 60: ^{1}H-NMR (500MHz, CD_3OD) spectrum of Nephtheidae extract

So, the extract was submitted to a first fractionation procedure, through flash chromatography, in gradient conditions of H_2O as solvent A and CH_3CN as solvent B, starting from 100% of A until 100% of B in 35 minutes, followed also by isocratic conditions in CH_3OH. After a first spectroscopic analysis, through LC-MS and ^{1}H-NMR, two fractions, CFRP3 and CFRP4, were selected for a further purification. They were purified through HPLC using a column XTerra 5u C18 110A (150x10mm) with H_2O and CH_3OH as solvent A and B respectively, starting from 20% of B in 3 minutes to 70% of B, and then to 100% of B in 39 minutes.

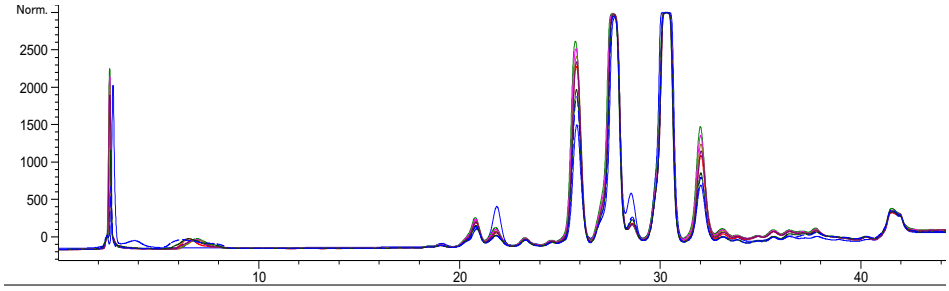

Figure 61: HPLC profile of CFRP3

All the fractions obtained from the HPLC purification of the fraction CFRP3 (FIGURE 61) were submitted to a dereplication analysis with spectroscopic techniques; three fractions showed the presence of a single, pure metabolite RP3-H1, RP3-H2 and RP3-H4. Comparing our NMR data with the literature we identified three different cembranoids (FIGURE 62-65) in each fraction: Dendronpholide C Sandensolide and Sinulariolide. All the structural hypothesis were also confirmed by the HRESI-MS spectrum showing respectivily a major peak at m/z= 389.22 $[M+Na]^+$ (calcd. for m/z=389.2298) in agreement with the molecular formula $C_{21}H_{34}O_5$ (calcd. for m/z=366.2406) for Dendronpholide C; a major peak at m/z= 357.20 $[M+Na]^+$ (calcd. for *m/z* 357.2036) in agreement with the molecular formula $C_{20}H_{30}O_4$ (calcd. for *m/z* 334.2144) for Sandensolide; a major peak at m/z= 357.20 $[M+Na]^+$ (calcd. for *m/z* 357.2036) in agreement with the molecular formula $C_{20}H_{30}O_4$ (calcd. for *m/z* 334.2144) for Sinulariolide.[126,127]

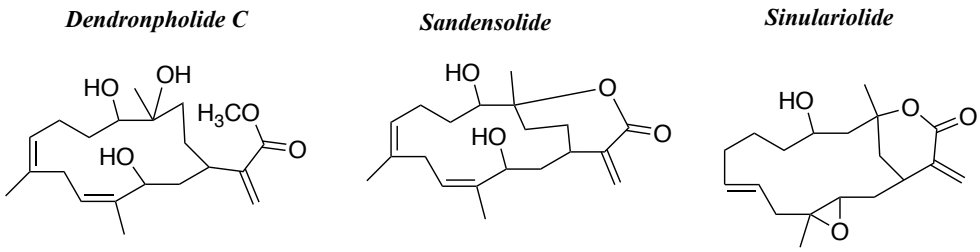

Figure 62: Pure compounds isolated from HPLC fraction CFRP3

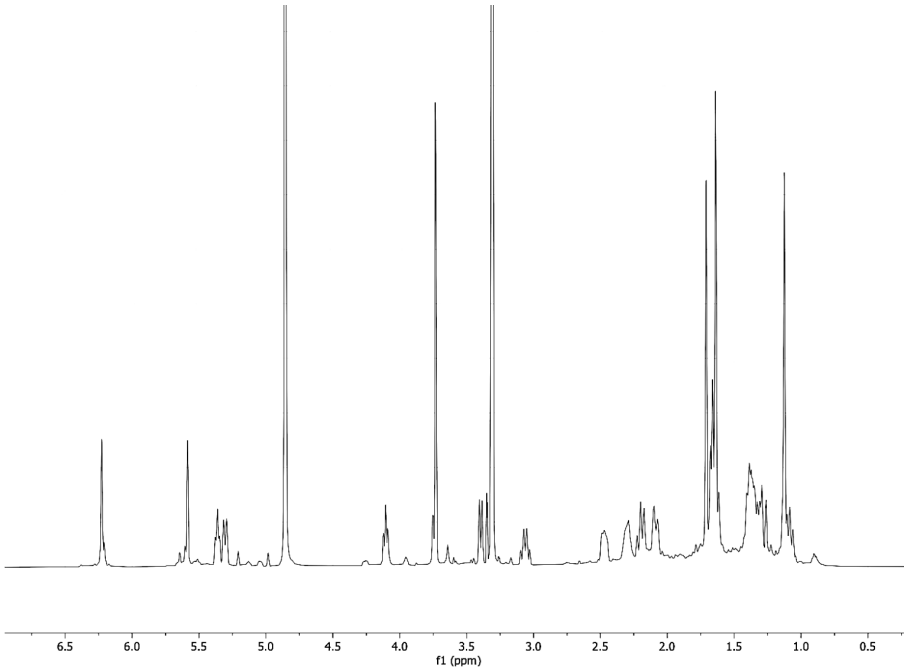

Figure 63: ^{1}H-NMR (500MHz, CD_3OD) spectrum of Dendronpholide C

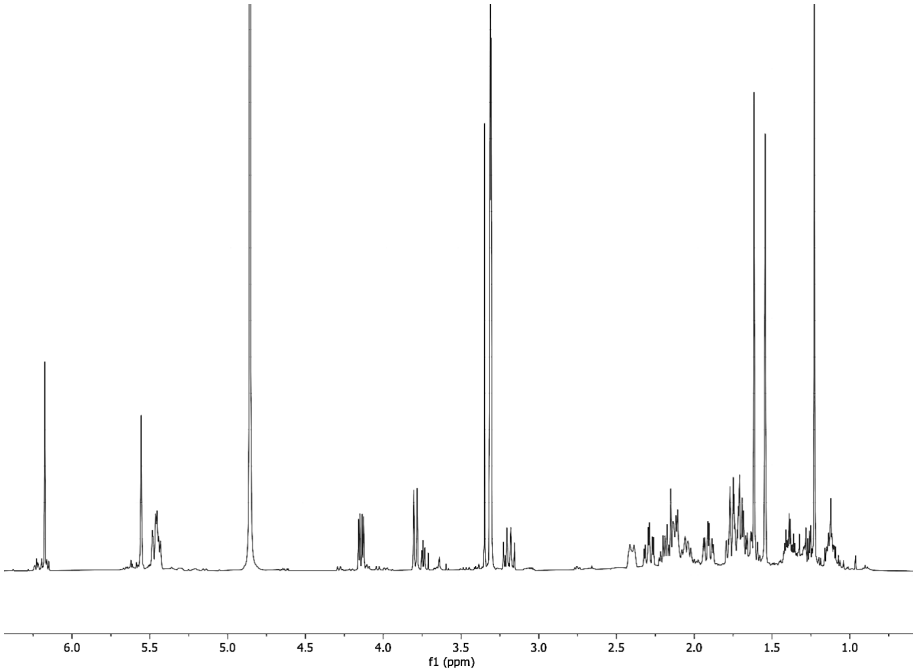

Figure 64: ^{1}H-NMR (500MHz, CD_3OD) spectrum of Sandensolide

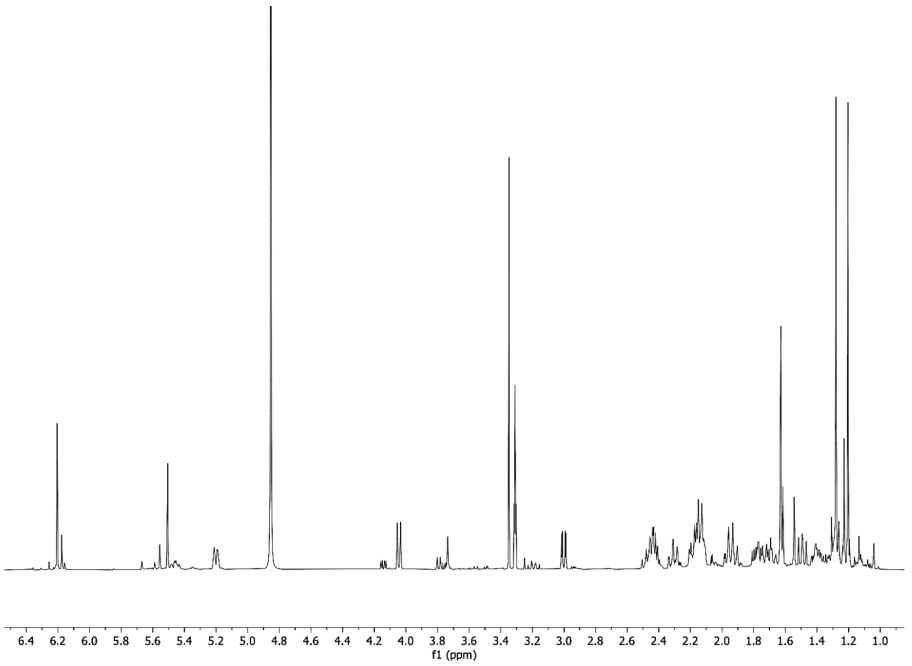

Figure 65: ^{1}H-NMR (500MHz, CD_3OD) spectrum of Sinulariolide

The same procedure was applied also for the fractions obtained with the HPLC purification of the fraction CFRP4 (FIGURE 66), even in this case three pure compounds were isolated in three different fractions: RP4-H1, RP4-H2 and RP4-H3.

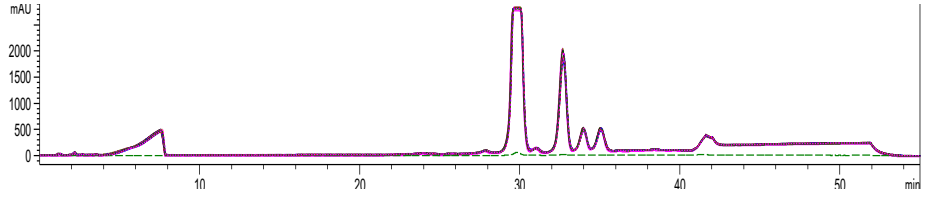

Figure 66: HPLC profile of CFRP4

Comparing our NMR data with the literature we identified three different cembranoids (FIGURE 67-70) in each fraction: Dendronpholide F, 11-epi-sinulariolide acetate and 11-epi-sinulariolide. All the structural hypothesis were also confirmed by the HRESI-MS spectrum showing respectively a major peak at m/z= 415.22 $[M-H_2O+Na]^+$ (calcd. for *m/z*$[M+Na]^+$ 433.2196) in agreement with the molecular formula $C_{22}H_{34}O_7$ (calcd. for *m/z* 410.23) for Dendronpholide F; a major peak at m/z= 399.22 $[M+Na]^+$ (calcd. for *m/z* 399.2142) in agreement with the molecular formula $C_{22}H_{32}O_5$ (calcd. for *m/z* 376.2249) for 1-epi-sinulariolide acetate; a major peak at m/z= 355.20 $[M-H_2O+Na]^+$ (calcd. for $[M+Na]^+$ 335.1879) in agreement with the molecular formula $C_{20}H_{28}O_4$ (calcd. for *m/z* 332.1987) for 1-epi-sinulariolide.[126,128]

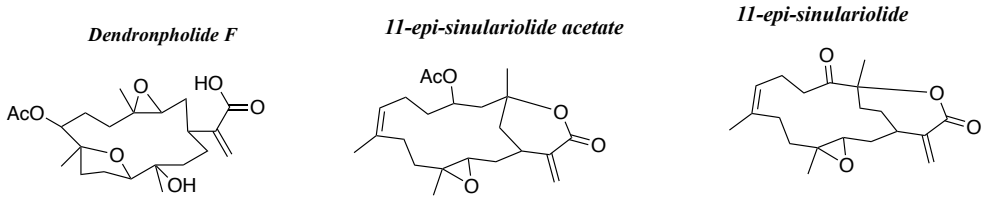

Figure 67: Pure compounds isolated from HPLC fraction CFRP4

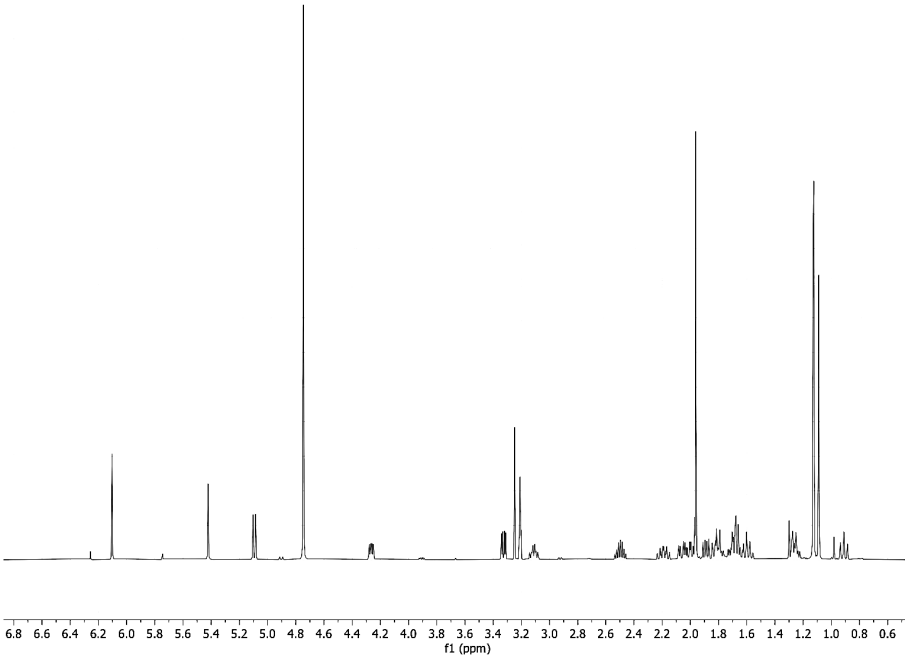

Figure 68: ^{1}H-NMR (500MHz, CD_3OD) spectrum of Dendronpholide F

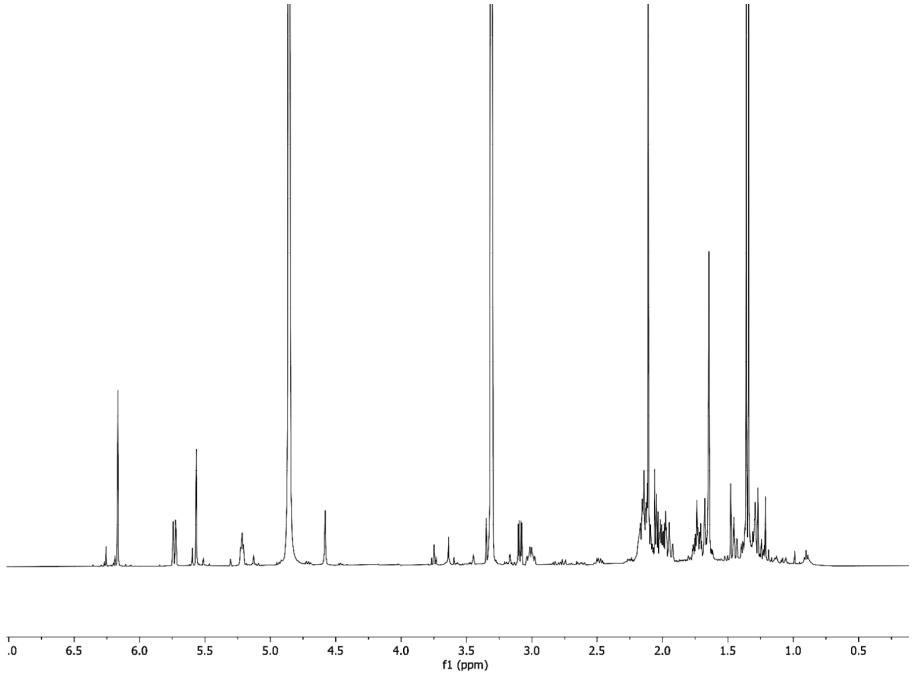

Figure 69: ^{1}H-NMR (500MHz, CD_3OD) spectrum of 1-epi-sinulariolide acetate

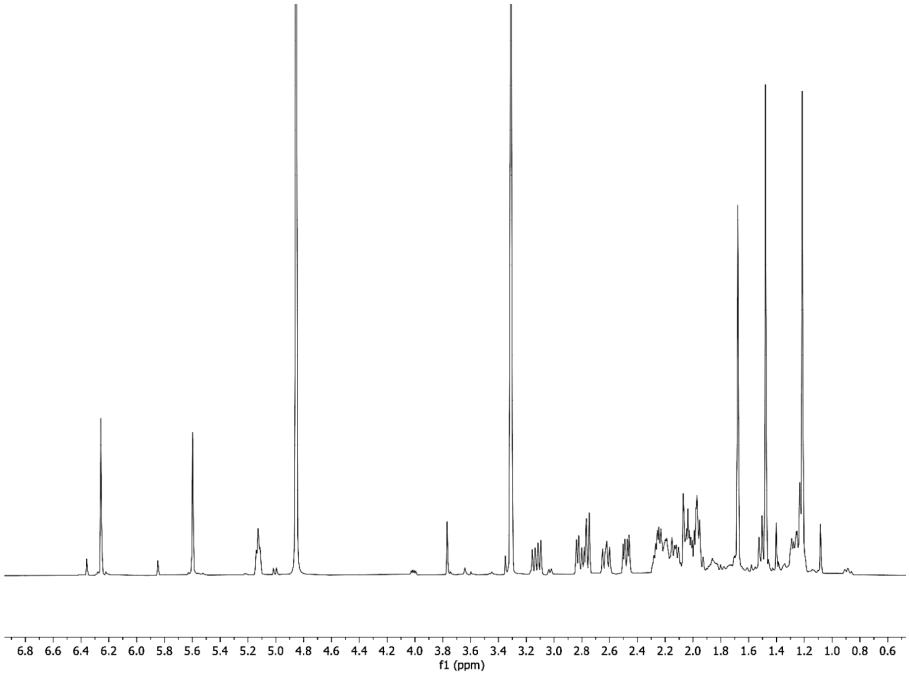

Figure 70: ^{1}H-NMR (500MHz, CD_3OD) spectrum of 1-epi-sinulariolide

5) CONCLUSIONS

This PhD thesis was aimed on identification of marine natural products for the development of immunoceuticals and candidate drugs, in pharmacological and "cosmeceutical" fields. The rationale behind my PhD project was to focus on small molecules that could achieve new "non-conventional" biological roles in the framework of the innate immune system, from marine sources. Moreover, about the cosmeceutical field, given the increased demand of anti-oxidant products, our purpose was to find potential antioxidant activity in microalgal extracts.

For these aims, two different approaches were developed:

- Bioassay-guided approach
- MS-based approach

The bioassay-guided approach was employed for the evaluation of the anti-oxidant activity and the ICD activity. Instead, the chemical approach was dedicated to research of metabolites constituted by specific structural functionalization, correlated to the potential immunomodulant activity.

Anti-oxidant activity: For dermo-cosmetic applications, three marine microalgae extract were analyzed, resulted to have the highest antioxidant property, suggesting the presence of natural products with promising potential as scavenger ingredients. All microalgal extracts exhibited a good scavenging ability in the ABTS assay, but the most promising outcome was obtained with the green microalga *T. chuii*. After fractionation, fraction B of *C. cryptica* showed the best results in DPPH and ORAC assays. Fractions B of *C. cryptica* and *I. galbana*, fractions A and C of *T. chuii* showed a removal of the ABTS radical higher than 90%. Regarding the content of conventional anti-oxidant molecules in each species: the highest phenolic content was found in fractions B and E of *I. galbana*

and fraction E of *T. chuii*; fraction B of *I. galbana* was the richest in carotenoids; the highest vitamin content was found in the fraction E of *T. chuii*. Fraction B of *C. cryptica* yielded the best results as candidate for developments of new natural antioxidants, due to the optimal results showed in the four assays. However, the highest antioxidant property of this fraction did not correlate with conventional antioxidant molecules, such as phenolic or flavonoid compounds, thus suggesting the presence of potential non-conventional scavenging metabolites, as ingredients for cosmeceutical formulations. Starting from these, the upcoming goal will be the deeper investigation of the metabolites presents in the selected enriched fractions and the evaluation of their immunoceuticals properties.

ICD and cytotoxic activity: A bioassay guided fractionation approach, through orthogonal fractionations step, led us to isolated several pure compounds or family of metabolites, from more than 300 different species present in the ICB-CNR library. In this PhD thesis, case studies of three marine species were reported and the lead compounds isolated from them (FIGURE 71):

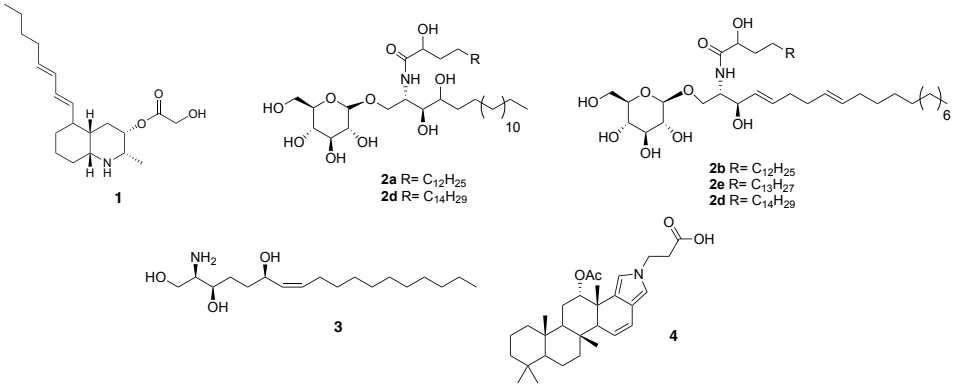

Figure 71: Chemical structure of potential anti-tumour compounds

This allowed us to distinguish how the same work approach led us to obtain molecules with several chemical variability and, most of all, with a different biological activity in the tumor microenvironment (TME). Lepadin A (**1**) works as an immune-based chemotherapy agent, unlike cerebrosides (**2**), halisphingosine (**3**) and Molliorin F (**4**) that act as conventional chemotherapy agents. Thus, showing Lepadin A (**1**) as the best candidate immunogenic anti-cancer drug. Future purposes will be the study of the immune-based effects and the mechanism of action of this potential chemotherapeutic agent.

MS-based approach:

Starting from the need to find new potential bioactive metabolites able to trigger two innate immune system receptors TREM-2 and Dectin-1, we developed a mass-based deconvolution approach. In the first case, guided by the bioassays and by the knowledge of characterized anionic ligands for TREM-2 receptors, we applied a targeted chemical filter searching for sulphur metabolites. Instead, in the second case the chemical filter choice was based entirely by the results of the bioassays.

Sulphur moiety compounds: through the diagnostic fragment in the MS/MS spectrum for both sulphated and sulphonated compounds, we were able to highlight the presence of sulphur compounds in five marine species. Noteworthy, the identification of a family of minoritary metabolites: halo-sulpho lipids, isolated for the first time from *Ophiura Ophiura* species, collected in the Mediterranean Sea. Evaluation of biological activity, as potential TREM2 agonist, are still on going.

Pyridine moiety compounds: the combination of a mass deconvolution approach, through the *MZmine* software, allowed to show the presence of known and unknown structure ascribable to 3-alkypiridines, in the mollusc *Haminoea orbygnana*. Two already reported compounds, such as Haminol-1 (**1)** and Haminol-2 (**2)** and the unknown compound (**3)**, that we suggest to be a dimeric

alkylpyridine. (FIGURE 80) Evaluation of biological activity on Dectin-1 reporter cells are still on going.

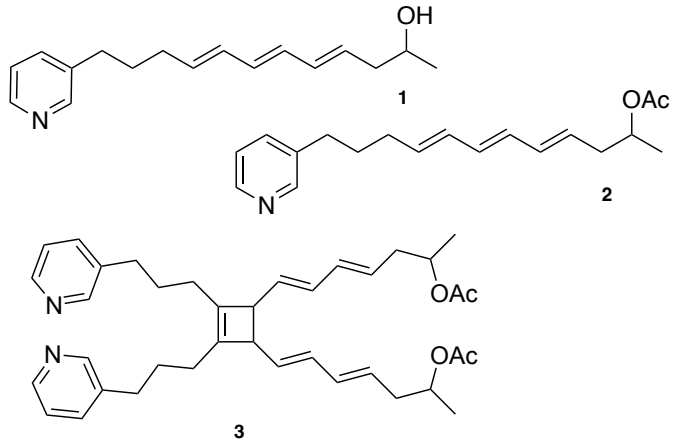

Figure 72: 3-alkylpyridine compounds

According to this PhD project, part of this thesis was developed at the drug discovery leader company Pharmamar S.p.a (Madrid, Spain). According to the company policy, we worked with six marine extracts with a potential cytotoxic activity. In this thesis I can report just six of the sixteen structures isolated (FIGURE 81) and I can't describe the biological activity for all of them, for privacy company reasons.

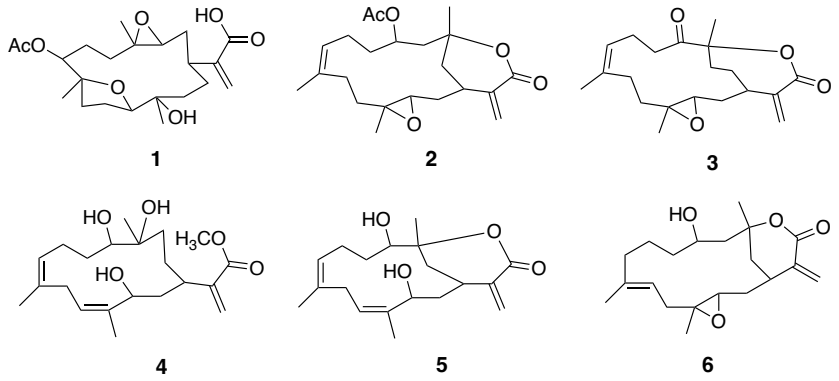

Figure 73: Compounds isolated in Pharmamar company

The results reported in this PhD thesis represent a part of a multidisciplinary research activity, in which chemical and biology aspects must be integrated. Future investigation pathways will be focused on the exploration of known and unknown marine natural products, in the framework of innate immune system, able to modulate immunity response, in a “broad sense”, with novelty mechanism of action.

6) REFERENCES

1. Atanasov, A. G. *et al.* Discovery and resupply of pharmacologically active plant-derived natural products: A review. *Biotechnology Advances* vol. 33 1582–1614 Preprint at https://doi.org/10.1016/j.biotechadv.2015.08.001 (2015).
2. Nuzzo, G. *et al.* Antitumor Potential of Immunomodulatory Natural Products. *Marine Drugs* vol. 20 Preprint at https://doi.org/10.3390/md20060386 (2022).
3. Newman, D. J. & Cragg, G. M. Natural Products as Sources of New Drugs over the Nearly Four Decades from 01/1981 to 09/2019. *Journal of Natural Products* vol. 83 770–803 Preprint at https://doi.org/10.1021/acs.jnatprod.9b01285 (2020).
4. de la Torre, B. G. & Albericio, F. The Pharmaceutical Industry in 2023: An Analysis of FDA Drug Approvals from the Perspective of Molecules. *Molecules* vol. 29 Preprint at https://doi.org/10.3390/molecules29030585 (2024).
5. Al Musaimi, O., Al Shaer, D., Albericio, F. & de la Torre, B. G. 2022 FDA TIDES (Peptides and Oligonucleotides) Harvest. *Pharmaceuticals* **16**, (2023).
6. Cragg, G. M. & Pezzuto, J. M. Natural Products as a Vital Source for the Discovery of Cancer Chemotherapeutic and Chemopreventive Agents. in *Medical Principles and Practice* vol. 25 41–59 (S. Karger AG, 2016).
7. Olsen, E. K. *et al.* Cytotoxic activity of marine sponge extracts from the sub-Antarctic Islands and the Southern Ocean. *S Afr J Sci* **112**, (2016).
8. Parkin, J. & Cohen, B. An overview of the immune system. *Lancet* vol. 357 1777–1789 Preprint at https://doi.org/10.1016/S0140-6736(00)04904-7 (2001).

9. Govardhanagiri, S., Bethi, S. & Nagaraju, G. P. Small Molecules and Pancreatic Cancer Trials and Troubles. in *Breaking Tolerance to Pancreatic Cancer Unresponsiveness to Chemotherapy* 117–131 (Elsevier, 2019). doi:10.1016/b978-0-12-817661-0.00008-1.
10. Tan, L. T. Impact of Marine Chemical Ecology Research on the Discovery and Development of New Pharmaceuticals. *Marine Drugs* vol. 21 Preprint at https://doi.org/10.3390/md21030174 (2023).
11. Lu, W. Y., Li, H. J., Li, Q. Y. & Wu, Y. C. Application of marine natural products in drug research. *Bioorg Med Chem* **35**, (2021).
12. Banday, A. H. *et al.* Exploring the potential of marine natural products in drug development: A comprehensive review. *Phytochem Lett* **59**, 124–135 (2024).
13. Molinski, T. F., Dalisay, D. S., Lievens, S. L. & Saludes, J. P. Drug development from marine natural products. *Nature Reviews Drug Discovery* vol. 8 69–85 Preprint at https://doi.org/10.1038/nrd2487 (2009).
14. Grey, J. L. & Thompson, D. H. Challenges and opportunities for new protein crystallization strategies in structure-based drug design. *Expert Opinion on Drug Discovery* vol. 5 1039–1045 Preprint at https://doi.org/10.1517/17460441.2010.515583 (2010).
15. Faulkner, D. J. *Marine Pharmacology*. *Antonie van Leeuwenhoek* vol. 77 (2000).
16. Liang, X., Luo, D. & Luesch, H. Advances in exploring the therapeutic potential of marine natural products. *Pharmacological Research* vol. 147 Preprint at https://doi.org/10.1016/j.phrs.2019.104373 (2019).
17. Ghareeb, M. A., Tammam, M. A., El-Demerdash, A. & Atanasov, A. G. Insights about clinically approved and Preclinically

investigated marine natural products. *Current Research in Biotechnology* vol. 2 88–102 Preprint at https://doi.org/10.1016/j.crbiot.2020.09.001 (2020).

18. Espinosa-Leal, C. A. & Garcia-Lara, S. Current Methods for the Discovery of New Active Ingredients from Natural Products for Cosmeceutical Applications. *Planta Medica* vol. 85 535–551 Preprint at https://doi.org/10.1055/a-0857-6633 (2019).
19. Rotter, A. *et al.* Marine cosmetics and the blue bioeconomy: From sourcing to success stories. *iScience* vol. 27 Preprint at https://doi.org/10.1016/j.isci.2024.111339 (2024).
20. Thiyagarasaiyar, K., Goh, B. H., Jeon, Y. J. & Yow, Y. Y. Algae metabolites in cosmeceutical: An overview of current applications and challenges. *Marine Drugs* vol. 18 Preprint at https://doi.org/10.3390/md18060323 (2020).
21. Valacchi, G. *et al.* Vitamin C compound mixtures prevent ozone-induced oxidative damage in human keratinocytes as initial assessment of pollution protection. *PLoS One* **10**, (2015).
22. Scaglioni, P. T. *et al.* Inhibition of enzymatic and oxidative processes by phenolic extracts from Spirulina sp. and Nannochloropsis sp. *Food Technol Biotechnol* **56**, 344–353 (2018).
23. Coulombier, N., Jauffrais, T. & Lebouvier, N. Antioxidant compounds from microalgae: A review. *Marine Drugs* vol. 19 Preprint at https://doi.org/10.3390/md19100549 (2021).
24. Sansone, C. *et al.* The green microalga Tetraselmis suecica reduces oxidative stress and induces repairing mechanisms in human cells. *Sci Rep* **7**, (2017).
25. Sansone, C. & Brunet, C. Promises and challenges of microalgal antioxidant production. *Antioxidants* **8**, (2019).

26. Anand, U. *et al.* Cancer chemotherapy and beyond: Current status, drug candidates, associated risks and progress in targeted therapeutics. *Genes and Diseases* vol. 10 1367–1401 Preprint at https://doi.org/10.1016/j.gendis.2022.02.007 (2023).
27. Tsung, K. & Norton, J. A. Lessons from Coley's Toxin. *Surg Oncol* **15**, 25–28 (2006).
28. Hodi, F. S. *et al.* Improved Survival with Ipilimumab in Patients with Metastatic Melanoma. *New England Journal of Medicine* **363**, 711–723 (2010).
29. Topalian, S. L. *et al.* Safety, Activity, and Immune Correlates of Anti–PD-1 Antibody in Cancer. *New England Journal of Medicine* **366**, 2443–2454 (2012).
30. Vasievich, E. A. & Huang, L. The suppressive tumor microenvironment: A challenge in cancer immunotherapy. *Molecular Pharmaceutics* vol. 8 635–641 Preprint at https://doi.org/10.1021/mp1004228 (2011).
31. Wu, Y., Yang, Z., Cheng, K., Bi, H. & Chen, J. Small molecule-based immunomodulators for cancer therapy. *Acta Pharmaceutica Sinica B* vol. 12 4287–4308 Preprint at https://doi.org/10.1016/j.apsb.2022.11.007 (2022).
32. Trenn, ', G., Pettit, G. R., Takayahm, H., Hu-Li, J. & Sitkovskf, M. V. *IMMUNOMODULATING PROPERTIES OF A NOVEL PROTEIN KINASE C ACTIVATORS SERIES OF The Bryostatins*. *THE JOURNAL OF lMMUROLOGY* http://journals.aai.org/jimmunol/article-pdf/140/2/433/1038828/433.pdf.
33. Cooper, E. L. & Yao, D. Diving for drugs: Tunicate anticancer compounds. *Drug Discovery Today* vol. 17 636–648 Preprint at https://doi.org/10.1016/j.drudis.2012.02.006 (2012).

34. Gallo, C. *et al.* A New Bioassay Platform Design for the Discovery of Small Molecules with Anticancer Immunotherapeutic Activity. *Mar Drugs* **18**, (2020).
35. Ahmad, B., Shah, M. & Choi, S. Oceans as a source of immunotherapy. *Marine Drugs* vol. 17 Preprint at https://doi.org/10.3390/md17050282 (2019).
36. Bracci, L., Schiavoni, G., Sistigu, A. & Belardelli, F. Immune-based mechanisms of cytotoxic chemotherapy: Implications for the design of novel and rationale-based combined treatments against cancer. *Cell Death and Differentiation* vol. 21 15–25 Preprint at https://doi.org/10.1038/cdd.2013.67 (2014).
37. De Ridder, T., Reddell, P., Jones, P., Brown, G. & Campbell, J. Tigilanol Tiglate-Mediated Margins: A Comparison With Surgical Margins in Successful Treatment of Canine Mast Cell Tumours. *Front Vet Sci* **8**, (2021).
38. De Ridder, T., Ruppin, M., Wheeless, M., Williams, S. & Reddell, P. Use of the Intratumoural Anticancer Drug Tigilanol Tiglate in Two Horses. *Front Vet Sci* **7**, (2020).
39. Schcolnik-Cabrera, A. *et al.* Calreticulin in phagocytosis and cancer: opposite roles in immune response outcomes. *Apoptosis* vol. 24 245–255 Preprint at https://doi.org/10.1007/s10495-019-01532-0 (2019).
40. Fucikova, J. *et al.* Detection of immunogenic cell death and its relevance for cancer therapy. *Cell Death and Disease* vol. 11 Preprint at https://doi.org/10.1038/s41419-020-03221-2 (2020).
41. Lichtman, A. H. *Basic Immunology: Functions and Disorders of the Immune System*. (2009).
42. Janeway, C. et al. *Immunobiology: The Immune System in Health and Disease.* . vol. 2 (New York, 2001).

43. Corthay, A. How do regulatory t cells work? *Scandinavian Journal of Immunology* vol. 70 326–336 Preprint at https://doi.org/10.1111/j.1365-3083.2009.02308.x (2009).
44. Unanue, E. R. Perspective on antigen processing and presentation. *Immunological Reviews* vol. 185 86–102 Preprint at https://doi.org/10.1034/j.1600-065X.2002.18510.x (2002).
45. Steinman:~, R. M. & Cohn, Z. A. *I D E N T I F I C A T I O N OF A NOVEL CELL T Y P E I N P E R I P H E R A L L Y M P H O I D ORGANS OF M I C E * II. FUNCTIONAL PROPERTIES IN VITRO*.
46. Van Brussel, I., Berneman, Z. N. & Cools, N. Optimizing dendritic cell-based immunotherapy: Tackling the complexity of different arms of the immune system. *Mediators of Inflammation* vol. 2012 Preprint at https://doi.org/10.1155/2012/690643 (2012).
47. Goubier, A. *et al.* Plasmacytoid Dendritic Cells Mediate Oral Tolerance. *Immunity* **29**, 464–475 (2008).
48. Montuori, E., de Pascale, D. & Lauritano, C. Recent Discoveries on Marine Organism Immunomodulatory Activities. *Marine Drugs* vol. 20 Preprint at https://doi.org/10.3390/md20070422 (2022).
49. Drummond, R. A. & Brown, G. D. The role of Dectin-1 in the host defence against fungal infections. *Current Opinion in Microbiology* vol. 14 392–399 Preprint at https://doi.org/10.1016/j.mib.2011.07.001 (2011).
50. Hardison, S. E. & Brown, G. D. C-type lectin receptors orchestrate antifungal immunity. *Nature Immunology* vol. 13 817–822 Preprint at https://doi.org/10.1038/ni.2369 (2012).
51. Lefèvre, L. *et al.* The C-type Lectin Receptors Dectin-1, MR, and SIGNR3 Contribute Both Positively and Negatively to the

Macrophage Response to Leishmania infantum. *Immunity* **38**, 1038–1049 (2013).

52. Zhao, Y. *et al.* Dectin-1-activated dendritic cells trigger potent antitumour immunity through the induction of Th9 cells. *Nat Commun* **7**, (2016).
53. Chen, J. *et al.* Dectin-1-activated dendritic cells: A potent Th9 cell inducer for tumor immunotherapy. *Oncoimmunology* **5**, (2016).
54. Zhao, X. *et al.* β-amyloid binds to microglia Dectin-1 to induce inflammatory response in the pathogenesis of Alzheimer's disease. *Int J Biol Sci* **19**, 3249–3265 (2023).
55. Kober, D. L. & Brett, T. J. TREM2-Ligand Interactions in Health and Disease. *Journal of Molecular Biology* vol. 429 1607–1629 Preprint at https://doi.org/10.1016/j.jmb.2017.04.004 (2017).
56. Balducci, C. & Forloni, G. Novel targets in Alzheimer's disease: A special focus on microglia. *Pharmacological Research* vol. 130 402–413 Preprint at https://doi.org/10.1016/j.phrs.2018.01.017 (2018).
57. Song, W. *et al.* Alzheimer's disease-associated TREM2 variants exhibit either decreased or increased ligand-dependent activation. *Alzheimer's and Dementia* **13**, 381–387 (2017).
58. Daws, M. R. *et al.* Pattern Recognition by TREM-2: Binding of Anionic Ligands. *The Journal of Immunology* **171**, 594–599 (2003).
59. Manzo, E. *et al.* Chemical synthesis of marine-derived sulfoglycolipids, a new class of molecular adjuvants. *Mar Drugs* **15**, (2017).
60. Gallo, C. *et al.* Sulfavant A as the first synthetic TREM2 ligand discloses a homeostatic response of dendritic cells after receptor engagement. *Cellular and Molecular Life Sciences* **79**, (2022).

61. Nuzzo Genoveffa et al. *Fractionation Protocol of Marine Metabolites." Marine Genomics: Methods and Protocols.* . (New York, 2022).
62. Cutignano, A. *et al.* Development and application of a novel SPE-method for bioassay-guided fractionation of marine extracts. *Mar Drugs* **13**, 5736–5749 (2015).
63. Brand-Williams, W., Cuvelier, M. E. & Berset, C. *Use of a Free Radical Method to Evaluate Antioxidant Activity*. vol. 28 (1995).
64. Stengel, D. B. , & C. S. *Natural Products from Marine Algae: Methods and Protocols. Natural Products From Marine Algae: Methods and Protocols*. (2015).
65. Huang, D., Boxin, O. U. & Prior, R. L. The chemistry behind antioxidant capacity assays. *Journal of Agricultural and Food Chemistry* vol. 53 1841–1856 Preprint at https://doi.org/10.1021/jf030723c (2005).
66. Iverson, S. J. , S. L. L. and M. H. C. Comparison of the Bligh and Dyer and Folch methods for total lipid determination in a broad range of marine tissue. *Lipids* 1283–1287 (2011).
67. Fischer, J., Treblin, M., Sitz, T. & Rohn, S. Development of a targeted HPLC-ESI-QqQ-MS/MS method for the quantification of sulfolipids from a cyanobacterium, selected leafy vegetables, and a microalgae species. doi:10.1007/s00216-021-03164-3/Published.
68. Lopalco, P. *et al.* Alteration of Cholesterol Sulfate/Seminolipid Ratio in Semen Lipid Profile of Men With Oligoasthenozoospermia. *Front Physiol* **10**, (2019).
69. Kessner, D., Chambers, M., Burke, R., Agus, D. & Mallick, P. ProteoWizard: Open source software for rapid proteomics tools development. *Bioinformatics* **24**, 2534–2536 (2008).

70. McMullin, D. R., Hoogstra, S., McDonald, K. P., Sumarah, M. W. & Renaud, J. B. Natural Product Discovery with LC-MS/MS Diagnostic Fragmentation Filtering: Application for Microcystin Analysis. *Journal of Visualized Experiments* **2019**, (2019).
71. Tan, D. *et al.* A class of anti-inflammatory lipids decrease with aging in the central nervous system. *Nat Chem Biol* **19**, 187–197 (2023).
72. Spinella, A., Alvarez, L. A., Passeggio, A. & Cimino, G. *New 3-Alkylpyridines from Three Mediterranean Cephalaspidean Molluscs: Structure, Ecological Role and Taxonomic Relevance*. vol. 49 (1993).
73. Sadeer, N. B., Montesano, D., Albrizio, S., Zengin, G. & Mahomoodally, M. F. The versatility of antioxidant assays in food science and safety—chemistry, applications, strengths, and limitations. *Antioxidants* vol. 9 1–39 Preprint at https://doi.org/10.3390/antiox9080709 (2020).
74. Benzie, I. F. F. & Strain, J. J. *The Ferric Reducing Ability of Plasma (FRAP) as a Measure of ‘“Antioxidant Power”’: The FRAP Assay*. *ANALYTICAL BIOCHEMISTRY* vol. 239 (1996).
75. Zulueta, A., Esteve, M. J. & Frígola, A. ORAC and TEAC assays comparison to measure the antioxidant capacity of food products. *Food Chem* **114**, 310–316 (2009).
76. Jeong, S., Jung, J. H., Jung, K. W., Ryu, S. & Lim, S. From microbes to molecules: a review of microbial-driven antioxidant peptide generation. *World Journal of Microbiology and Biotechnology* vol. 40 Preprint at https://doi.org/10.1007/s11274-023-03826-7 (2024).
77. Manzo, E. *et al.* Immunostimulatory Phosphatidylmonogalactosyldiacylglycerols (PGDG) from the

marine diatom Thalassiosira weissflogii: Inspiration for a novel synthetic toll-like receptor 4 agonist. *Mar Drugs* **17**, (2019).

78. Manzo, E. *et al.* A new marine-derived sulfoglycolipid triggers dendritic cell activation and immune adjuvant response. *Sci Rep* **7**, (2017).
79. Casertano, M., Menna, M. & Imperatore, C. The ascidian-derived metabolites with antimicrobial properties. *Antibiotics* vol. 9 1–30 Preprint at https://doi.org/10.3390/antibiotics9080510 (2020).
80. Raub, M. F. , et al. Clavepictines A and B: cytotoxic quinolizidines from the tunicate Clavelina picta. in *Journal of the American Chemical Society* 3178–3180 (1991).
81. Steffan, B. *LEPADIN A, A DECAHYDROQUINOLINE ALKALOID FROM THE TUNICATE CLAVELINA LEPADIFORMIS*. *Tetrahedron* vol. 41 (1991).
82. Kubanek, J., Williams, D. E., Dilip De Silva, E., Allen, T. & Andersen, R. J. *Cytotoxic Alkaloids from the Flatworm Prostheceraeus Villatus and Its Tunicate Prey Clavelina Lepadiformis*. *Tetrahedron Letters* vol. 36 (1995).
83. Wright, A. D., Goclik, E., König, G. M. & Kaminsky, R. Lepadins D-F: Antiplasmodial and antitrypanosomal decahydroquinoline derivatives from the tropical marine tunicate Didemnum sp. *J Med Chem* **45**, 3067–3072 (2002).
84. Davis, R. A., Carroll, A. R. & Quinn, R. J. Lepadins F-H, new cis-decahydroquinoline alkaloids from the Australian ascidian Aplidium tabascum. *J Nat Prod* **65**, 454–457 (2002).
85. Ómarsdóttir, S., Wang, X., Liu, H. B., Duggan, B. M. & Molinski, T. F. Lepadins I-K, 3- O-(3′-Methylthio)acryloyloxy-decahydroquinoline Esters from a Bahamian Ascidian Didemnum

sp. Assignment of Absolute Stereostructures. *Journal of Organic Chemistry* **83**, 13670–13677 (2018).

86. Nuzzo, G. *et al.* Identification of the Marine Alkaloid Lepadin A as Potential Inducer of Immunogenic Cell Death. *Biomolecules* **12**, (2022).
87. Bezu, L. *et al.* Combinatorial strategies for the induction of immunogenic cell death. *Frontiers in Immunology* vol. 6 Preprint at https://doi.org/10.3389/fimmu.2015.00187 (2015).
88. Wang, Y. J., Fletcher, R., Yu, J. & Zhang, L. Immunogenic effects of chemotherapy-induced tumor cell death. *Genes and Diseases* vol. 5 194–203 Preprint at https://doi.org/10.1016/j.gendis.2018.05.003 (2018).
89. Del Prete, A. *et al.* Dendritic cell subsets in cancer immunity and tumor antigen sensing. *Cellular and Molecular Immunology* vol. 20 432–447 Preprint at https://doi.org/10.1038/s41423-023-00990-6 (2023).
90. Carbone, D. *et al.* Marine natural product lepadin A as a novel inducer of immunogenic cell death via CD91-dependent pathway. *Nat Prod Bioprospect* **13**, (2023).
91. Li, K. and K. R. G. Sesterterpenoids: chemistry, biology, and biosynthesis. in *Natural Product Reports* 1251–1281 (2021).
92. De Stefano, D. *et al.* Cacospongionolide and scalaradial, two marine sesterterpenoids as potent apoptosis-inducing factors in human carcinoma cell lines. *PLoS One* **7**, (2012).
93. De Rosa, S. S. D. S. and N. Z. Cacospongionolide. A new antitumoral sesterterpene, from the marine sponge Cacospongia mollior. *J Org Chem* 5020–5023 (1988).

94. Fattorusso, E., Magno, S., Sa~jtacr~ce, C. & Sica, D. *SCALARIN, A NEW PENTACYCLIC C-25 TERPENOID FROM THE SPONGE CACOSPONGIA SCALAR19*. *Tetrahedron* vol. 28.
95. Cafieri, F., De Napoli, L., Fattorusso, E. & Santacroce, C. *Specialia EXPERIENTIA 33/8 Molliorin-B, a Second Scalarin-like Pyrroloterpene from the Sponge Cacospongia Mollior 1*.
96. Cafieri, F., De Napoli, L., Iengo, A. & Santacroce, C. *Specialia EXPERIENTIA 34/3 Molliorin-e, a Further Pyrroloterpene Present in the Sponge Cacospongia Mollior 1*.
97. Cafieri, F., De Napoli, L., Iengo, A. & Santacroce, C. *Minor Pyrroloterpenoids from the Marine Sponge Cacospongia Mollior I*.
98. Federico, S. *et al.* Identification of the New Cytotoxic Pyrrole-Terpene Molliorin F from the Mediterranean Sponge Cacospongia Mollior. *Journal of Biotechnology and Biomedicine* **7**, (2024).
99. Kumar, M. S. Chemical Constituents and Anti-inflammatory Properties of the Marine Sponge Haliclona cratera from Konkan, India. *Russ J Mar Biol* **48**, 285–296 (2022).
100. Mansoor, T. A. *et al.* Renierosides, cerebrosides from a marine sponge Haliclona (Reniera) sp. *J Nat Prod* **70**, 1481–1486 (2007).
101. Park, T. *et al. New Cerebrosides from a Marine Sponge Haliclona (Reniera) Sp*. *Chem. Pharm. Bull* vol. 57 (2009).
102. Ruocco, N. *et al.* Potential of Polar Lipids Isolated from the Marine Sponge Haliclona (Halichoclona) vansoesti against Melanoma. *Int J Mol Sci* **25**, (2024).
103. Biegelmeye, R. *et al.* Sphingosines derived from marine sponge as potential multi-target drug related to disorders in cancer development. *Mar Drugs* **13**, 5552–5563 (2015).

104. Careaga, V. P. & Maier, M. S. Cerebrosides from Marine Organisms. in 59–81 (2014). doi:10.1016/b978-0-444-63281-4.00003-3.

105. Nadar, V. M., Manivannan, S., Chinnaiyan, R., Govarthanan, M. & Ponnuchamy, K. Review on marine sponge alkaloid, aaptamine: A potential antibacterial and anticancer drug. *Chemical Biology and Drug Design* vol. 99 103–110 Preprint at https://doi.org/10.1111/cbdd.13932 (2022).

106. Thakur, N., Choudhary, P., Kaushik, N. & Sharma, A. A review on pharmacological and pharmaceutical properties of Genus Stelletta from Marine Sponges. in *Materials Today: Proceedings* vol. 81 1034–1039 (Elsevier Ltd, 2021).

107. Roman, D. *et al.* Structure Revision of a Widespread Marine Sulfonolipid Class Based on Isolation and Total Synthesis. *Angewandte Chemie - International Edition* **63**, (2024).

108. Nuzzo, G. *et al.* Isolation of Chamigrene Sesquiterpenes and Absolute Configuration of Isoobtusadiene from the Brittle Star Ophionereis reticulata. *J Nat Prod* **80**, 3049–3053 (2017).

109. Fedorov, S. N., Levina, E. V, Kalinovsky, A. I., Dmitrenok, P. S. & Stonik, V. A. *SULFATED STEROIDS FROM PACIFIC BRITTLE STARS OPHIOPHOLIS ACULEATA, OPHIURA SARSI, AND STEGOPHIURA BRACHIACTIS*. *Journal of Natural Products* vol. 57 https://pubs.acs.org/sharingguidelines (1994).

110. Valeria, M. D., Gomez Paloma, L., Mínale, L., Riccio, R. & Zampella, A. *ON THE COMPOSITION OF SULFATED POLYHYDROXYSTEROIDS IN SOME OPHIUROIDS AND THE STRUCTURE DETERMINATION OF SIX NEW CONSTITUENTS*. *Journal of Natural Products* vol. 58 https://pubs.acs.org/sharingguidelines (1995).

111. Klimenko, A. *et al.* Shallow- and Deep-Water Ophiura Species Produce a Panel of Chlorin Compounds with Potent Photodynamic Anticancer Activities. *Antioxidants* **12**, (2023).
112. Haines, T. H. , et al. Microbial sulpholipids:(R)-13-choro-1-(R)-14-docosanediol disulphate and polychlorosulpholipids in Ochromonas danica. *Biochemical Journal* (1969).
113. Elovson, J. and P. R. V. A new class of lipids: Chlorosulfolipids. in *Proceedings of the National Academy of Sciences* 957–963 (1969).
114. White, A. R., Duggan, B. M., Tsai, S. C. & Vanderwal, C. D. The Alga Ochromonas danica Produces Bromosulfolipids. *Org Lett* **18**, 1124–1127 (2016).
115. Cutignano, A., Cimino, G., Giordano, A., D'Ippolito, G. & Fontana, A. Polyketide origin of 3-alkylpyridines in the marine mollusc Haminoea orbignyana. *Tetrahedron Lett* **45**, 2627–2629 (2004).
116. Cimino, G., Passeggio, A., Sodano, G., Spinella, A. & Villani, G. *Alarm Pheromones from the Mediterranean Opisthobranch Haminoea Navicula i 61*. *Research Articles Experientia* vol. 47 (1991).
117. Epifanio, N. M. et al. Systematic Review of Chemical and Biological Activity Studies of Extracts and Isolated Compounds from Nudibranchs. (2023).
118. Cutignano, A. *et al.* Fusaripyrones, novel polypropionates from the Mediterranean mollusc Haminoea fusari. *Tetrahedron* **63**, 12935–12939 (2007).
119. Cimino G. et al al. Metabolites of marine opisthobranchs: chemistry and biological activity. in (ed. Taylor and Francis) 577–637 (London, 2001).

120. Elcombe, S. E. *et al.* Dectin-1 Regulates IL-10 Production via a MSK1/2 and CREB Dependent Pathway and Promotes the Induction of Regulatory Macrophage Markers. *PLoS One* **8**, (2013).
121. Dillon, S. *et al.* Yeast zymosan, a stimulus for TLR2 and dectin-1, induces regulatory antigen-presenting cells and immunological tolerance. *Journal of Clinical Investigation* **116**, 916–928 (2006).
122. Slack, E. C. *et al.* Syk-dependent ERK activation regulates IL-2 and IL-10 production by DC stimulated with zymosan. *Eur J Immunol* **37**, 1600–1612 (2007).
123. Einarsdottir, E. *et al.* Metabolic profiling as a screening tool for cytotoxic compounds: Identification of 3-alkyl pyridine alkaloids from sponges collected at a shallow water hydrothermal vent site North of Iceland. *Mar Drugs* **15**, (2017).
124. Campuzano, I. *et al.* Structural characterization of drug-like compounds by ion mobility mass spectrometry: Comparison of theoretical and experimentally derived nitrogen collision cross sections. *Anal Chem* **84**, 1026–1033 (2012).
125. Dodds, J. N. & Baker, E. S. Ion Mobility Spectrometry: Fundamental Concepts, Instrumentation, Applications, and the Road Ahead. *J Am Soc Mass Spectrom* **30**, 2185–2195 (2019).
126. Ma, A. *et al.* Dendronpholides A-R, Cembranoid diterpenes from the chinese soft coral Dendronephthya sp. *J Nat Prod* **71**, 1152–1160 (2008).
127. Nguyen, N. B. A. *et al.* Towards Sustainable Medicinal Resources through Marine Soft Coral Aquaculture: Insights into the Chemical Diversity and the Biological Potential. *Marine Drugs* vol. 20 Preprint at https://doi.org/10.3390/md20100640 (2022).

128. Su, J.-H. *et al. Oxygenated Cembranoids from the Cultured and Wild-Type Soft Corals Sinularia Flexibilis*. *Chem. Pharm. Bull* vol. 57 (2009).

7) SUPPLEMENTARY MATERIAL

	500µg/mL	1000µg/mL	2000 µg/mL
EXT	23,98 ± 1,80	16,32 ± 1,47	0 ± 0
	125µg/mL	250µg/mL	500µg/mL
A	5,00 ± 0,56 %	9,68 ± 0,56 %	23,59 ± 0,48%
B	23,65 ± 4,67%	21,58 ± 0,30 %	13,03 ± 0,43 %
C	7,15 ± 1,30 %	13,78 ± 0,10%	21,79 ± 0,81%
D	7,00 ± 0,04 %	10,18 ± 0,02 %	15,11 ± 1,17 %
E	14,95 ± 0,63 %	16,56 ± 0,86 %	19,01 ± 1,10 %

Table S 1: DPPH• assay for T. chuii extracts and HRX-fraction. Values are expressed as mg TE (Trolox Equivalent)/g DS (Dried Sample).

	125µg/mL	250µg/mL	500µg/mL
EXT	88,53 ± 0,01 %	88,25 ± 0,01%	86,21 ± 0,02%
A	56,38 ± 0,27 %	86,62 ± 0,01 %	89,61 ± 0,04%
B	88,32 ± 0,02 %	87,58 ± 0,01 %	86,03 ± 0,03%
C	67,39 ± 0,12 %	89,73 ± 0,01 %	89,29 ± 0,03%
D	75,47 ± 0,01%	91,05 ± 0,01%	91,17 ± 0,03%
E	87,40 ± 0,02%	85,70 ± 0,02 %	82,72 ± 0,04 %

Table S 2: ABTS$^{\bullet+}$ assay for T. chuii extracts and HRX-fractions. Values are expressed as mg TE (Trolox Equivalent)/g DS (Dried Sample).

	500µg/mL	**2000µg/mL**
EXT	290,58 ± 0,64	175,48 ± 6,30
A	57,22 ± 1,65	
B	322,98 ± 5,55	
C	88,56± 0,66	
D	80,25± 1,56	
E	353,90± 31,56	

Table S 3: FRAP assay for T. chuii extracts and HRX-fractions. Values are expressed as mg TE (Trolox Equivalent)/g DS (Dried Sample).

	2000µg/mL
EXT	0,00 ± 0,00
	500µg/mL
A	11,60 ± 0,26
B	1,05 ± 0,05
C	13,16 ± 0,33
D	2,44 ± 0,85
E	0,00 ± 0,00

Table S 4: ORAC assay for T. chuii extracts and HRX-fractions. Values are expressed as mg TE (Trolox Equivalent)/g DS (Dried Sample).

	500µg/mL	1000µg/mL	2000 µg/mL
EXT	23,45 ± 0,81 %	22,91 ± 1,20 %	0,00 ± 0,00 %
	125µg/mL	250µg/mL	500µg/mL
A	14,44 ± 0,22 %	19,79 ± 1,06 %	24,16 ± 0,34 %
B	23,32 ± 1,05 %	36,59 ± 0,41 %	58,91 ± 0,68 %
C	20,93 ± 1,70 %	25,54 ± 1,30%	40,09± 0,81%
D	0,00 ± 0,00%	0,00 ± 0,00%	0,00 ± 0,00%
E	17,16 ± 0,18 %	17,91 ± 0,24 %	21,20 ± 1,22 %

Table S 5: DPPH$^{\bullet}$ assay for C. cryptica extracts and HRX-fraction. Values are expressed as mg TE (Trolox Equivalent)/g DS (Dried Sample).

	125µg/mL	250µg/mL	500µg/mL
EXT	62,29 ± 0,10 %	78,82 ± 0,15 %	89,62 ± 0,02 %
A	21,17 ± 0,23 %	9,90 ± 0,27 %	40,70 ± 0,25 %
B	31,09 ± 0,50 %	52,57 ± 0,53 %	89,54 ± 0,27 %
C	29,36 ± 0,22 %	50,84 ± 0,33 %	87,14 ± 0,69 %
D	63,26 ± 0,14 %	88,22 ± 0,27 %	91,48 ± 0,06 %
E	76,39 ± 0,10 %	85,95 ± 0,02 %	88,27 ± 0,06 %

Table S 6: ABTS$^{\bullet+}$ assay for C. cryptica extracts and HRX-fractions. Values are expressed as mg TE (Trolox Equivalent)/g DS (Dried Sample).

	500µg/mL	2000µg/mL
EXT	238,83 ± 2,04	82,70 ± 2,26
A	19,46 ±0,85	
B	48,88 ± 1,38	
C	64,65 ± 3,30	
D	81, 79 ± 0,05	
E	104,14 ± 3,87	

Table S 7: FRAP assay for C. cryptica extracts and HRX-fractions. Values are expressed as mg TE (Trolox Equivalent)/g DS (Dried Sample).

	2000µg/mL
EXT	0,16 ± 0,03
	500 µg/mL
A	12,60 ± 0,69
B	18,61 ± 0,35
C	19,09 ± 0,82
D	0,00 ± 0,00
E	12,24 ± 0,60

Table S 8: ORAC assay for C. cryptica extracts and HRX-fractions. Values are expressed as mg TE (Trolox Equivalent)/g DS (Dried Sample).

	500µg/mL	1000µg/mL 2000 µg/mL	
EXT	15,10 ± 0,53 %	21,12 ± 0,18 %	0,00 ± 0,00 %
	125µg/mL	250µg/mL	500µg/mL
A	3,19 ± 0,63 %	6,32 ± 0,92 %	10,19 ± 0,49 %
B	9,72 ± 0,43 %	17,14 ± 0,37 %	29,57 ± 0,23 %
C	10,50 ± 0,85 %	22,41 ± 0,18 %	41,37 ± 0,74%
D	1,98 ± 1,04 %	0,00 ± 0,00 %	0,00 ± 0,00 %
E	16,05 ± 1,10 %	19,64 ± 0,24 %	0,00 ± 0,00 %

Table S 9: DPPH˙ assay for I. galbana extracts and HRX-fraction. Values are expressed as mg TE (Trolox Equivalent)/g DS (Dried Sample).

	125µg/mL	250µg/mL	500µg/mL
EXT	54,41 ± 0,07 %	84,63 ± 0,05 %	91,52 ± 0,00 %
A	56,95 ± 0,14 %	78,49 ± 0,19 %	90,60 ± 0,08 %
B	65,99 ± 0,12 %	84,43 ± 0,09 %	91,67 ± 0,02 %
C	56,96 ± 0,07 %	84,60 ± 0,09 %	91,63 ± 0,00 %
D	35,67 ± 0,08 %	67,33 ± 0,05 %	88,20 ± 0,06 %
E	79,58 ± 0,09 %	91,29 ± 0,01 %	90,84 ± 0,02 %

Table S 10: $ABTS^{\bullet+}$ assay for I. galbana extracts and HRX-fractions. Values are expressed as mg TE (Trolox Equivalent)/g DS (Dried Sample).

	500µg/mL	2000µg/mL
EXT	56,72 ± 0,74	44,42 ± 0,79
A	25,40 ± 0,72	
B	45,84 ± 0,56	
C	43,43 ± 0,68	
D	81,16 ± 0,96	
E	81,93 ± 0,18	

Table S 11: FRAP assay for I. galbana extracts and HRX-fractions. Values are expressed as mg TE (Trolox Equivalent)/g DS (Dried Sample).

	2000µg/mL
EXT	0,62 ± 0,05
	500 µg//mL
A	25,48 ± 0,52
B	27,22 ± 0,42
C	19,78± 0,06
D	11,66 ± 0,15
E	3,72 ± 0,19

Table S 12: ORAC assay for C. cryptica extracts and HRX-fractions. Values are expressed as mg TE (Trolox Equivalent)/g DS (Dried Samples)

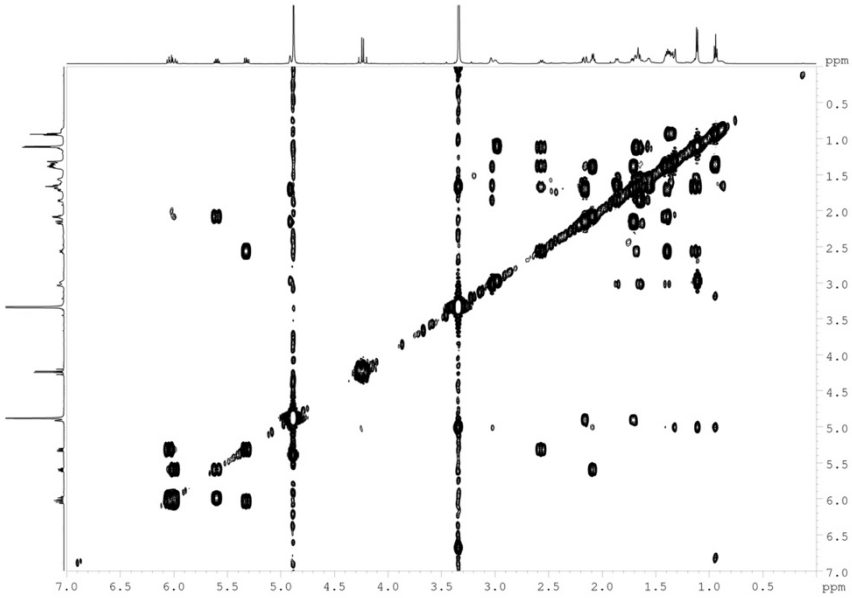

Figure S 13: ^{1}H-^{1}H COSY of Lepadin A (CD_3OD, Brucker 600MHz)

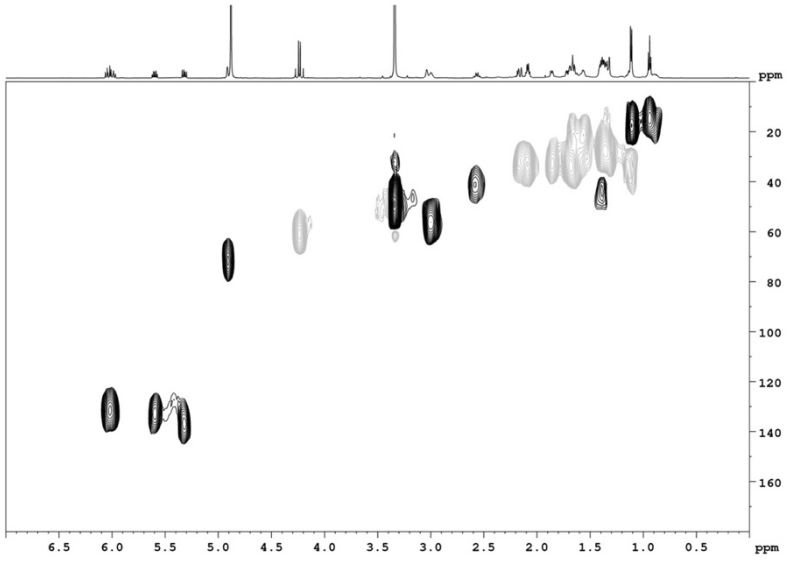

Figure S 14: HSQCed of Lepadin A (CD_3OD, Brucker 600MHz)

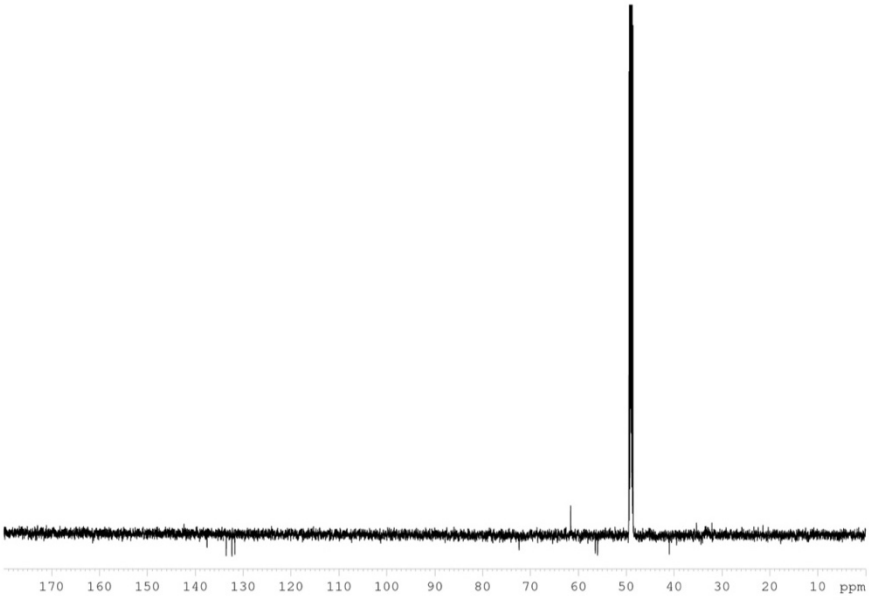

Figure S 15: ^{13}C-jmod of Lepadin A (CD_3OD, Brucker 600MHz)

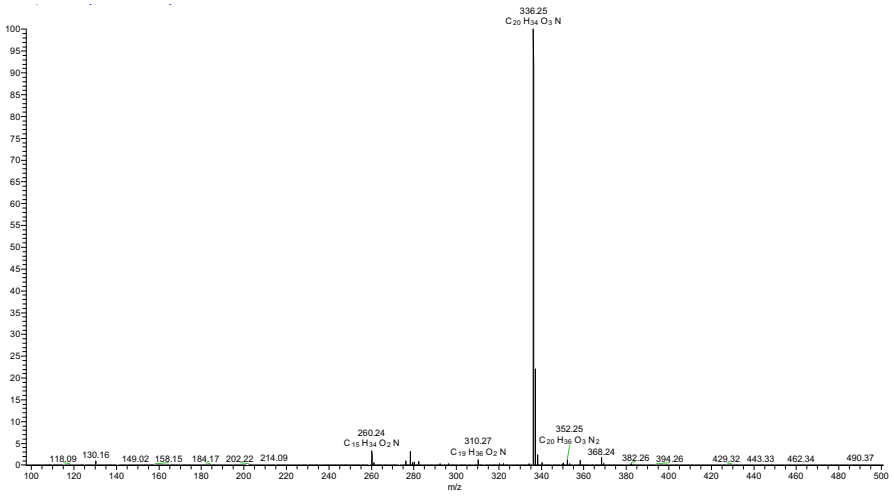

Figure S 16: HRESI-MSMS of Lepadin A

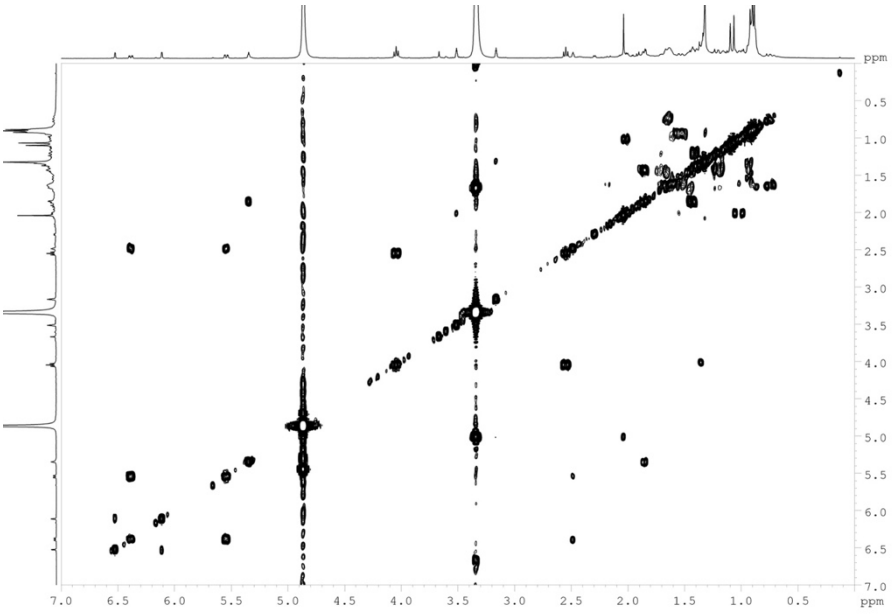

Figure S 27: ^{1}H-^{1}H COSY of Molliorin F (CD_3OD, Brucker 600MHz).

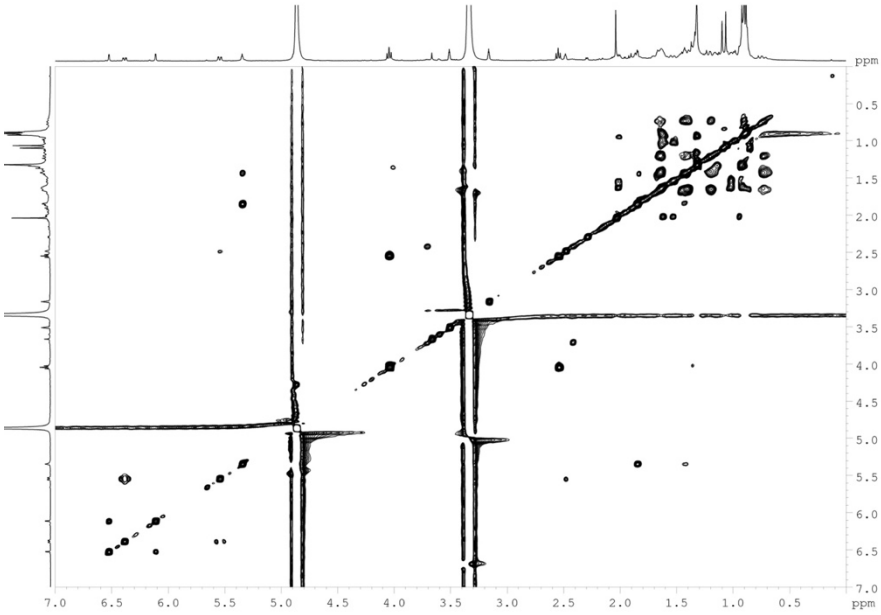

Figure S 18: ^{1}H-^{1}H TOCSY of Molliorin F (CD_3OD, Brucker 600MHz).

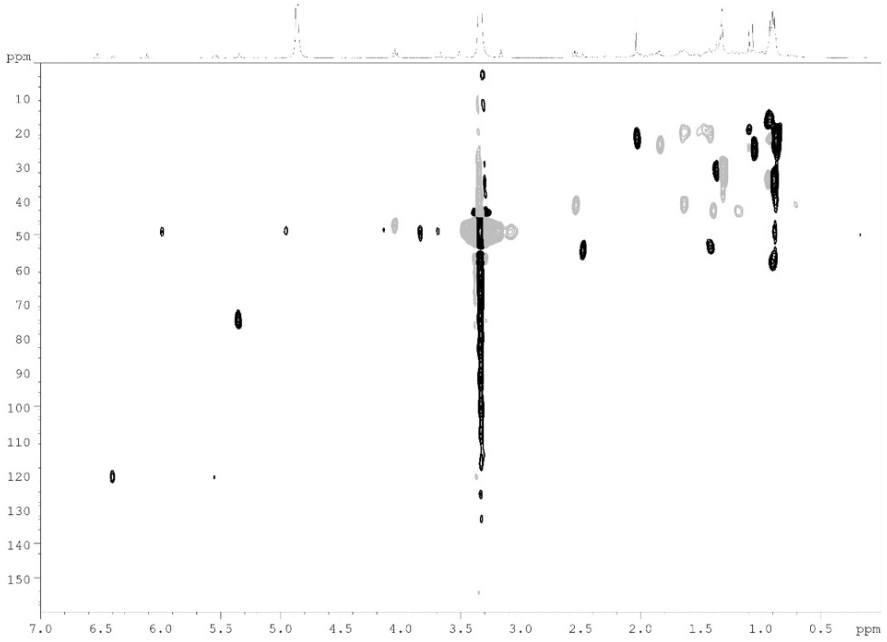

Figure S 19: HSQCed of Molliorin F (CD_3OD, Brucker 600MHz).

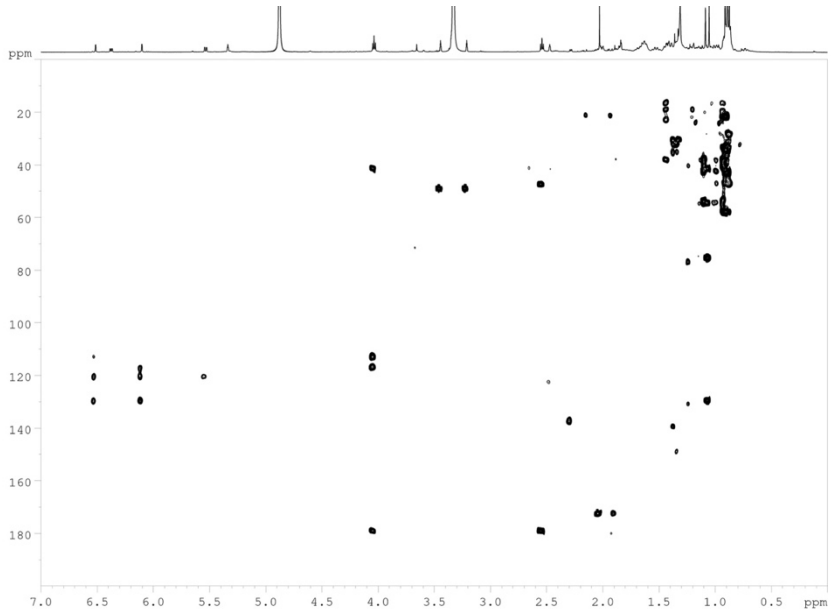

Figure S 20: HMBC of Molliorin F (CD_3OD, Brucker 600MHz).

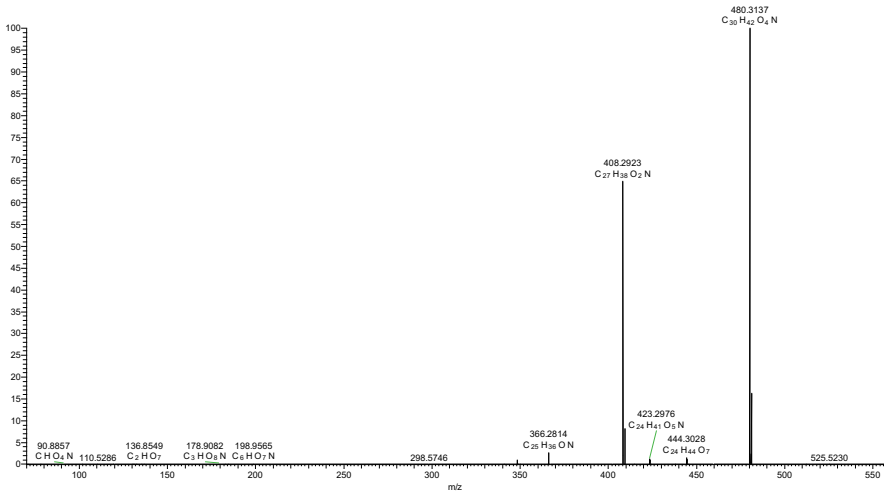

Figure S 21: HRESI-MSMS (ESI mode (+)) of Molliorin F.

RT (min)	m/z IonPeak $[M- H]^-/[M+Cl]^-$	m/z Fragment $[M-H-Glc]^-$	Molecular Formula	Exact Mass
19.20	732.56/768.54	570.52	$C_{40}H_{79}NO_{10}$	733.5704
20.97	712.54/748.53	550.49	$C_{40}H_{75}NO_9$	713.5442
22.49	726.56/762.54	564.50	$C_{41}H_{77}NO_9$	727.5962
23.02	760.60/796.59	598.54	$C_{42}H_{83}NO_{10}$	761.6017
23.79	740.57/776.56	578.52	$C_{42}H_{79}NO_9$	741.5755
26.64	816.66/852.65	654.61	$C_{46}H_{91}NO_{10}$	817.6643
27.29	830.67/866.65	668.62	$C_{46}H_{89}NO_{11}$	831.6436

Table S 13: Main Ion Peak and related fragment for HILIC fraction C, from H. Vansoesti.

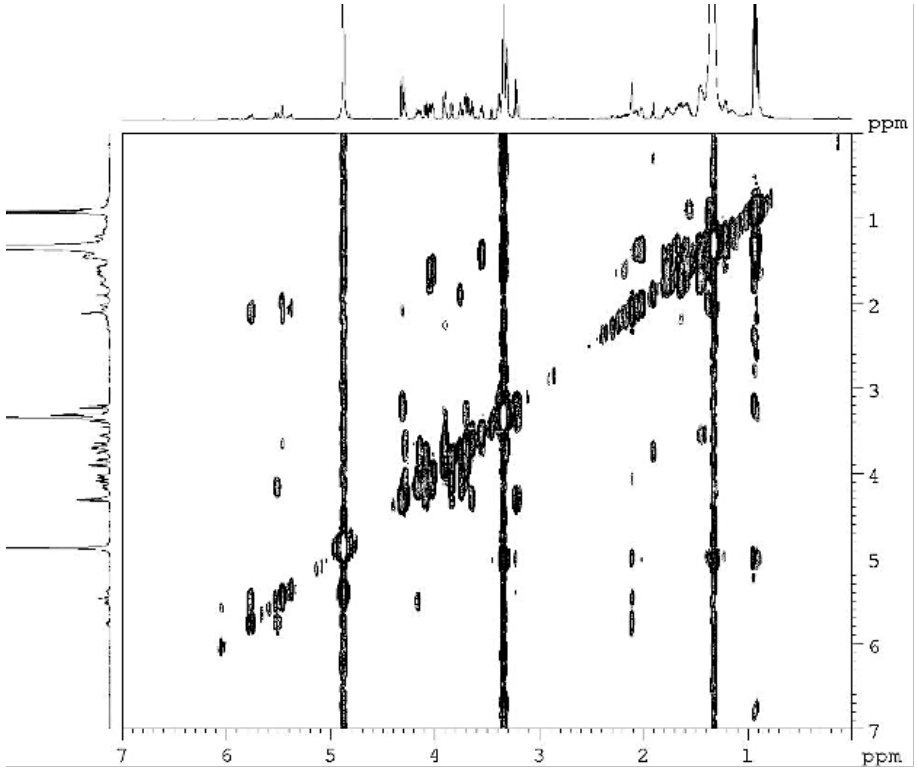

Figure S 22: ^1H-^1H COSY of HILIC Fraction C from H. vansoesti (CD_3OD, Brucker 600MHz).

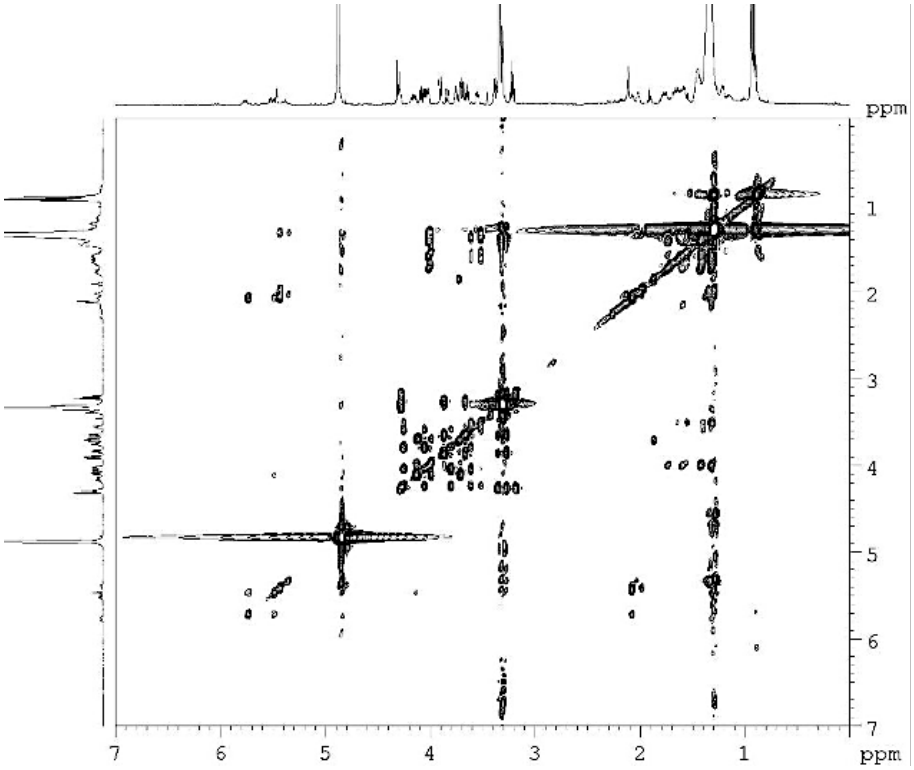

Figure S 23: ^{1}H-^{1}H TOCSY of HILIC Fraction C from H. vansoesti (CD_3OD, Brucker 600MHz).

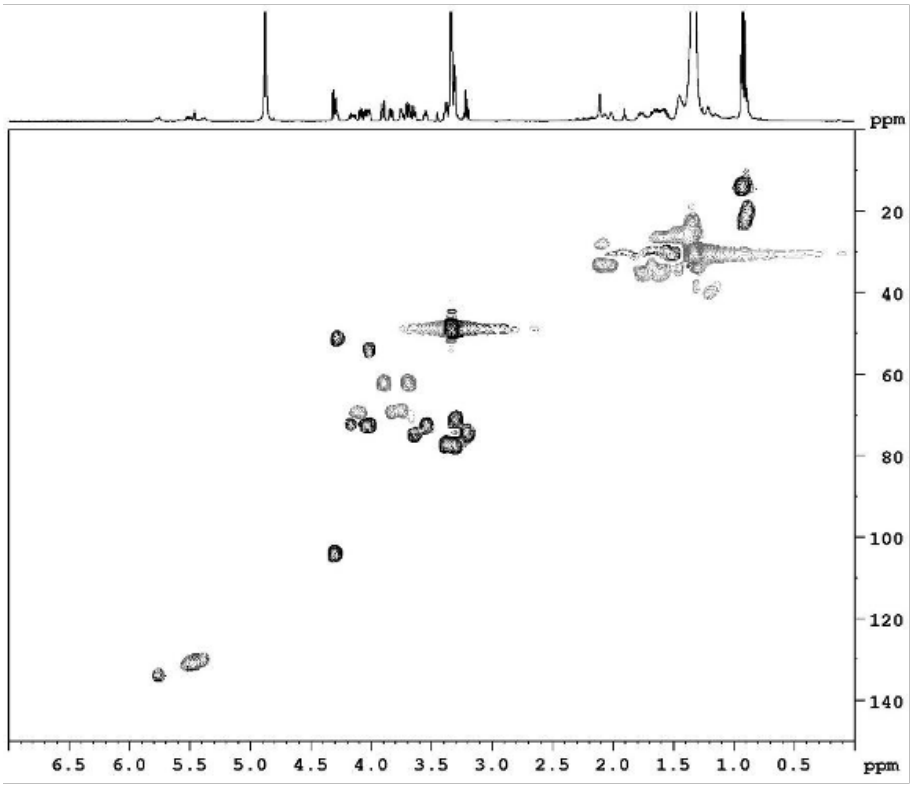

Figure S 24: HSQCed of HILIC Fraction C from H. vansoesti (CD_3OD, Brucker 600MHz).

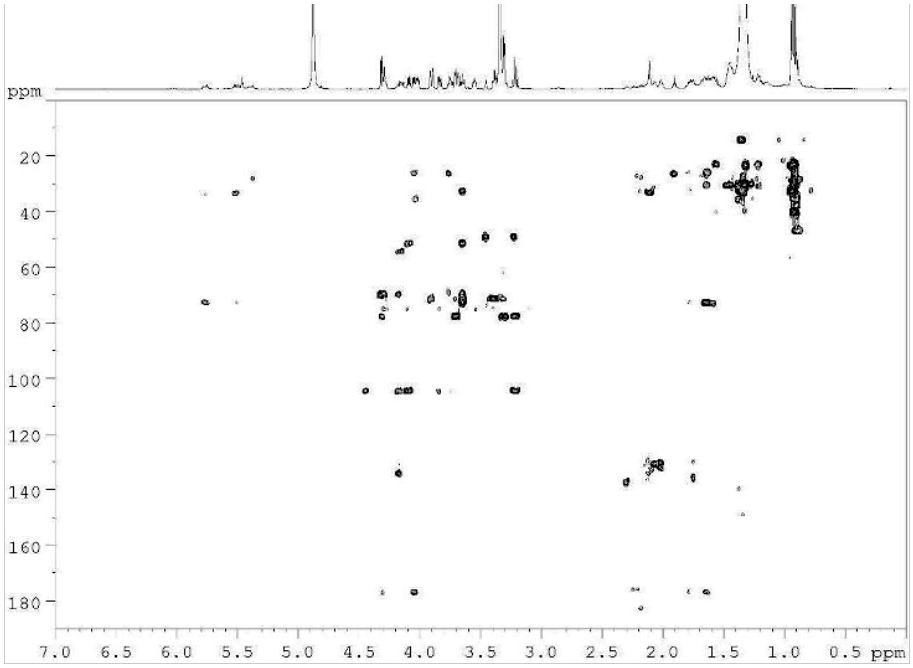

Figure S 25: HMBC of HILIC Fraction C from H. vansoesti (CD_3OD, Brucker 600MHz).

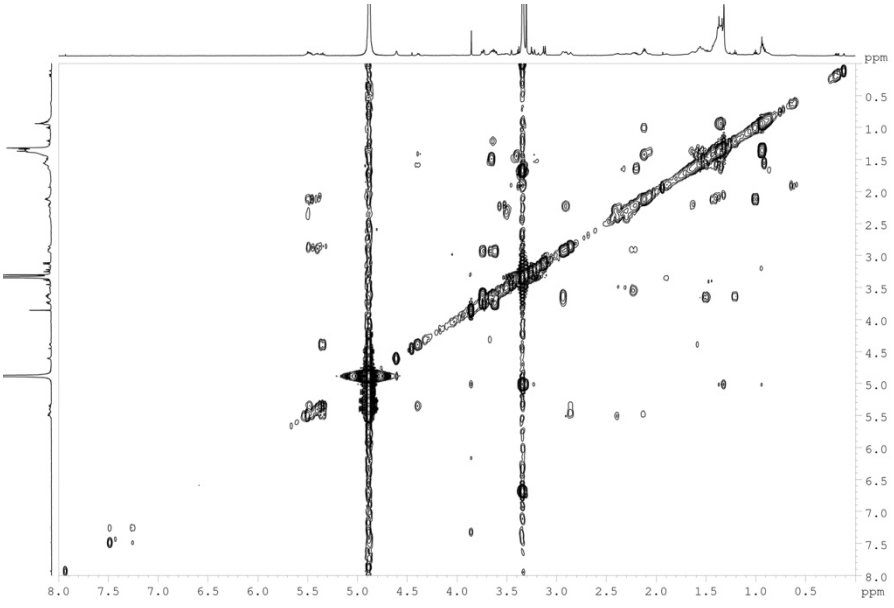

Figure S 26: ^{1}H-^{1}H COSY of HILIC Fraction D from H. vansoesti (CD_3OD, Brucker 600MHz).

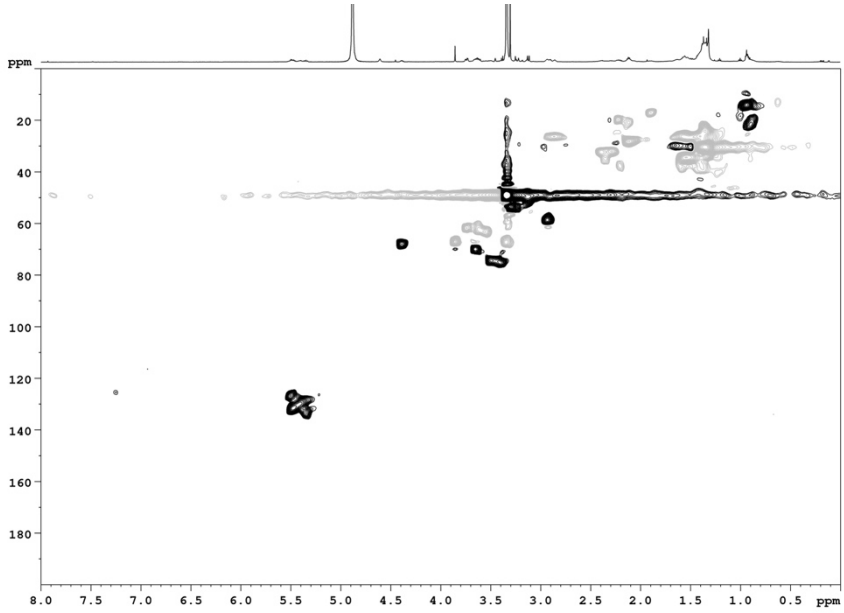

Figure S 27: HSQCed of HILIC Fraction D from H. vansoesti (CD_3OD, Brucker 600MHz).

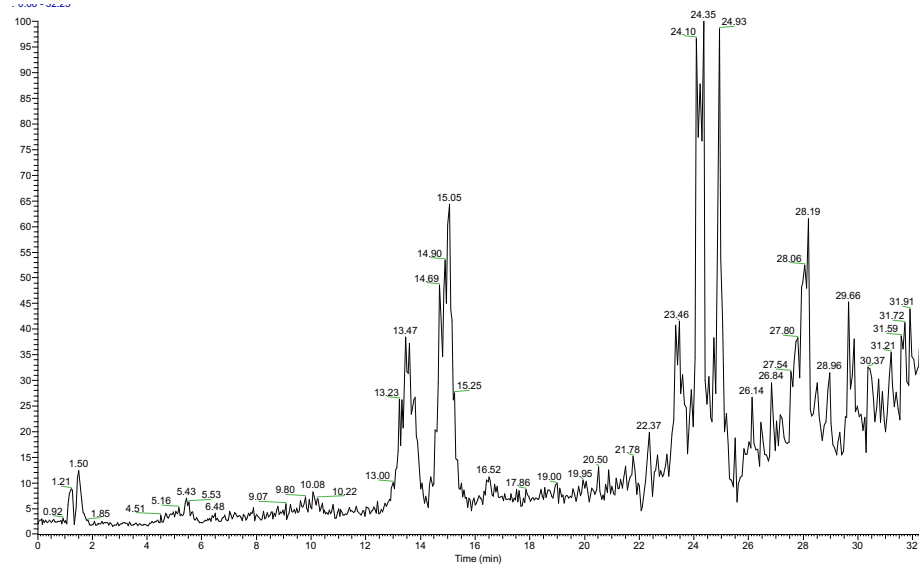

Figure S 28: HRESI-LCMS (ESI mode (-)) of Halo-sulpholipids (HILIC fraction B B of Ophiura ophiura)

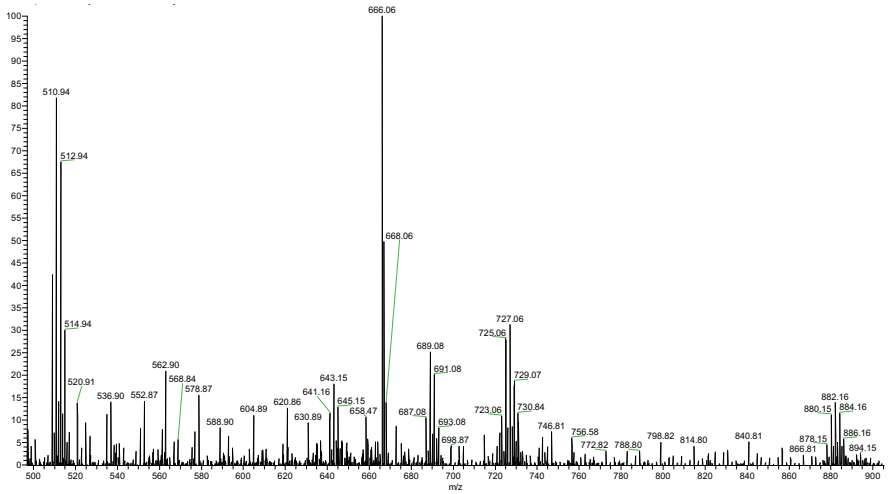

Figure S 29: HRESI-MS (ESI mode (-)) of Halo-sulpholipids (HILIC fraction B of Ophiura ophiura)

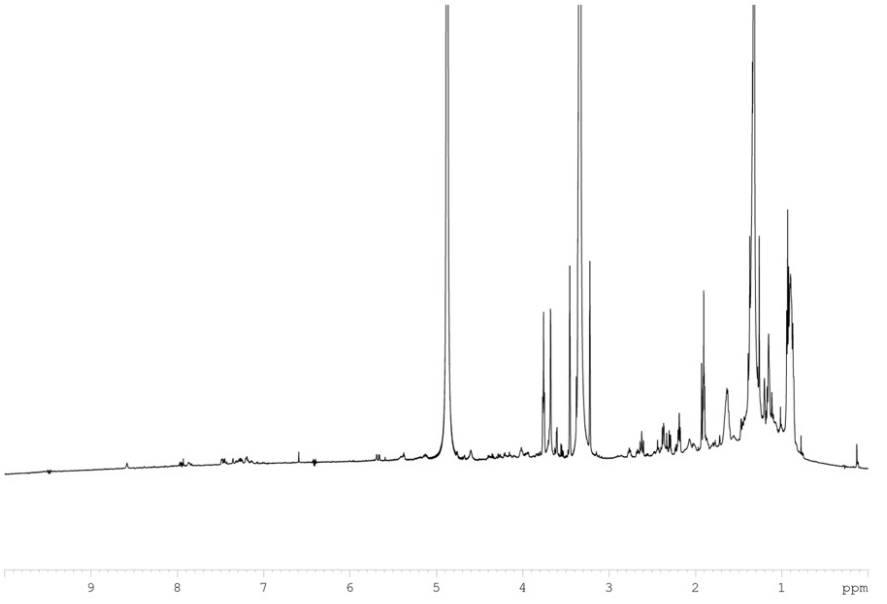

Figure S 30: ^{1}H NMR of HILIC fraction B (600 MHz, CD_3OD)

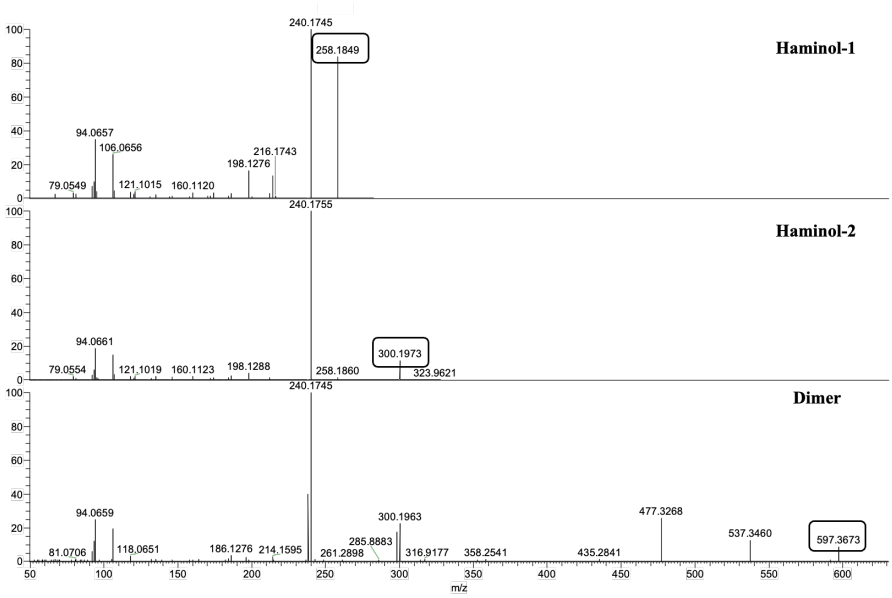

Figure S 31: HRESI-MSMS (ESI mode (+)) of Haminol-1, Haminol-2 and Dimer

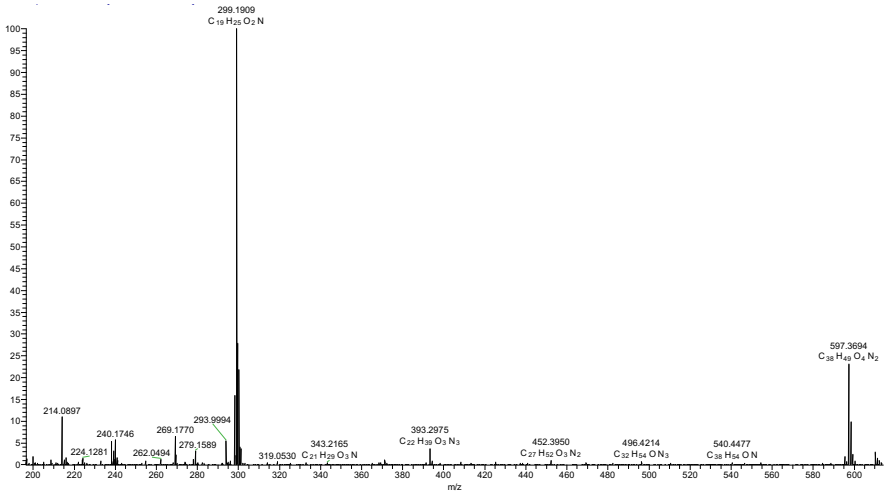

Figure S 32: HRESI-MS (ESI mode (+)) of Dimer from H. orbygnana.

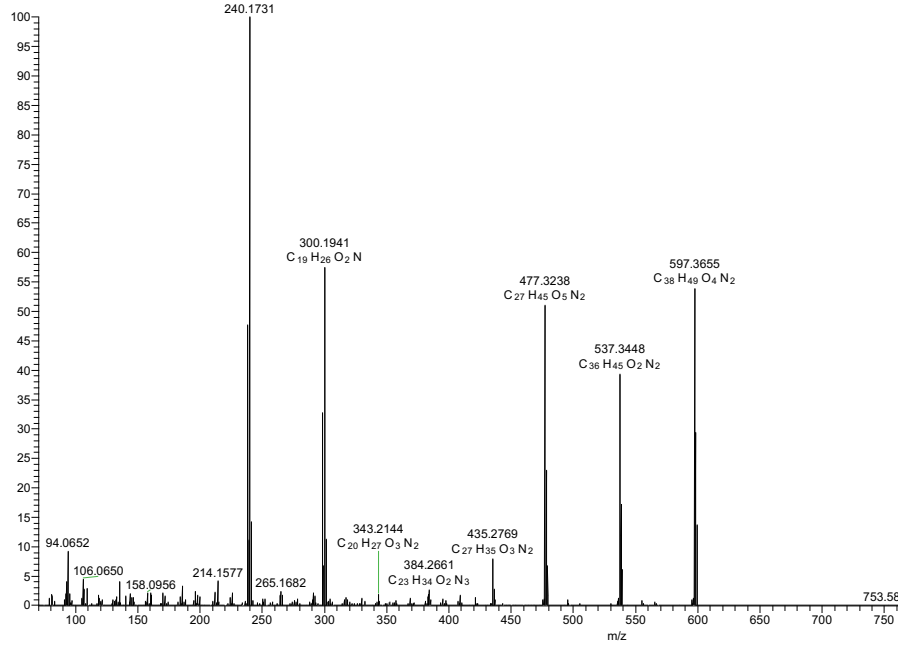

Figure S 33: HRESI-MSMS (ESI mode (+)) of Dimer from H. orbygnana

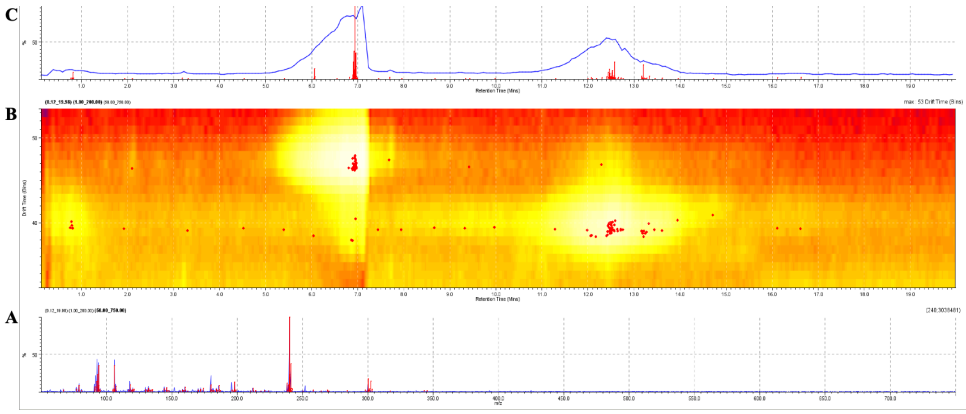

Figure S 34: IMS-MS of first sonicate of H. orbygnana; A) TIC B) Mobility trace C) Base peak m/z 299.19